NASA CONTRACTOR REPORT

NASA CR-2451

NASA CR-2451



# DEVELOPMENT AND APPLICATION OF A NON-GAUSSIAN ATMOSPHERIC TURBULENCE MODEL FOR USE IN FLIGHT SIMULATORS

*by P. M. Reeves, G. S. Campbell, V. M. Ganzer, and R. G. Joppa*

*Prepared by*
UNIVERSITY OF WASHINGTON
Seattle, Wash.
*for Ames Research Center*

NATIONAL AERONAUTICS AND SPACE ADMINISTRATION • WASHINGTON, D. C. • SEPTEMBER 1974

| 1. Report No. | 2. Government Accession No. | 3. Recipient's Catalog No. |
|---|---|---|
| NASA CR 2451 | | |

| 4. Title and Subtitle | 5. Report Date |
|---|---|
| "Development and Application of a Non-Gaussian Atmospheric Turbulence Model for Use in Flight Simulators" | September 1974 |
| | 6. Performing Organization Code |

| 7. Author(s) | 8. Performing Organization Report No. |
|---|---|
| P.M. Reeves, G.S. Campbell, V.M. Ganzer, and R.G. Joppa | |
| | 10. Work Unit No. |

| 9. Performing Organization Name and Address | 11. Contract or Grant No. |
|---|---|
| University of Washington<br>Department of Aeronautics & Astronautics<br>Seattle, Washington | NASA NGR 48-002-085 |
| | 13. Type of Report and Period Covered |
| 12. Sponsoring Agency Name and Address | Contractor Report |
| National Aeronautics & Space Administration<br>Washington, D.C. 20546 | 14. Sponsoring Agency Code |

15. Supplementary Notes

16. Abstract

A method is described for generating time histories which models the frequency content and certain non-Gaussian probability characteristics of atmospheric turbulence. The method also reproduces the large gusts and "patchy" nature of turbulence. Methods for producing such time histories using either analog or digital computation are described.

An experiment was performed in which a STOL airplane was programmed into a 6-degree-of-freedom flight simulator at NASA Ames, and turbulence time histories from several atmospheric turbulence models, including the non-Gaussian model, were introduced. The pilots' reactions to the various models are described.

| 17. Key Words (Suggested by Author(s)) | 18. Distribution Statement |
|---|---|
| Aircraft, atmospheric turbulence, flight simulators, gusts, piloted simulators, simulation, STOL, turbulence, turbulence models. | UNCLASSIFIED-UNLIMITED<br>CAT. 02 |

| 19. Security Classif. (of this report) | 20. Security Classif. (of this page) | 21. No. of Pages | 22. Price* |
|---|---|---|---|
| UNCLASSIFIED | UNCLASSIFIED | 147 | 4.75 |

*For sale by the National Technical Information Service, Springfield, Virginia 22151

# FOREWORD

This report was prepared under NASA Grant No. NGR 48-002-085 between the University of Washington, Seattle, Washington, and the National Aeronautics and Space Administration. The NASA technical monitor was Richard L. Kurkowski. The evaluation pilots were Gordon H. Hardy and Glen W. Stinnett, Jr. from NASA, Ames Research Center, and Lt. Col. Daniel C. Dugan from the Ames Directorate of the Army Air Mobility Research and Development Laboratory.

The authors gratefully acknowledge the invaluable help of the NASA and the University of Washington personnel associated with this project.

TABLE OF CONTENTS

FIGURE INDEX

# DEVELOPMENT AND APPLICATION OF A NON-GAUSSIAN ATMOSPHERIC TURBULENCE MODEL FOR USE IN FLIGHT SIMULATORS

By P. M. Reeves,* G. S. Campbell,* V. M. Ganzer,† and R. G. Joppa†

## SUMMARY

The use of flight simulators for the study of airplane handling qualities has proven to be much more valuable when disturbances in the form of artificially simulated turbulence are introduced into the system. Several methods have been used to generate the turbulence signals, the best known of which uses a Gaussian white-noise generator whose output is linearly shaped to match the power spectrum of the turbulence. This procedure results in a Gaussian probability density distribution which is not a precise representation of the probability characteristics of real turbulence.

In this report a method is described for artificially generating turbulence time histories which accurately models both the frequency content of atmospheric turbulence and its non-Gaussian nature. In particular it correctly reproduces the large gusts and the "patchy" nature of turbulence which are lacking in a Gaussian simulation. Although the present report discusses only the application of this method to ground based flight simulators, the method should also be of use in airborne flight simulators, in computer studies of stability, stability augmentation, and guidance systems, and for aircraft structural problems.

Four turbulence time histories, two of which were generated by this new method, were used in a ground-based simulator experiment, consisting of an IFR tracking task, which was intended to determine if pilots are sensitive to the non-Gaussian characteristics of turbulence and if the turbulence generated by the method described herein might be more satisfactory than that obtained by other methods. The four turbulence time histories were an actual recording of atmospheric turbulence, one derived using the Gaussian probability distribution, and two non-Gaussian models differing in patchiness and probability distribution.

The results of the investigation were mixed. The time histories generated by the new method showed characteristics which appeared to be much more similar to the real turbulence than did those generated using the Gaussian model. This would indicate that the new model should give more realistic results when used in the simulator experiment as well as in structural studies.

---

*Research Associate

†Professor, Department of Aeronautics and Astronautics

The simulator experiment produced results which were not conclusive. Although the pilots judged that the simulator response to the turbulence generated by this new method indicated that this model produced turbulence somewhat more realistic, "patchy", and less monotonous than that generated from the Gaussian model, the other subjective information obtained as pilot opinion was inconclusive regarding distinguishing the various types of turbulence inputs. It is concluded that more extensive experience is required to evaluate the worth of this new model in handling qualities studies.

## INTRODUCTION

The widespread use of flight simulators to evaluate vehicle handling qualities, pilot workload, ride quality, and other design factors which must be evaluated with a human pilot in the control loop, has resulted in the development of highly sophisticated simulators, including six degree-of-freedom moving base simulators and complex variable stability aircraft.

It has been found that realism requires the presence of an external disturbance representing atmospheric turbulence. A realistic representation of turbulence becomes especially important in the simulation of STOL vehicles because of their sensitivity to turbulence, as even light to moderate turbulence may seriously degrade the controllability and ride quality of these vehicles.

Several methods of generating turbulence signals for use in simulators have been developed. Some of these will be mentioned below, along with their shortcomings.

The most direct method is the use of recorded gust time histories obtained from flight experiments (ref. 1). This form is certainly realistic, and may even be especially useful when the turbulence is generated by terrain and obstacles, but for general studies it has several disadvantages. It is difficult to modify such records to fit anything except the specific situation recorded, which may or may not be typical, and there is a possibility that pilots may become familiar with the time histories if they are used repeatedly. Therefore a large number of recordings representing a wide variety of turbulence conditions becomes necessary.

A more useful turbulence simulation might result if one could generate non-repeating random time histories with proper statistical properties of the actual atmospheric turbulence being simulated. Such a method should allow continuous

adjustment of these properties in order to simulate changes in the flight environment. Three such techniques are described.

The first of these represents turbulence by a summation of sinusoidal waves with various amplitudes and frequencies (ref. 2). The principal objection to this method is that it attempts to model a process containing an infinite number of frequencies by using a small number of sinusoids, and therefore valuable information may be lost. Nevertheless, the sum of sine waves model does produce a non-repeating time history and has been used in flight simulation.

A second method generating random time histories uses a linearly filtered Gaussian white noise signal (ref. 3). This Gaussian model or Gaussian simulation requires only inexpensive equipment and is not particularly complicated if the gust components are uncorrelated. This Gaussian model has two major deficiencies. First, the artificial turbulence produced is necessarily Gaussian, whereas real turbulence is non-Gaussian. This results in an underestimation of the large gusts by the Gaussian model which is a serious deficiency in that the large gusts cause the greatest control problems and result in the greatest passenger discomfort. Secondly, the Gaussian model does not truly represent the patchy nature of real turbulence. Turbulence occurs in patches of relatively intense activity separated by intervals of relative calm. These deficiencies result in a model which produces turbulence inputs which pilots classify as too continuous or monotonous compared to real turbulence.

A third method, proposed by one of the authors of this paper (ref. 4) consists of using the product of two Gaussian processes, one representing a constant intensity turbulence time history and the other representing the time varying standard deviation. This method produces a non-Gaussian model and has the same versatility as the Gaussian model. However, the simulation is not as realistic as might be hoped. The approach described in this paper is a modification and extension of this third method.

The purpose of the study described in this report was to develop a technique for producing artificial turbulence which would overcome the deficiencies of the techniques described, and yet retain the practical advantages of the Gaussian simulation in ease of application. Such a technique was developed and put into a form which could be used in simulators. The application of this new non-Gaussian model is somewhat more complex than that of the Gaussian model, but the new model does include the possibility of producing the large gusts and patchy characteristics of turbulence lacking in the Gaussian model.

This new model and others were mechanized to be included in a flight simulator experiment in order to determine to what extent pilots are sensitive to changes in the "patchiness" of a turbulence model. Pilots were asked to fly a constant altitude tracking task for a typical STOL aircraft in the landing configuration with four different turbulence models, recorded real atmospheric turbulence, a Gaussian model, and two non-Gaussian models of differing patchiness. These models differed only in their probability densities.

The following sections of this report describe the proposed turbulence simulation and the flight simulator experiment in detail. Briefly the sections consist of:

a.) Description of Turbulence Simulation. This section describes the characteristics of real turbulence and several simulations now in use. The proposed new simulation is then discussed and it is shown that this simulation produces an improved representation of atmospheric turbulence. The manner in which the statistics of the spatial distribution of gusts over the vehicle surface are obtained is presented. The section also includes the method used to introduce the artificial turbulence into the flight simulator.

b.) Flight Simulator Experiment. Here are found details of the flight simulator experiment, in which pilots were asked to rate the realism of the various turbulence models.

c.) Results. This section summarizes and discusses the results of the previous sections.

d.) Conclusions.

e.) Appendixes. Five appendices are included.

Appendix A describes the details of the turbulence simulations used in the flight simulator experiment.

Appendix B describes the equations of motion used in the experiment.

Appendix C describes the flight simulator motion compensation.

Appendix D presents the pilot question sheet.

Appendix E presents additional results of the pilot questionnaire not presented in the main text.

## SYMBOLS

$a$ random function of time

$b$ wingspan, m ; also, a random function of time

$c$ wing chord, m ; also, a random function of time

$C_D = \dfrac{\text{Drag}}{(1/2)\ \rho u_o^2 S}$ , nondimensional drag coefficient of the airplane

$C_{D_{CT}} = \left(\dfrac{\partial C_D}{\partial C_T}\right)_o$

$C_L = \dfrac{\text{Lift}}{(1/2)\ \rho u_o^2 S}$ , nondimensional lift coefficient of the airplane

$C_{L_{CT}} = \left(\dfrac{\partial C_L}{\partial C_T}\right)_o$

$C_\ell = \dfrac{\text{Rolling Moment}}{(1/2)\ \rho u_o^2 Sb}$ , nondimensional rolling moment coefficient of the airplane

$C_{\ell_p} = \left(\dfrac{2u_o}{b}\right)\left(\dfrac{\partial C_\ell}{\partial p}\right)_o$

$C_{\ell_r} = \left(\dfrac{2u_o}{b}\right)\left(\dfrac{\partial C_\ell}{\partial r}\right)_o$

$C_{\ell_{ug}}$ contribution to $C_\ell$ from the distribution of head-on gusts across the wingspan

$C_{\ell_{wg}}$ contribution to $C_\ell$ from the distribution of vertical gusts across the wingspan

$C_{\ell_\beta} = \left(\dfrac{\partial C_\ell}{\partial \beta}\right)_o$

$C_{\ell_{\delta a}} = \left(\dfrac{\partial C_\ell}{\partial \delta_a}\right)_o$

$C_{\ell_{\delta r}} = \left(\frac{\partial C_\ell}{\partial \delta_r}\right)_o$

$C_m = \frac{\text{Pitching Moment}}{(1/2)\ \rho u_o^2 Sc}$, nondimensional pitching-moment coefficient of the airplane

$C_{m_{CT}} = \left(\frac{\partial C_m}{\partial C_T}\right)_o$

$C_{m_q} = \left(\frac{2u_o}{c}\right)\left(\frac{\partial C_m}{\partial q}\right)_o$

$C_{m_t} = \left(\frac{2}{\rho u_o^2 Sc}\right)$. (pitching moment about airplane c.g. due to horizontal tail only)

$C_{m_{tu}} = (u_o)\left(\frac{\partial C_{mt}}{\partial u}\right)_o$

$C_{m_{t\alpha}} = \left(\frac{\partial C_{mt}}{\partial \alpha}\right)_o$

$C_{m_{t\dot{\alpha}}} = \left(\frac{2u_o}{c}\right)\left(\frac{\partial C_{mt}}{\partial \dot{\alpha}}\right)_o$

$C_{m_\alpha} = \left(\frac{\partial C_m}{\partial \alpha}\right)_o$

$C_{m_{\dot{\alpha}}} = \left(\frac{2u_o}{c}\right)\left(\frac{\partial C_m}{\partial \dot{\alpha}}\right)_o$

$C_{m_{\delta e}} = \left(\frac{\partial C_m}{\partial \delta e}\right)_o$

$C_n = \frac{\text{Yawing Moment}}{(1/2)\rho u_o^2 Sb}$, nondimensional yawing-moment coefficient of the airplane

$C_{n_p} = \left(\frac{2u_o}{b}\right)\left(\frac{\partial C_n}{\partial p}\right)_o$

$C_{n_r} = \left(\frac{2u_o}{b}\right)\left(\frac{\partial C_n}{\partial r}\right)_o$

$C_{n_t} = \left(\frac{2}{\rho u_o^2 Sb}\right)$ .(Yawing moment about airplane c.g. due to vertical tail only

$C_{n_{t\beta}} = \left(\frac{\partial C_{nt}}{\partial \beta}\right)_o$

$C_{n_{ug}}$ contribution to $C_n$ from the distribution of head-on gusts across the wingspan

$C_{n_{wg}}$ contribution to $C_n$ from the distribution of vertical gusts across the wingspan

$C_{n_\beta} = \left(\frac{\partial C_n}{\partial \beta}\right)_o$

$C_{n_{\delta a}} = \left(\frac{\partial C_n}{\partial \delta a}\right)_o$

$C_{n_{\partial r}} = \left(\frac{\partial C_n}{\partial r}\right)_o$

$C_T = \frac{\text{Thrust}}{(1/2)\ \rho u_o^2 S}$ , thrust coefficient

$C_{T_{\delta T}} = \left(\frac{\partial C_T}{\partial \delta T}\right)_o$

$C_{uu}$ autocorrelation of random process u(t)

$C_{uv}$ cross correlation of random processes u(t) and v(t)

$C_x = \left(\frac{2}{\rho u_o^2 S}\right)$ . (x-component of aerodynamic force acting on the airplane)

$C_{x_\alpha} = \left(\frac{\partial C_x}{\partial \alpha}\right)_o$

$C_y = \left(\frac{2}{\rho u_o^2 S}\right)$ . (y-component of aerodynamic force acting on the airplane)

$$C_{Y_p} = \left(\frac{2u_o}{b}\right)\left(\frac{\partial C_Y}{\partial p}\right)_o$$

$$C_{Y_r} = \left(\frac{2u_o}{b}\right)\left(\frac{\partial C_Y}{\partial r}\right)_o$$

$$C_{Y_t} = \left(\frac{2}{\rho u_o^2 S}\right) \cdot \text{(y-force due to vertical tail only)}$$

$$C_{Y_{t\beta}} = \left(\frac{\partial C_{Yt}}{\partial \beta}\right)_o$$

$$C_{Y_\beta} = \left(\frac{\partial C_Y}{\partial \beta}\right)_o$$

$$C_{Y_{\delta a}} = \left(\frac{\partial C_Y}{\partial \delta a}\right)_o$$

$$C_{Y_{\delta r}} = \left(\frac{\partial C_Y}{\partial \delta r}\right)_o$$

$$C_z = \left(\frac{2}{\rho u_o^2 S}\right) \cdot \text{(z-component of aerodynamic force acting on the airplane)}$$

$$C_{z_q} = \left(\frac{2u_o}{c}\right)\left(\frac{\partial C_z}{\partial q}\right)_o$$

$$C_{z_t} = \left(\frac{2}{\rho u_o^2 S}\right) \cdot \text{(z-force due to horizontal tail only)}$$

$$C_{z_{t\alpha}} = \left(\frac{\partial C_{zt}}{\partial \alpha}\right)_o$$

$$C_{z_{t\dot{\alpha}}} = \left(\frac{2u_o}{c}\right)\left(\frac{\partial C_{zt}}{\partial \dot{\alpha}}\right)_o$$

$$C_{z_\alpha} = \left(\frac{\partial C_z}{\partial \alpha}\right)_o$$

$$C_{z_{\dot{\alpha}}} = \left(\frac{2u_o}{c}\right)\left(\frac{\partial C_z}{\partial \dot{\alpha}}\right)_o$$

$C_{z_{\delta e}} = \left(\frac{\partial C_z}{\partial \delta e}\right)_o$

$d$ random function of time

$f$ frequency, hertz

$(F_{E_x}, F_{E_y}, F_{E_z})$ x, y, and z-components of engine force, N

$(F_{T_x}, F_{T_y}, F_{T_z})$ x, y, and z-components of total force on the airplane (excluding gravity), N

$P_{max}$ maximum engine power, W

$K_o$ modified Bessel function of second type, order zero

$L$ longitudinal scale-length of atmospheric turbulence, m

$\ell_t$ distance from airplane c.g. to tail mean-aerodynamic-center, m

$m$ airplane mass, kg

$(M_{E_x}, M_{E_y}, M_{E_z})$ x, y, and z-components of moment due to engines, kgm

$M_n$ $n^{th}$ normalized central moment

$(M_{T_x}, M_{T_y}, M_{T_z})$ x, y, and z-components of total moment on the airplane (excluding gravity) kgm

$n$ integer

$p$ roll rate (right wing down, positive), rad/sec

$P$ probability density

$\mathbb{P}$ cumulative probability distribution

$q$ pitch rate (nose-up, positive), rad/sec

$\bar{q} = (1/2)\rho V_{RW}^2$, dynamic pressure, $N/m^2$

$r$ yaw rate (nose right, positive), rad/sec

$s$ Laplace transform variable

$S$ wing area, $m^2$

$S_k$ Sears function for a two-dimensional wing in a sinusoidal upwash

STOL short take-off and landing

$t$ time, sec

$T$ total time history length (sec)

$u_o$ reference flight speed in still air, m/sec

$(u, v, w)$ x, y, and z-components of airplane velocity with respect to still air, m/sec

$(u_B, v_B, w_B)$ x, y, and x-components of airplane velocity with respect to gusty air (i.e., $u_B = u + u_{g_c}$, etc.), m/sec

$(u_{g_c}, v_{g_c}, w_{g_c})$ x, y, and z-components of gusts at the airplane c.g. ($u_{g_c}$, $v_{g_c}$, $w_{g_c}$ are positive when in the direction of negative x, y, and z), m/sec

$(u_{g_t}, v_{g_t}, w_{g_t})$ components of gusts at the airplane tail (same sign convention as c.g. gusts), m/sec

$(V_N, V_E, V_D)$ north, east, and down components of the airplane velocity with respect to still air, m/sec

$V_{RW} = \sqrt{u_B^2 + v_B^2 + w_B^2}$, airplane speed with respect to gusty air, m/sec

$(x, y, z)$ distances measured in airplane body axes; (body-axes are centered at aircraft c.g., attached to the airplane, and have x-axis through the nose, y-axis out the right side of the airplane, and z-axis downward with respect to the airplane), m

$(X_N, X_E, X_D)$ distance airplane has travelled in the north, east, and downward directions, m

$\alpha = \tan^{-1} \frac{w_B}{u_B}$, airplane angle of attack, rad

$\alpha_o$ angle of attack of the zero-lift line of the wing, rad

$\beta = \tan^{-1} \dfrac{v_B}{\sqrt{u_B^2 + w_B^2}}$, sideslip angle, rad

$\delta_a$ angle moved by one aileron surface, rad (positive $\delta_a$ gives positive rolling moment)

$\delta_e$ angle moved by elevator surface (trailing-edge up, positive), rad

$\delta_r$ angle moved by rudder surface (trailing-edge right, positive), rad

$\delta T$ pilot's throttle movement (throttle forward is positive), measured in % of full throttle

$\eta$ Gaussian white noise

$\sigma$ standard deviation

$\rho$ atmospheric density, $kg/m^3$

$\phi_i(f)$ power spectral density of the variable i , in (units of the variable i)$^2$/hertz

$\phi_{ij}(f)$ cross spectral density of variables i and j in (units of variable i) (units of variable j)/hertz

Subscripts:

u, v, w denotes u, v, or w gust component

$(\dot{\ }) = \dfrac{d(\ )}{dt}$

$(\ )_o$ = value at reference-flight condition with no wind

## TURBULENCE SIMULATIONS

In this section the general problem of statistically modeling atmospheric turbulence is discussed, and detailed descriptions are given of various techniques for accomplishing this modeling, including the proposed non-Gaussian model.

First, basic definitions of statistical properties of atmospheric turbulence are reviewed. Then the statistical properties of atmospheric turbulence which are to be used in the various models are discussed in the light of presently available information. Next, presently used simulation techniques are discussed in some detail. Finally, a non-Gaussian simulation method is proposed, and it is shown that this technique can closely model the statistical properties of real turbulence including spatial effects, providing proper information and data regarding the real turbulence are available.

### Review of Basic Definitions

The following is a collection of definitions applying to the statistical quantities used throughout this report.

Stationarity.- A random process is stationary if its statistical properties are not dependent on the time of their measurement. One could, for example, collect an infinite number of time histories which are representative of the process. This set of histories is called an ensemble, and could look as below.

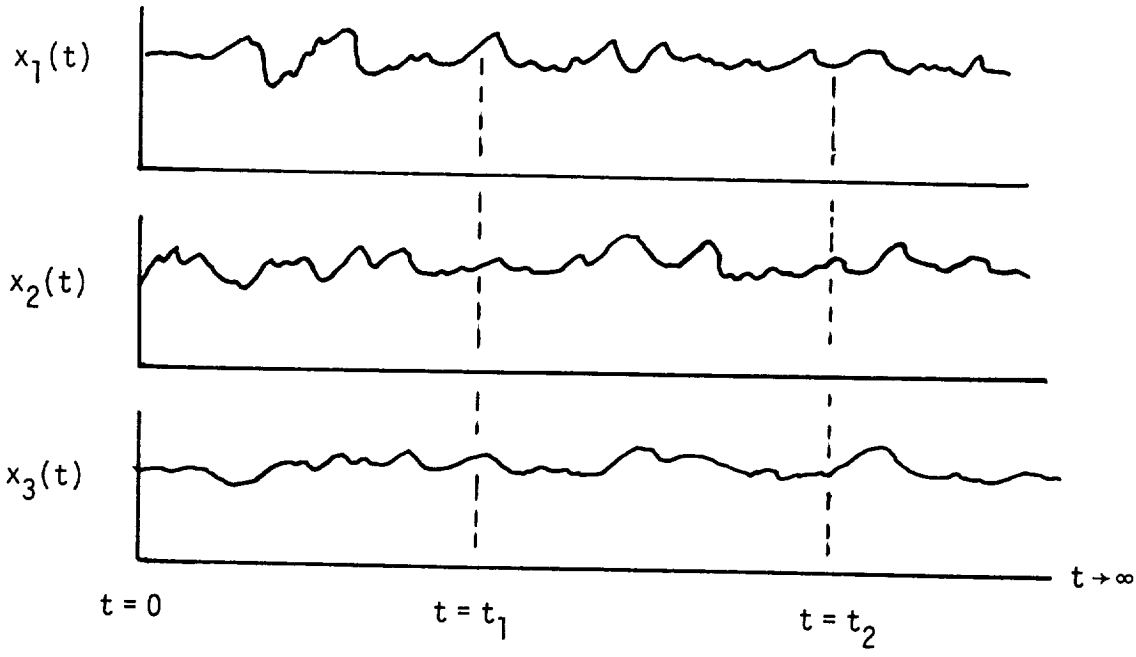

If one takes an ensemble average across the ensemble, at $t_1$ and at $t_2$, etc., and if these ensemble averages are not functions of time the process is stationary.

All of the definitions which follow assume stationarity, with the exception of homogeneity.

Homogeneity.- A random process is homogeneous if its statistical properties are independent of position. Thus, if atmospheric turbulence were homogeneous (which it is not), its statistical properties would be independent of altitude and geographical location. If one is concerned with turbulence models to be used for simulator studies of STOL airplanes in approaches to airport, during which altitude varies, the lack of homogeneity becomes important since the statistical properties vary with altitude.

Ergodicity.- Since, in turbulence measurements, it is virtually impossible to obtain ensembles of turbulence data from atmospheric measurements, it is necessary to use time averages to get statistical information. If such a time average gives the same statistical properties as the ensemble average the process is called ergodic. Note that ergodicity implies stationarity.

In the various methods of turbulence simulation it is not always necessary to assume either stationarity or ergodicity since it may be possible, if desired, to vary the statistical properties with time. However, in the reduction of experimental data, whether turbulence, flight, or flight simulation data, only a few relatively short time histories are generally available, and as a result one usually assumes ergodicity.

Note that all the quantities defined below employ time averages and therefore assume ergodicity.

Average or Mean Value.- The mean value of an ergodic random process is

$$\text{Mean of } u = \bar{u} = \lim_{T\to\infty} \frac{1}{2T} \int_{-T}^{T} u(t)\, dt \qquad (1)$$

For practical evaluation of the mean value the limit process is not required and $\bar{u}$ can be approximated by the equation

$$\bar{u} \simeq \frac{1}{T} \int_0^T u(t)\, dt \qquad (2)$$

where $T$ is large.

This approximate representation is especially useful for processes such as turbulence which are probably not stationary over very large time periods. However, the time interval $T$ must be large enough so the averages approach the asymptotic value one would obtain for a stationary process, but small enough to be assured that the process has approximately constant statistical properties during this time interval.

Variance.- The variance of $u$ is defined as

$$\text{Variance of } u = \sigma_u^2 = \lim_{T\to\infty} \frac{1}{2T} \int_{-T}^{T} [u(t)-\bar{u}]^2\, dt \qquad (3)$$

As before for practical purposes the variance can be approximated by

$$\sigma_u^2 \simeq \frac{1}{T} \int_0^T [u(t)-\bar{u}]^2\, dt \qquad (4)$$

for sufficiently large $T$.

Standard Deviation, Root Mean Square.- The standard deviation is defined as the square root of the variance, or

$$\text{Standard deviation} = \sigma_u = \sqrt{\sigma_u^2}\ , \qquad (5)$$

which is the root mean square of the departure from the mean value. In this report it is assumed that $\bar{u}$ is equal to zero, or that signals are measured from the mean value. Thus the standard deviation becomes the root mean square of the signal itself.

Normalized Central Moment.- The $N^{th}$ normalized central moment, or more simply the $N^{th}$ moment, of a random process $u(t)$ is

$$M_n = \lim_{T\to\infty} \frac{1}{2T} \int_{-T}^{T} \left[\frac{u(t)-\bar{u}}{\sigma_u}\right]^n dt \, , n = 1 \, , \, 2 \, , \, 3 \, . \, . \, . \qquad (6)$$

or approximately

$$M_n \simeq \frac{1}{T} \int_{o}^{T} \left[\frac{u(t)-\bar{u}}{\sigma_u}\right]^n dt \, , n = 1 \, , \, 2 \, , \, 3 \, . \, . \, . \qquad (7)$$

The moment is called central because the mean value $\bar{u}$ is substracted from $u(t)$ , and is nondimensionalized with respect to $u$ by dividing by the standard deviation $\sigma_u$ . Inspection shows that $M_1$ is thus zero, and $M_2$ becomes $(\frac{\sigma_u}{\sigma_u})^2 = 1$ .

Cumulative Probability Distribution.- The cumulative probability distribution is defined as

$$\mathbb{P}_u(x) = \text{Probability that } u \leq x \qquad (8)$$

Two important properties of the cumulative probability are that $\mathbb{P}_u(-\infty) = 0$ , which implies that no value of $u$ will be less than $-\infty$ , and $\mathbb{P}_u(+\infty) = 1$ , or that all values of $u$ will be $\leq +\infty$ . If a random function is distributed symmetrically about $\bar{u} = 0$ , that is, there is just as much probability of having a negative signal of a certain size as a positive signal, $\mathbb{P}_u(0)$ will be $0.5$ , and the cumulative probability distribution will look about as shown below.

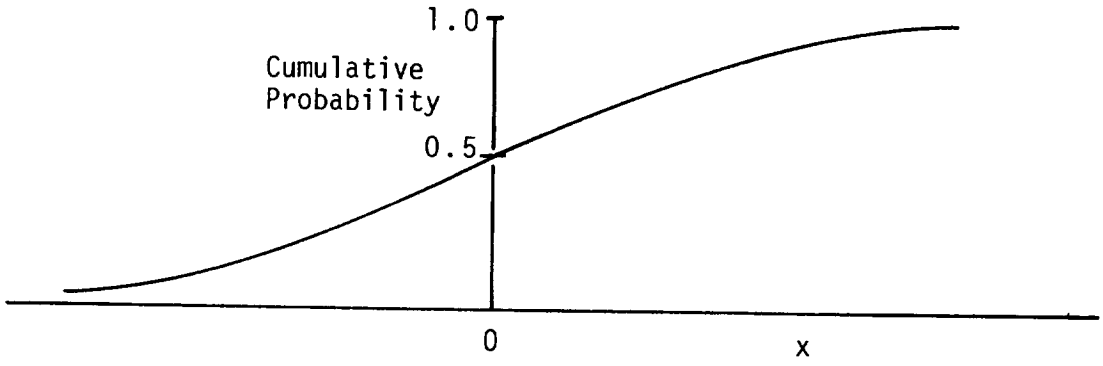


Probability Density Distribution.- Since for random processes it is difficult to conceive of the probability of an exact event occurring, such as having a gust of exactly 10 m/sec (such a probability would be almost zero), the probability density distribution is defined as,

$$\text{Probability density} = P_u(x)dx = \text{Probability that } x < u \leq x + dx \tag{9}$$

The probability density is related to the cumulative probability by differentiation.

$$P_u(x) = \frac{d}{dx} \mathbb{P}_u(x) \tag{10}$$

Some important properties of $P_u(x)$ are

$P_u(+\infty) = P_u(-\infty) = 0$ , or probabilities that $|u|$

will be greater than $\infty$ are zero, and

$\int_{-\infty}^{\infty} P_u(x)dx = 1$ , or the probability that $u$

will lie between $\pm\infty$ is 1 .

Gaussian Probability Density Distribution.- The most commonly known probability density distribution is the Gaussian or normal distribution

$$P_u(x) = \frac{1}{\sigma_u\sqrt{2\pi}} \exp\left[-1/2\left(\frac{x-\bar{u}}{\sigma_u}\right)^2\right] \tag{11}$$

When $\bar{u}$ is assumed to be zero, as it is in this report,

$$P_u(x) = \frac{1}{\sigma_u\sqrt{2\pi}} \exp\left[-1/2\left(\frac{x}{\sigma_u}\right)^2\right] \tag{12}$$

Examples of the Gaussian distribution for two values of $\sigma_u$ are shown below, where $\bar{u} = 0$ .

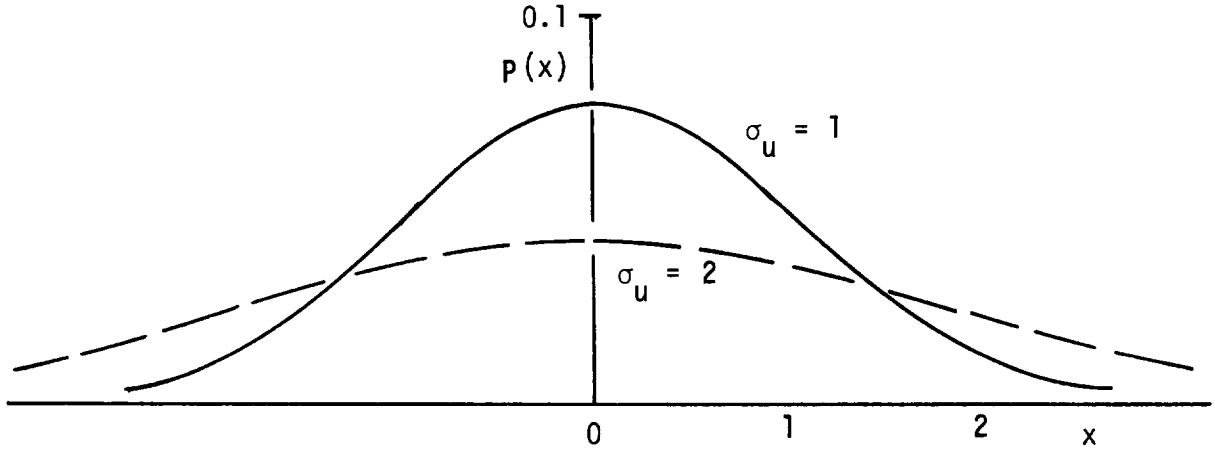


Modified Bessel Probability Density Distribution.- A probability density distribution which will be referred to frequently in the following report is characterized by the modified Bessel function of the second kind and order zero, $K_0$ .

$$P_u(x) = \frac{1}{\pi\sigma_u} K_0\left(\frac{x}{\sigma_u}\right) \tag{13}$$

A comparison of the modified Bessel function probability density and the Gaussian probability density for $\sigma_u = 1$ m/sec is shown below

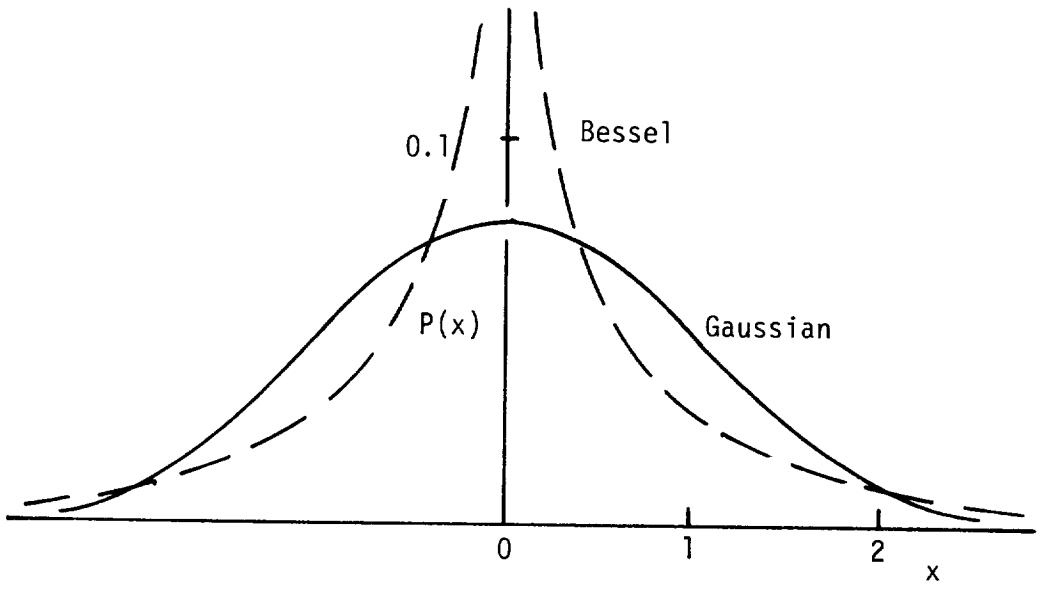


An examination of these probability density distributions shows that:

1.) The Bessel function shows greater probability for small gusts (0.5m/sec or less) than does the Gaussian.

2.) Between gusts of about 0.5m/sec and 2 m/sec the Bessel function indicates less probability of occurrence than does the Gaussian.

3.) The Gaussian shows almost no probability of reaching gust velocities of over 3 m/sec, while the Bessel function shows much greater probability of reaching such higher gust velocities.

Higher Moments.- As mentioned on page 15, the $N^{th}$ moment of a process in which $\bar{u} = 0$ is

$$M_n \approx \frac{1}{T} \int_0^T \left(\frac{u(t)}{\sigma_u}\right)^n dt \ , \ n = 1 \ , \ 2 \ , \ 3 \qquad (14)$$

As indicated the 1st moment is zero, and the second moment becomes 1 . The higher moments are important in the description of the probability density distribution. The third

moment is called the "skewness" moment, and if a process is not symmetrical about the mean value the third moment will be non-zero as shown below.

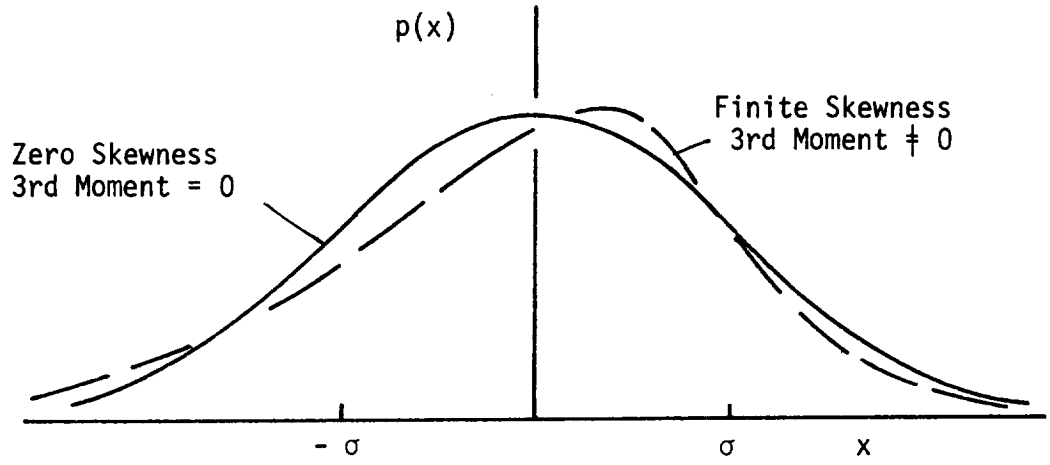


Since in this report all processes are assumed to be symmetric about the average, the third and higher odd moments will be zero.

The fourth moment,

$$M_4 \approx \frac{1}{T} \int_0^T \left(\frac{u(t)}{\sigma_u}\right)^4 dt \qquad (15)$$

is called the kurtosis or flatness factor, and probability densities with small and large kurtosis could look as below, for the same value of $\sigma$ .

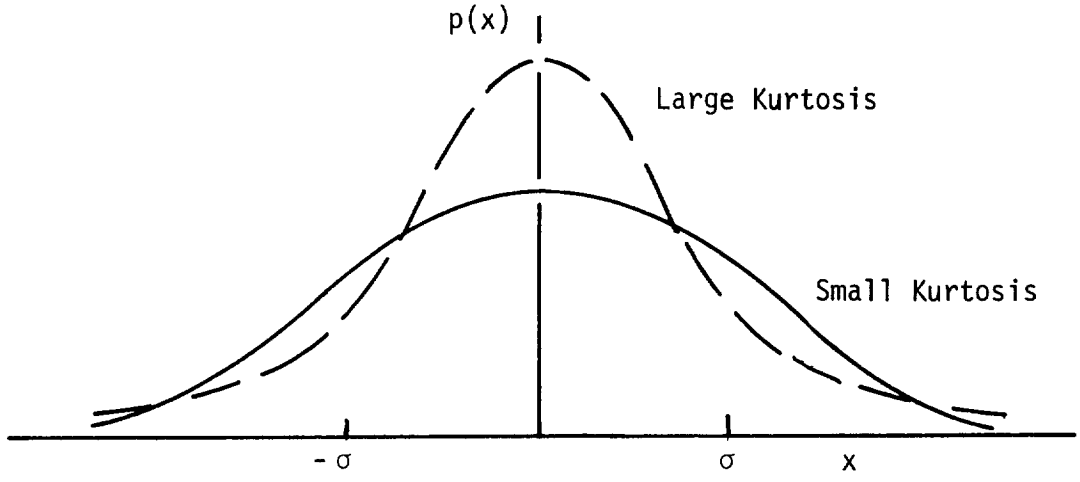

Comparison of these curves shows that the higher (even) moments are very important in defining the shape of the probability density, and that probability densities with larger kurtosis have higher probability of obtaining large values of the gust velocity. It will be noted that this same characteristic has been pointed out on page 18 in regard to the Bessel function, which has higher probability of having large gusts than does the Gaussian probability density.

Cross Correlation Function.- The cross correlation function of two random processes $u(t)$ and $w(t)$ is

$$C_{uw}(\tau) = \lim_{T\to\infty} \frac{1}{2T} \int_{-T}^{T} u(t)w(t+\tau)\, dt \tag{16}$$

Correlations are the measure of the predictability of a signal at some future time $(t+\tau)$ based on the knowledge of a signal at the time $t$. Since the modeling of a random process such as turbulence consists of developing techniques for predicting the time-wise behavior of that process it can be seen that correct duplication of the correlation functions is very important, since these are measures of predictability.

Autocorrelation Function.- The autocorrelation function of a random process is a special case of the cross correlation function defined above in which $w(t) = u(t)$, so

$$C_{uu}(\tau) = \lim_{T\to\infty} \frac{1}{2T} \int_{-T}^{T} u(t)u(t+\tau)\, dt \tag{17}$$

Integral Scale Length.- A statistical parameter of special importance in atmospheric turbulence studies is the integral scale length, also called simply the scale length,

$$L_u = \frac{u_o}{\sigma_u^2} \int_{-\infty}^{\infty} C_{uu}(\tau)\, d\tau \tag{18}$$

where $u_o$ is the reference steady state flight speed of the aircraft flying through the turbulence.

In random process theory an integral scale time is defined as

$$\mathcal{T} = \int_{-\infty}^{\infty} \frac{C_{uu}(\tau)}{\sigma_u^2} \, d\tau \ . \tag{19}$$

As shown below, this value of $\mathcal{T}$ is a measure of the strength of the correlation, and gives a rough idea of the time interval during which the process is correlated with itself.

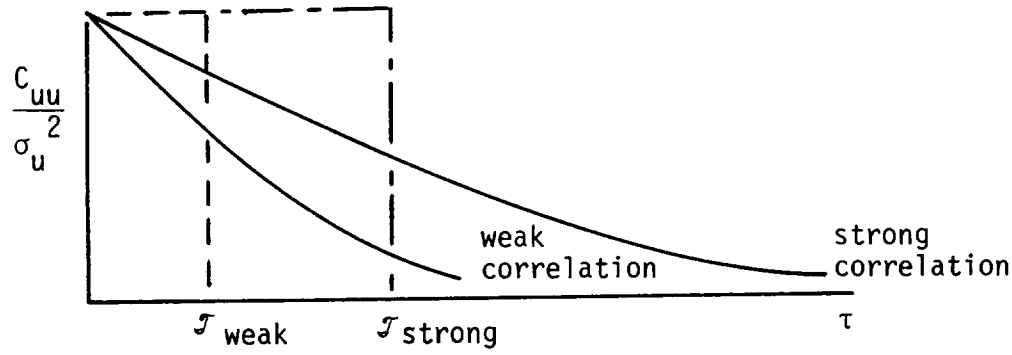


In work concerning the flight of an aircraft through turbulence it is more convenient to turn this time into a distance by multiplying by the steady flight speed, or

$$L_u = u_o \mathcal{T} , \tag{20}$$

so the scale length becomes an approximate measure of the distance an aircraft flies through turbulence which is correlated with itself.

Cross Spectral Density.- The cross spectrum of two random processes $u(t)$ and $w(t)$ is defined as the Fourier transform of their cross correlation.

$$\phi_{uw}(f) = \int_{-\infty}^{\infty} C_{uw}(\tau) \exp(-i2\pi f\tau) \, d\tau \tag{21}$$

where $f$ = frequency in hertz .

The Fourier Transform of an aperiodic function such as $C_{uw}$ can be interpreted as a continuous spectrum of Fourier series coefficients for that function. Thus $\phi_{uw}$ is a harmonic representation of $C_{uw}$.

The cross spectral density of two random processes is generally a complex function of frequency. The phase angle at any frequency represents the average phase difference of the Fourier components of the two processes at that frequency.

It is also noted that in this report, for mathematical convenience. $\phi_{uw}$ is a function of both positive and negative $f$, although negative $f$ has no physical significance.

Power Spectral Density.- The power spectral density of a random process is the Fourier transform of its autocorrelation function, or

$$\phi_u(f) = \int_{-\infty}^{\infty} C_{uu}(\tau) \exp(-i2\pi f\tau)\, d\tau \tag{22}$$

Unlike $\phi_{uw}$, $\phi_u$ is always real since there is no phase information contained in an autocorrelation function.

$\phi_u$ can be interpreted physically as the average contribution to the variance $\sigma_u^2$ from the frequency component $f$. The variance of $u(t)$ can be obtained from $\phi_u$ by integration.

$$\sigma_u^2 = \int_{-\infty}^{\infty} \phi_u(f)\, df \tag{23}$$

White Noise.- White noise is a random process for which the power spectral density is a constant, independent of frequency. That is

$$\phi_u(f) = K \tag{24}$$

where $K$ is a constant for all $f$. True white noise cannot be realized physically since its variance

$$\sigma_u^2 = \int_{-\infty}^{\infty} \phi_u(f)\, df \qquad (25)$$

would be infinite. However, random processes for which the power spectrum is constant over a broad frequency range can be generated. This is called band limited white noise. When band limited white noise is used as the input of a system which responds only to frequencies in the constant power band of the noise, then all of the theoretical results obtained by assuming true white noise are valid.

## Description of Atmospheric Turbulence

Before specifying the statistical properties of a realistic turbulence simulation it is necessary to review the characteristics of actual turbulence. In this report the statistical properties which are judged to be of most importance are the probability distribution, power spectral density, cross spectral density, and patchy characteristic of the gust field. At this time only the gust components occurring at one point in space will be considered. Later in this section, when discussing the method of turbulence model input to the simulator, the properties of real turbulence described here will be expanded to include the spatial characteristics of the gust field.

Probability Distribution.- The probability distribution of a random function provides information concerning the range of values assumed by that function and the frequency with which they occur. There are several ways to present such information. The methods described here are the cumulative probability distribution (eq. (8) ), the probability density distribution (eq. (9) ), and the normalized central moments (eq. (14) ).

The cumulative probability distribution and the probability density of a random process are related by differentiation as shown in equation (10), and therefore contain identical information. However, this information is presented by the two distributions so as to make apparent different aspects of the random process. The probability density function, usually plotted on linear scales, is useful for comparing differences in the probability of small values of a random process. The cumulative distribution on the other hand, especially when plotted in probability coordinates (see fig. 1) shows the behavior of extreme values of the process.

A third way to present the same sort of information is through the use of normalized central moments. Though these

moments do not contain the amount of information present in the cumulative probability or probability density functions, they are much easier to estimate and do give some indication of the occurrence of large values of the random process.

As there is little experimental data available which distinguishes between probability distributions of the different gust components, no distinction will be made in this report. That is, all components of the turbulence model will be assumed to have the same probability distribution.

Cumulative Probability Distribution.- Figure 1 presents data from reference 5 showing typical cumulative probability distributions of atmospheric turbulence. The straight line in that figure represents the result expected from a Gaussian process. The departure of the turbulence data from the Gaussian curve clearly indicates the increased probability of large gusts. Data are shown for two different altitudes, and similar tendencies are seen in both cases. An analysis of unpublished data collected by the University of Washington Department of Atmospheric Sciences from a four meter tower during times of strong winds, and therefore nearly neutral stability conditions, indicates that data of the form shown in figure 1 is indeed representative of low altitude turbulence.

Probability Density Distribution.- A typical probability density (eq. (9) ) obtained from low altitude turbulence is compared with the Gaussian distribution in figure 2. The increased probability of large and small gusts in real turbulence is apparent.

Normalized Central Moments.- The table below compares the fourth and sixth normalized central moments (eq. (14) ) measured in low altitude turbulence with those expected from a Gaussian process. These data were obtained from LO-LOCAT Tests, Phase 3, Test 1141. The larger values measured in real turbulence indicate the presence of larger gust velocities than would be expected from a Gaussian process.

TABLE 1.- COMPARISON OF FOURTH AND SIXTH NORMALIZED CENTRAL MOMENTS OF TURBULENCE WITH THOSE OF A GAUSSIAN PROCESS

| | $M_4$ | $M_6$ |
|---|---|---|
| Atmospheric Turbulence* | 3.5 | 21.7 |
| Gaussian Process | 3.0 | 15.0 |

*Data from 76.2 m altitude, neutral stability, strong winds

It should be noted here that no attention has been given to the odd moments of turbulence such as $M_3$ or $M_5$. Experimental measurements of laboratory generated turbulence (ref. 6) indicate that these odd moments are not zero. However, there does not appear to be any detailed data on these moments measured in atmospheric turbulence. In any case there does not appear to be any convenient way to introduce these odd moments into a turbulence simulation and they have been neglected in this report.

Power Spectral Density.- The power spectral density of a random process (eq. (22) ) provides information on the average contribution to the process from the frequency components which make it up. It is therefore a most important statistical description. Several possible algebraic forms have been suggested for the power spectral density of the three turbulence gust components. A comparison of the most popular forms presented in reference 7 indicates that the most accurate form is that suggested by Theodore von Karman (ref. 8) to represent isotropic turbulence

$$\phi_u(f) = \frac{\sigma_u^2 L}{u_o} \frac{2}{\left[1 + \left(1.339 \frac{2\pi Lf}{u_o}\right)^2\right]^{5/6}} \tag{26}$$

$$\phi_v(f) = \frac{\sigma_v^2 L}{u_o} \frac{\left[1 + \frac{8}{3}\left(1.339 \frac{2\pi Lf}{u_o}\right)^2\right]}{\left[1 + \left(1.339 \frac{2\pi Lf}{u_o}\right)^2\right]^{11/6}} \tag{27}$$

$$\phi_w(f) = \frac{\sigma_w^2 L}{u_o} \frac{\left[1 + \frac{8}{3}\left(1.339 \frac{2\pi Lf}{u_o}\right)^2\right]}{\left[1 + \left(1.339 \frac{2\pi Lf}{u_o}\right)^2\right]^{11/6}} \tag{28}$$

These shapes are not convenient for turbulence model work because they cannot be exactly matched using linear filters. (See discussion of linearly filtered Gaussian white noise turbulence simulation which follows in this section.) This is because of the non-integer powers appearing in the denominators. The error resulting from the use of linear filters to produce these spectra can be reduced as far as desired by adding poles and zeros to the filter transfer function, but this adds to the complexity of the system and is generally felt to be not worth the trouble. This problem is usually overcome by assuming the spectra suggested by H. L. Dryden (ref. 9).

$$\phi_u(f) = \frac{\sigma_u^2 L}{u_o} \frac{2}{\left[1 + \left(\frac{2\pi L f}{u_o}\right)^2\right]} \tag{29}$$

$$\phi_v(f) = \frac{\sigma_v^2 L}{u_o} \frac{\left[1 + 3\left(\frac{2\pi L f}{u_o}\right)^2\right]}{\left[1 + \left(\frac{2\pi L f}{u_o}\right)^2\right]^2} \tag{30}$$

$$\phi_w(f) = \frac{\sigma_w^2 L}{u_o} \frac{\left[1 + 3\left(\frac{2\pi L f}{u_o}\right)^2\right]}{\left[1 + \left(\frac{2\pi L f}{u_o}\right)^2\right]^2} \tag{31}$$

These spectral shapes can be exactly matched using linear filters. Since the difference between the Dryden shapes and those proposed by von Karman are quite small in the frequency range of interest in most flight simulation studies, there is no reason to believe that these spectra are not sufficiently realistic.

In this report a slightly modified form of the Dryden spectra will be used. The changes introduced are: (1) replacement of the single scale length $L$ with independent values for each gust component. This change is consistent with much experimental data (ref. 10 for example) which shows that the scale length does vary among the components of atmospheric turbulence; (2) replacement of the lateral power spectrum $\phi_v$ with a form similar to that used for the longitudinal spectrum $\phi_u$. This change is suggested by low altitude data (ref. 10) showing the lateral spectrum to be more like $\phi_u$ than like $\phi_w$. It is not a strict requirement of the turbulence simulation schemes to be described presently, but does simplify them slightly.

The gust component power spectral densities to be used in this report are:

$$\Phi_u(f) = \frac{\sigma_u^2 L_u}{u_o} \frac{2}{\left[1 + \left(\frac{2\pi L_u f}{u_o}\right)^2\right]} \tag{32}$$

$$\Phi_v(f) = \frac{\sigma_v^2 L_v}{u_o} \frac{2}{\left[1 + \left(\frac{2\pi L_v f}{u_o}\right)^2\right]} \tag{33}$$

$$\Phi_w(f) = \frac{\sigma_w^2 L_w}{u_o} \frac{\left[1 + 3\left(\frac{2\pi L_w f}{u_o}\right)^2\right]}{\left[1 + \left(\frac{2\pi L_w f}{u_o}\right)^2\right]^2} \tag{34}$$

These spectra are presented non-dimensionally in figure 3.

It should be noted that these spectra are assumed valid for any heading of the simulated vehicle relative to the mean wind. In general the scale length and standard deviation of each gust component are expected to be functions of the heading angle, altitude, atmospheric stability and mean wind speed relative to the surface, though explicit relationships are not needed for the work reported here. Many reports describing the dependence of $L$ and $\sigma$ upon the above mentioned conditions, with the exception of heading angle, can be found in the current literature if explicit functional relationships are required. (See ref. 11 for example.) The dependence upon heading angle is generally unknown.

Cross Spectral Densities.- The cross spectral density (eq. (21)) of two random processes provides information on the phase relationships of their frequency components. At the present time little is known about the cross spectral densities of the $u$, $v$, and $w$ gust components, particularly the variation of these cross spectra with altitude, heading angle relative to the mean wind direction, and other variables of interest in flight simulator work. Because convenient algebraic forms for these spectra are not currently available, and because their inclusion in a turbulence simulation significantly complicates the simulation technique, cross spectra are usually neglected in flight simulations. However, one would expect non-zero cross spectra in any turbulent boundary layer flow, and therefore in most low altitude turbulence. Indeed Elderkin (ref. 10) finds a consistent low frequency cospectrum (real part of the complex cross spectrum) relating the longitudinal and vertical gust components measured from a tower.

In general it would seem prudent to make some provision for low frequency cross spectra in a turbulence simulation even if no specific form is known. In this report a low frequency cross spectrum relating the longitudinal and lateral gust components will be assumed. The form of this spectrum is determined

primarily by the technique in which the artificial turbulence time histories are to be generated, and therefore involves parameters which are dependent upon the simulation method itself. Details of the cross correlation method used in this report and the physical significance of the parameters will be found in Appendix 1. The cross spectral density assumed in this report is

$$\phi_{uw}(f) = \frac{-\sigma_u \sigma_w \sqrt{2}}{R^2+1}\left\{\frac{2R^2}{A^2}\left(\frac{L_w}{u_o}\right)^2\left(\frac{L_u}{u_o}\right)\left[\frac{[1+3(\pi Af)^2]-i(2\pi Af)}{[1+(\pi Af)^2]^2}\right]\right.$$

$$\left.+\sqrt{\frac{L_u L_w}{u_o^2}}\left[\frac{1+i\sqrt{3}\left(2\pi\frac{L_w}{u_o}f\right)}{\left[1+i\left(2\pi\frac{L_w}{u_o}f\right)\right][1+(2\pi Bf)^2]}\right]\right\} \qquad (35)$$

where A , B , and R are arbitrary parameters satisfying the conditions

$$A > \frac{2L_w}{u_o} \quad , \quad A > \frac{2L_u}{u_o} \qquad (36)$$

$$B > \frac{L_w}{u_o} \quad , \quad B > \frac{L_u}{u_o} \qquad (37)$$

$$R \geq 0 \qquad (38)$$

Patchy Nature.- It is known that turbulence has a patchy structure. That is, atmospheric turbulence seems to occur in patches of relatively intense motion separated by areas of relative calm. It is not easy to formulate a model of this phenomenon in terms applicable to flight simulator work. Nor is it easy to see a patchy structure in turbulence velocity time histories, although the derivative of a gust velocity time history as shown in figure 4 does reveal distinct bursts or patches of activity. (Reference LO-LOCAT Phase 3, Test 1145.) Since there are no available models of this patchy characteristic, figure 4 will be used as a standard of comparison in this report.

## Presently Used Simulation Techniques

The preceding pages of this section have discussed the statistical properties of atmospheric turbulence which are to be modeled by a realistic turbulence simulation. In this section several presently used simulation techniques will be described from the standpoint of their statistical realism and suitability for use in flight simulators.

Flight Recordings of Atmospheric Turbulence.- Perhaps the most obvious method of producing a realistic simulation of atmospheric turbulence is to use recorded time histories obtained under the same flight conditions as those being simulated. There can be no question as to whether or not these time histories are an accurate representation of atmospheric turbulence. However, this method has several serious drawbacks. First, the time history must be obtained under the same conditions as are to be simulated. This means that variables such as altitude and true airspeed must be matched, as well as meterological variables. This implies that a flight simulator facility which is to provide realistic simulations of a wide variety of flight conditions must have a complete library of time histories available. A second problem associated with the use of recorded time histories is that the length of each time history is fixed. Longer run times cannot be accommodated without an interruption of the simulated turbulence. One further problem with recorded time histories is that repeated use of the same time histories may permit the pilot to become familiar with some of their characteristics, such as the occurrence of large gusts. This would, of course, negate the principle purpose of the artificial turbulence, which is to provide an unpredictable external disturbance to the flight simulation.

The recorded time history turbulence model does have advantages in certain circumstances. For example, it can be used to simulate statistically rare occurrences such as encounters with isolated large gusts. Since this event is very infrequent, a turbulence simulation employing the statistics of typical turbulence, described earlier in this section, would produce such an encounter only very infrequently. This is, of course, an unacceptable situation for a practical flight simulator program.

In summary, the recorded time history turbulence simulation does have application to the simulation of situations which are not adequately described by the statistics of typical turbulence discussed earlier in this section. However, it lacks the versatility to simulate a wide variety of flight conditions, is limited in the length of its time histories, and may permit the pilot to become familiar with time histories which are used repeatedly. It is, therefore, not suitable for the simulation of typical turbulence.

Sum of Sine Waves.- Another technique which has been used to simulate atmospheric turbulence is the sum of sine waves model. This technique involves summing ten or twenty sinusoidal waves of different frequencies and magnitudes. The resultant time history is then used to represent a time history of turbulence. This method does provide a random appearing, non-repeating time history, but cannot be said to represent atmospheric turbulence, which contains an infinite number of frequency components. If the number of sinusoids is increased in an attempt to provide a smoother power spectrum, the resultant time history will become Gaussian by virtue of the central limit theorem. As discussed previously in this section, atmospheric turbulence is not Gaussian. Hence the sum of sine waves turbulence simulation is not statistically representative of atmospheric turbulence.

Linearly Filtered Gaussian White Noise.- The most commonly used turbulence simulation is the linearly filtered Gaussian white noise technique. Each component of this simulation is produced by passing Gaussian white noise through a linear filter as shown in figure 5. As noted in that figure, the power spectral density of the simulated time history is determined by the transfer function of the filter. Any power spectral shape can be approximated as closely as desired by using a sufficient number of poles and zeros in the transfer function.

This turbulence simulation is remarkably easy to implement and can be generalized (see for example reference 12) to produce several simultaneous random time histories with specified power spectral densities and cross spectral densities. Furthermore these spectra and cross spectra are continuously variable by changing the parameters of the filter transfer functions.

Despite these desirable characteristics, this type of turbulence simulation also has its deficiencies. Since a Gaussian process remains Gaussian when passed through a linear filter, the artificial turbulence time histories produced by this method will always be Gaussian. As already noted, atmospheric turbulence is not Gaussian.

It is also easily shown that the Gaussian white noise turbulence model does not reproduce the desired patchy nature of turbulence. Figure 6 compares the derivative of an artificial-turbulence time history produced by the Gaussian model with the typical example of atmospheric turbulence from figure 4. Care was taken to match the power spectral densities of the two curves, so both time histories have the same frequency content. Note that the Gaussian time history completely lacks the patchy nature of real turbulence.

In addition to the criticisms based on the poor statistical characteristics of the Gaussian turbulence simulation, there are also indications that this method produces time histories which do not "feel" like turbulence when used in a flight simulator. Pilots complain that compared to real turbulence, the artificial turbulence is too regular and does not require corrective control motions, because a disturbance in one direction is soon followed by a compensating disturbance in the opposite direction (ref. 13). It must be concluded therefore that the artificial turbulence generated by the linearly filtered Gaussian white noise turbulence simulation is not sufficiently realistic for flight simulator applications.

In summary, the Gaussian turbulence simulation has many convenient features. It is easily generated and can be generalized to produce a number of simultaneous time histories with specified power spectra and cross spectra. However, the method does not model the non-Gaussian nature of atmospheric turbulence, nor does it model the patchy character of real turbulence. It is therefore unsuitable for realistic flight simulator applications.

Method of Orthogonal Functions.- A recent report by Dutton and Deaven (ref. 14) describes a method by which turbulence time histories are decomposed into eigenfunctions of the covariance matrix. Simulated turbulence time histories are then generated by recombining these eigenfunctions. Only preliminary results are presented, however it appears that even though the $-5/3$ slope of the power spectral density is correctly modeled, the procedure as now proposed does not correctly model the non-Gaussian nature of turbulence. The method also shares some problems of the recorded time history simulation in that the time history length is fixed, and maneuvers of the simulated vehicle cannot be correctly simulated unless they are known in detail before the simulator experiment, and the appropriate data have been collected. The primary advantage of this method is that the probability of occurrence of any particular time history can be computed a priori and therefore the degree to which the results are representative is known. In summary, the method of orthogonal functions almost certainly has flight simulator applications in the area of rare event simulation, such as the isolated large gust encounter described previously in this section, but does not provide the versatility being sought in this report.

## A Proposed Non-Gaussian Turbulence Simulation

The preceding parts of this section have discussed the properties of atmospheric turbulence and several simulation techniques. Of the simulations described, the linearly filtered Gaussian white noise method is the most easily produced and is the method

most readily adaptible to simulating complex situations involving time-varying power spectra and cross spectra. Unfortunately the artificial turbulence which it produces is always Gaussian and is therefore unrealistic. It seems reasonable to suppose that a turbulence simulation similar to the Gaussian method, but with a non-Gaussian probability distribution, will be more realistic. A simulation of this type will now be proposed.

Consider the patchy nature of turbulence. The existence of patches suggests that atmospheric turbulence might be simulated by a product of Gaussian processes, the first representing a constant-intensity turbulence time history and the other representing the time varying standard deviation. This idea has already been pursued in reference 4, and a non-Gaussian turbulence simulation has been proposed. Furthermore, reference 4 shows that this new simulation has the same versatility as the Gaussian model. That is, it is possible to generate the required power spectra and cross spectra, with time-varying characteristics to represent vehicle maneuvers just as in the case of the Gaussian turbulence simulation. However, the Gaussian product simulation is not as realistic as might be hoped, as will be discussed later.

The probability density resulting from a product of Gaussian processes is the modified Bessel function distribution defined previously in this section (eq. (13) ). This distribution is compared with the normal distribution and a typical result for atmospheric turbulence in figure 7. Note that the probability density of real turbulence lies between the Gaussian and Modified Bessel distributions. This suggests that a more realistic probability density would be obtained by adding the two.

Typical patchy characteristics of the Modified Bessel process are compared to those of the Gaussian model and an actual turbulence time history in figure 8. All three functions shown in figure 8 have the same power spectral density and therefore the same frequency content. However, the Modified Bessel process is clearly far more patchy than atmospheric turbulence.

Table 2 below presents the fourth and sixth normalized central moments of Gaussian, real, and Modified Bessel processes, and shows that the Modified Bessel greatly overestimates the higher moments, while the Gaussian underestimates them. This is further evidence that a summation of Gaussian and Modified Bessel processes might produce a more realistic result than either of these above.

TABLE 2.- COMPARISON OF FOURTH AND SIXTH NORMALIZED CENTRAL MOMENTS OF TURBULENCE WITH THOSE OF GAUSSIAN AND MODIFIED BESSEL PROCESSES

| | $M_4$ | $M_6$ |
|---|---|---|
| Gaussian | 3.0 | 15.0 |
| Real Turbulence* | 3.5 | 21.7 |
| Modified Bessel | 9.0 | 225.0 |

*Data from 76.2 m , neutral stability, strong winds. Ref. LOLOCAT, Phase 3, Test 1141

The large moments of the Modified Bessel process indicate that it has much larger peak values than are found in typically measured low altitude turbulence. The Modified Bessel model may therefore be suitable for simulating some extremely violent flight environment, but it not very suitable for representing typical turbulence.

The non-Gaussian turbulence simulation proposed in this report, which consists of the addition of Gaussian and Modified Bessel processes, is shown schematically in figure 9. The detailed analysis of this system and its application to a specific turbulence simulation is both complicated and lengthy. It has therefore been placed in Appendix A. The following is a summary of some of the proposed simulations important features. In figure 9 $a(t)$ , $b(t)$ and $d(t)$ are Gaussian processes produced just as in the case of the linearly filtered Gaussian white noise turbulence simulation. Therefore $a(t)$ , $b(t)$ and $d(t)$ are independent Gaussian processes. The process $c(t)$ is generated by the multiplication of the Gaussian processes $a(t)$ and $b(t)$ , it is therefore a Modified Bessel process. The system output, $u(t)$ , is the sum of the Modified Bessel process $c(t)$ and the Gaussian process $d(t)$ .

The probability distribution and patchy character of $u(t)$ are determined by the standard deviation ratio

$$R = \frac{\sigma_c}{\sigma_d} \tag{39}$$

If $R$ is very small then $\sigma_c$ is much smaller than $\sigma_d$ , and the

process $c(t)$ can be neglected in comparison to $d(t)$. The system of figure 9 is then equivalent to the Gaussian simulation shown in figure 5, and the system output is therefore Gaussian. The characteristics of the output are then the same as those of the Gaussian process in figure 8 and Table 2. On the other hand, if $R$ is very large then $\sigma_c$ is much larger than $\sigma_d$. The Gaussian process $d(t)$ can be neglected and the system output is the Modified Bessel process. The characteristics of the output are then the same as those of the Modified Bessel process in figure 8 and Table 2.

It can be seen that the standard deviation ratio $R$ is a powerful control over the probability distribution, and that a close approximation of almost any reasonable experimentally determined distribution is available. It has been found that, in general, a good match with measured probability data is obtained when $R$ is of the order of unity, which results in a random process with properties lying between those of the Gaussian and Modified Bessel processes. As mentioned above, the theoretical analysis of the proposed non-Gaussian turbulence simulation and its application to the generation of specific turbulence models is quite lengthy and has been placed in Appendix A.

Some theoretical results showing the dependence of the system output characteristics upon the ratio $R$ are presented in the following mentioned figures in order to show the range of variation possible with the proposed model. Figure 10 presents the range of cumulative probability distribution which can be obtained. Note upon comparison with figure 1 that the probability of large gusts can be varied over a range which includes the distribution of real turbulence. Figure 11 presents the probability density distributions corresponding to the cumulative distributions of figure 10. The experimental data from figure 2 have been plotted in figure 11, and it is evident that the proposed model with $R$ approximately unity compares very favorably with these data. Figure 12 shows the dependence of $M_4$ and $M_6$ upon $R$. Figure 13 presents the time derivative of the system output for several values of $R$. All four time histories have exactly the same frequency content. Note that the patchy characteristics of turbulence as typified by figure 4 can be matched quite closely.

Figures 10 through 13 show that the various properties of turbulence can be matched quite well if $R$ is chosen properly in each case. Of course these properties are not independent of each other. They all depend upon $R$ and only one value of $R$ can be chosen for any given turbulence simulation. It is therefore necessary to choose a value which is in some sense best. A comparison of the above mentioned figures with the data presented for real turbulence in figures 1, 2, and 4 and Table 1 indicates that an $R$ value of slightly less than unity appears

to give very good results. Of course the final test of realism can only come from a practical flight simulator experiment. As yet no attention has been given to the explicit method by which the artificial turbulence time histories should be introduced into the simulator so as to provide a realistic representation of flight through turbulent air. This is the next subject of this report.

## Simulation of Spatial Distribution Effects

The simplest way to handle gust inputs is to assume the gusts are uniform everywhere over the aircraft and are equal to the gusts measured at the aircraft center of gravity (c.g.). These gusts are then fed into the airplane equations of motion through stability derivatives such as $C_{\ell_\beta}$ and $C_{m_\alpha}$, e.g.,

$$C_m = C_{m_\alpha}\alpha + C_{m_{\dot{\alpha}}}\frac{w_g}{u_o} + \cdots$$

This method is called the one-point model, and is in fact quite accurate for moderate and high altitudes, and away from strong shear surfaces, where the ratio $L/b$ of scale-length-to-span is very large (say > 20). ($L$ can be loosely thought of as being approximately the size of the average turbulent eddy. For wind driven turbulence in the lower part of the atmosphere, $L \approx h$, where $h$ is the altitude (ref. 15). For higher altitudes, above 533 m (1750 ft.), $L \approx 533$ m). For large values of $L/b$ the eddies are very large compared to the wing span, and the gusts are very nearly uniform over the whole airplane. As $L/b$ drops below 20, gradients in the gusts become significant across the wing span and from the c.g. to the tail, and these gradients cause forces and moments additional to those considered by the one-point model. For example, an up-gust at one wing-tip and a down-gust at the other causes a rolling moment on the aircraft. Also, an up-gust at the c.g. will probably be different from the up-gust at the horizontal tail. This would result in a nose-up or nose-down pitching moment not considered in the one-point model. The correct simulation of these effects is very important for a STOL airplane at low altitude. In this report, the De Havilland Twin Otter (with a wing span of 19.8 m (65 ft.) ) was simulated at an altitude of 76.3 m (250 ft.). For this case $L/b \approx 4$,

Several theories have been proposed to account for the effects of the spatial distribution of gusts over an aircraft. Etkin (ref. 16 & 17) expands the gusts in a Taylor series about the c.g. Using a second-order series, as high as one can go

before the method becomes unwieldy, results in the gust model being accurate for $L/b$ down to 6 (too high for the case considered in this report). Skelton (ref. 12) proposes a 3-point gust model, with the gusts considered as acting at the tail and mid-way along each wing. His method requires eight separate gust inputs, all properly cross-correlated, and still only depicts the gusts as being linearly distributed across the span. This method would be accurate for $L/b$ down to only about 12. Eggleston and Diederich (ref. 18) use a modified strip theory to calculate the power spectrum of the rolling and yawing moments on an aircraft wing in turbulence. Their method is good for any ratio of $L/b$, although they account only approximately for the unsteady aerodynamic effects. Franklin (ref. 19) makes use of their results in his flight-simulator investigation into lateral-directional flying qualities.

The method of handling the gusts in the present simulation generally follows Franklin's ideas, with the exception of three differences:

1.) The method of handling tail lags in that Franklin uses a linear-filter approximation to the Laplace transform of a time delay, $e^{-sT}$, whereas the present simulation utilizes a separate gust input at the tail;

2.) This report includes the effects of distributed $u_g$ gusts across the wing span (a necessary inclusion since a slow-flying STOL aircraft is flying at a large angle of attack); and

3.) The inclusion by Franklin of more unsteady-aerodynamic terms, by multiplying the $u_g$, $v_g$, and $w_g$ input power spectra by a Sears function (ref. 20).

In the present simulation, the gust components were handled in the following way:

a.) Side gust component, $v_g$

(1) Gust at airplane c.g.: $v_{g_c}(t)$.

This appears in the sideslip angle $\beta$ and is multiplied by the stability derivative of the tailless airplane. e.g., in the equation for yawing moment,

$$C_n = (C_{n_\beta} - C_{n_{t\beta}}) \frac{v_{gc}}{V_{RW}} + \ldots, \text{ where}$$

$C_{n_\beta}$ = the yawing-moment-due-to-sideslip stability derivative for the complete airplane,

$C_{n_{t\beta}}$ = the yawing-moment-due-to-sideslip stability derivative due to the tail only,

$v_{gc}/V_{RW}$ = the effective sideslip angle measured at the c.g.

(2) Gust at tail (gust at c.g. delayed):

$$v_{g_t}(t) = v_{g_c}(t - \frac{\ell_t}{u_o}) \quad . \tag{40}$$

This accounts for the finite time it takes for a gust to travel the distance $\ell_t$ between the wing and the tail. (The frozen-field hypothesis is assumed for the gust field, i.e., the gust field is assumed fixed, unchanging in space, while the airplane flies through.) The time-lag $\ell_t/u_o$ = .212 seconds was used here. $v_{g_t}(t)$ appears as a sideslip angle at the tail, and influences the equations through the tail contribution to the sideslip stability derivatives such as $C_{n_{t\beta}}$. The complete yawing moment coefficient due to gusts then becomes

$$C_n = (C_{n_\beta} - C_{n_{t\beta}}) \frac{v_{gc}}{V_{RW}} + C_{n_{t\beta}} \frac{v_{gt}}{V_{RW}} + \ldots$$

The tail-only stability derivatives were estimated using methods in references 21 and 22. The complete equation for the yawing moment is shown in Appendix B.

b.) Horizontal and vertical gust components, $u_g$ and $w_g$

(1) Gusts at airplane c.g.: $u_{g_c}(t)$ and $w_{g_c}(t)$.

These influence the equations of motion through the tail-off stability derivatives with the $w_{g_c}$ gust appearing as an effective $\alpha$ (and corresponding $\dot{\alpha}$ term).

(2) Gusts at tail (gusts at c.g. delayed):

$$u_{g_t}(t) = u_{g_c}\left(t - \frac{\ell_t}{u_o}\right) , \tag{41}$$

and

$$w_{g_t}(t) = w_{g_c}\left(t - \frac{\ell_t}{u_o}\right) . \tag{42}$$

These appear through the tail contribution to the stability derivatives, i.e., $C_{m_{t\alpha}}$ and $C_{m_{tu}}$.

(3) Rolling moments due to spatial effects on wing: $C_{\ell_{ug}}(t)$ and $C_{\ell_{wg}}(t)$

These appear as additive terms in the rolling moment equation, and are generated by taking two independent random-noise signals and passing them through appropriate filters to shape the power spectra to match those of Eggleston and Diederich (ref. 18), including the unsteady-aerodynamic effects. (See page 39.)

(4) Yawing moments due to spatial effects on wing: $C_{n_{ug}}(t)$ and $C_{n_{wg}}(t)$.

These are again additive terms in the yawing-moment equation. Reference 18 shows that these terms are simply a constant multiplied by the rolling-moment spatial effects:

$$C_{n_{ug}}(t) = \frac{C_{n_r}}{C_{\ell_r}} C_{\ell_{ug}}(t) \tag{43}$$

$$C_{n_{wg}}(t) = \frac{C_{n_p}}{C_{\ell_p}} C_{\ell_{wg}}(t) \tag{44}$$

In summary, the turbulence model consisted of the following: three gust inputs at the c.g. and acting on the tailless airplane; the same gusts delayed by $\ell_t/u_o$ and acting on the tail; and random rolling and yawing moments to account for the distribution of gusts over the wing span. Required for the simulation are three time delays (done digitally here) plus time histories

of the five inputs $u_{g_c}(t)$ , $v_{g_c}(t)$ , $w_{g_c}(t)$ , $C_{\ell_{ug}}(t)$ , and $C_{\ell_{wg}}(t)$ . In this simulation, these inputs were computed beforehand, recorded on FM tape, and input to the simulator as analog signals.

## Power Spectra of $C_{\ell_{ug}}$ and $C_{\ell_{wg}}$

The power spectra of the spatial effects $C_{\ell_{ug}}(t)$ and $C_{\ell_{wg}}(t)$ use the results of reference 18. In that report, Eggleston and Diederich considered a number of different wings in turbulent flow. These wings were such that they had differently shaped steady-state lift distributions for the steady-flow case. For the turbulent case, the authors used quasi-steady aerodynamics (in which the lift distribution is assumed to adjust instantaneously to changes in the local angle of attack) to derive power spectra for the rolling and yawing moments on the wing. Surprisingly, the resulting non-dimensional spectra turned out to be practically independent of the lift distribution assumed. Eggleston and Diederich suggested taking into account the unsteady-lift effects (i.e., the fact that the lift does not respond instantly to a change in local $\alpha$ ) by simply multiplying the power spectral density of the rolling moment due to each gust component by $\left|S_k\left(\frac{\omega c}{2u_o}\right)\right|^2$ , where $S_k$ is the Sears function (ref. 20). That was what was done here. The present simulation takes the power spectra from figures 7b and 9b of reference 18 for the elliptic span-loading case and $b/L = 0.25$ . Since the span $b$ of the Twin Otter is 19.8 m (65 ft.), this corresponds to a turbulence scale-length of 79.4 m (260 ft.), which corresponds roughly to the altitude of 76.3 m (250 ft.) used in the simulation. The resulting power spectra of rolling moments, $\Phi_{C_{\ell_{ug}}}$ and $\Phi_{C_{\ell_{wg}}}$ (in the present notation) are shown in figures 14 and 15 respectively. Unsteady-lift effects are included by using the Sears function as outlined above. Note that in converting from Eggleston and Diederich's curves to the present simulation, the value $\alpha_o = -.337$ was used for the zero-lift angle of attack of the wing. Note also that in reference 18 the power spectrum is defined as $1/\pi$ times the way it is defined in this report.

For convenience in generating the time histories of $C_{\ell_{ug}}(t)$ and $C_{\ell_{wg}}(t)$, Eggleston and Diederich's power spectra (with unsteady-lift effects included) were approximated by a linear-filter representation, i.e.

$$\frac{\Phi_{C_{\ell_{ug}}}}{\overline{u_g^2}} \doteq |H_u(i2\pi f)|^2 \tag{45}$$

and

$$\frac{\Phi_{C_{\ell_{wg}}}}{\overline{w_g^2}} \doteq |H_w(i2\pi f)|^2 \tag{46}$$

where

$$H_u(s) = \frac{.004842(1 + .7425s)(1 + .2270s)}{(1 + 1.2569s)(1 + .134115)(1 + .2653s)^2} \tag{47}$$

$$H_w(s) = \frac{.006331(1 + .7314s)(1 + .11542s)}{(1 + 1.2410s)(1 + .06803s)(1 + .19733s)^2} \tag{48}$$

These linear-filter approximations to the power spectra of the rolling moments are also shown in figures 14 and 15, and it can be seen that they compare very closely with the more exact curves of Eggleston and Diederich.

## FLIGHT SIMULATOR EXPERIMENT

This section describes the flight simulator experiment, including details of the aircraft simulated, the flight simulator itself, the pilot task, the pilot's experience, and the presentation of the results. The purpose of the experiment was to determine whether or not pilots are sensitive to the differences in patchiness between Gaussian and non-Gaussian turbulence for the case of a STOL aircraft in a landing approach configuration.

### Vehicle Simulated

It was decided to simulate a STOL aircraft on approach because the low frequency effects of turbulence become more pronounced as airspeed decreases. A STOL approach through

turbulence is a very demanding task for a pilot, and any differences between turbulence models should be the most noticeable for this configuration.

The aircraft simulated was the de Havilland DHC-6 Twin Otter, Series 300 (fig. 16), chosen because its linear characteristics are fairly well documented, and because some flight time in an actual Twin Otter was available in order to aid the pilots in their assessment of the simulator fidelity.

The configuration chosen was the following: STOL landing approach at a weight of 4989.5 kg., 36 m/sec., $40^0$ of flaps, and center of gravity at 20% m.a.c. Data were available for a power-off approach configuration, but since a constant-height task was desired (see page 45) and there were no data for this case, it was decided to use all the stability derivatives for the power-off case and simply add sufficient throttle to allow the airplane to fly level. No attempt was made to adjust the stability derivatives for the effects of power, other than by adding drag, lift, and pitching moment due to throttle changes from the reference flight condition. The aircraft is described in Table 3., and the equations used are discussed in Appendix B.

## Simulator

The NASA-Ames 6 degree-of-freedom, moving-base simulator was used (fig. 17). Because of mechanical stops, the cab travel is quite restricted (± 2.7 m (± 9 ft.) ) in the translational degrees of freedom, but quite adequate in angular rotations (± 45° in roll, pitch and yaw). Because of the restricted translational motions, it was necessary to wash out low-frequency accelerations with a high-pass filter in order to prevent them from integrating into motions which would cause the simulator to hit the travel limits. In addition, the simulator response was sluggish for high-frequency input signals, so compensation (in the form of a lead circuit) was added in order to improve the response in this frequency range. It was also found that large-amplitude input accelerations in the translational modes caused the simulator drive system to shut off, so commanded accelerations from the equations of motion were put through a limiting circuit. Details of the washout, compensation, and acceleration limits used are given in Appendix C.

The instrumentation and controls were somewhat different between the simulator and the actual Twin Otter; however the pilots did not seem to feel these differences would have too much effect on their evaluation of the realism of the turbulence models. The simulator had a stick instead of control yoke, and a single throttle (for both engines) on a console on

TABLE 3. - AIRPLANE DATA

Aircraft: de Havilland DHC-6 Twin Otter (Series 300)
de Havilland data used where available. Missing derivatives were supplied by the authors. Some derivatives were altered for the purposes of this study.

Airplane Parameters

| | | | |
|---|---|---|---|
| $u_o$ | = 36.03 m/sec (118.2 ft/sec) | $Z_{PIL}$ | = 0 |
| m | = 4989.5 kg (341.9 slugs) | $I_{XX}$ | = 21,621 $kgm^2$ (15,947 slug $ft^2$) |
| S | = 39.019 $m^2$ (420 $ft^2$) | $I_{YY}$ | = 31,824 $kgm^2$ (23,472 slug $ft^2$) |
| b | = 19.812 m (65 ft) | $I_{ZZ}$ | = 48,857 $kgm^2$ (36,035 slug $ft^2$) |
| $\ell_t$ | = 7.62 m (25 ft) | $I_{XZ}$ | = 1,482 $kgm^2$ (1,093 slug $ft^2$) |
| c | = 1.9812 m (6.5 ft) | $P_{max}$ | = $4.847 \times 10^5$ w (650 HP) per engine |
| $X_{PIL}$ | = 2.4384 m (8 ft) | $\delta T_o$ | = .725 |
| $Y_{PIL}$ | = 0 | $\rho$ | = 1.2256 $kg/m^3$ (.002378 $slugs/ft^3$) |

Stability Derivatives

| | | | |
|---|---|---|---|
| $C_{T_o}$ | = 0.320 | $C_{\ell_\beta}$ | = - 0.090/rad |
| $C_{x_\alpha}$ | = 0.9832/rad | $C_{\ell_r}$ | = 0.336 |
| $C_{D_o}$ | = 0.320 | $C_{\ell_p}$ | = - 0.777 |
| $C_{D_{CT}}$ | = - 0.75 | $C_{\ell_{\delta a}}$ | = .150/rad |
| $C_{y_\beta}$ | = - 0.775/rad | $C_{\ell_{\delta r}}$ | = - 0.045/rad |
| $C_{y_r}$ | = 0.513 | $C_{m_{CT}}$ | = - 0.1698 |
| $C_{y_p}$ | = - 0.131 | $C_{m_\alpha}$ | = - 2.026/rad |
| $C_{y_{\delta a}}$ | = 0.0108/rad | $C_{m_{\dot{\alpha}}}$ | = - 8.663/rad |
| $C_{y_{\delta r}}$ | = - 0.391/rad | $C_{m_q}$ | = - 28.76 |
| $C_{y_{t\beta}}$ | = - 0.39/rad | $C_{m_{\delta e}}$ | = 2.068/rad |
| $C_{L_o}$ | = 1.576 | $C_{m_{tu}}$ | = 1.24 |

TABLE 3.- AIRPLANE DATA - Continued

$C_{z_\alpha} = -6.109/rad$

$C_{z_{\dot{\alpha}}} = -2.150/rad$

$C_{z_q} = -7.144$

$C_{z_{\delta e}} = 0.5236/rad$

$C_{L_{CT}} = 0.55$

$C_{z_{t\alpha}} = -0.632/rad$

$C_{z_{t\dot{\alpha}}} = -2.09/rad$

$C_{m_{t\alpha}} = -2.43/rad$

$C_{m_{t\dot{\alpha}}} = -8.04/rad$

$C_{n_\beta} = 0.147/rad$

$C_{n_r} = -0.219$

$C_{n_{\delta a}} = -0.0219/rad$

$C_{n_{\delta r}} = 0.1565/rad$

$C_{n_{t\beta}} = 0.14/rad$

$C_{n_p} = -0.0935$

Resulting Characteristics of Airplane Dynamics

a.) Short-Period Mode

natural frequency = 2.322 rad/sec

damping ratio = .6538

frequency of oscillation = 1.757 rad/sec

period = 3.576 sec

time to half-amplitude = .4566 sec

b.) Phugoid Mode

natural frequency = .3265 rad/sec

damping ratio = .2186

frequency of oscillation = .3186 rad/sec

period = 19.72 sec

time to half-amplitude = 9.711 sec

c.) Roll Convergence

time to half-amplitude = .1167 sec

TABLE 3.- AIRPLANE DATA - Concluded

d.) Spiral Divergence

time to double-amplitude = 11.92 sec

e.) Dutch Roll

natural frequency = 1.519 rad/sec

damping ratio = .3431

frequency of oscillation = 1.427 rad/sec

period = 4.403 sec

time to half-amplitude = 1.330 sec

the left side as opposed to two throttles overhead on the pilot's right in the airplane. The Twin Otter had the normal ILS cross-pointer, needle and ball, directional gyro, and artificial horizon. The simulator however had all this information on one instrument, the attitude director indicator.

## Description of the Experiment

Turbulence Cases.- The tests were conducted for four cases composed of one set of measured turbulence data and three different statistical turbulence models, as follows.

(1) Real - using time histories of real atmospheric turbulence recorded during the LO-LOCAT (low level critical air turbulence) program.

(2) Gaussian model - a model having a Gaussian probability distribution.

(3) Matched non-Gaussian model - a non-Gaussian model characterized by a standard deviation ratio of unity (see equation (39) and related discussion). The probability characteristics of this model were chosen so as to be as much like those of real turbulence as possible. These characteristics are shown in figures 10 and 11 by the curves marked $R = 1$ .

(4) More patchy non-Gaussian model - a non-Gaussian model characterized by a standard deviation ratio of two. The probability characteristics of this model were chosen so as to produce more large gusts and more patchiness than are found in real turbulence. The curves marked $R = 2$ in figures 10 and 11 show the probability characteristics of this model.

The real data and the three models were scaled to the same rms intensities, had the same power spectra and cross-spectra, and had the effects of spatial distribution included as outlined on page 35. The only difference between the models was their different probability densities, resulting in differing amounts of "patchiness".

Pilot Task.- It was decided to have the pilots fly a constant - altitude tracking task in order not to introduce too many variables (such as changing the turbulence characteristics with height) that might distract the pilots from their primary goal of trying to distinguish differences between turbulence models. This hypothetical task consisted of tracking a constant-width ILS localizer and a constant-altitude glideslope parallel to the ground at an altitude of 76.3 m (250 ft.). The sensitivity

of the ILS needles was set so that full-scale deflections corresponded to 15.2 m (50 ft.) off the glideslope and 76.3 m (250 ft.) from the localizer. These full scale deviations would occur at a range of 1750 m (5730 ft.) from the runway for a 2 1/2° glideslope.) The pilot was told that his ILS tracking errors both in the vertical and horizontal were being measured, and that his primary task was to minimize these errors using rudder, aileron, elevator, throttle, and the flying techniques he would normally use on an approach.

Test Procedures.- Four to six runs, each of five minutes duration, were made in one pilot session, and in the course of the experiment each pilot flew each of the turbulence models from three to five times. The models were given to the pilot in random order so that no consecutive runs had the same model. Steady crosswinds of either 2.5 m/sec (5 knots), - 3.8 m/sec (- 7 1/2 knots), or 0 were fed in, and the pilot was told what the crosswind was. (He would receive this information from the tower in an actual approach.) After each run he was asked for his comments on the turbulence by means of a questionnaire (see Appendix D). This question sheet asked the pilot to estimate the turbulence intensity and realism, his workload, his task performance, and a Cooper rating (ref. 23) for the airplane/turbulence/task combination. Additional questions tried to find out why the pilot did or did not find the turbulence realistic. These included comments on the relative amplitudes of disturbances in roll, pitch, etc., whether the turbulence was too continuous or too patchy, and whether the motions contained annoying amounts of high or low frequencies.

During the flight a total of twenty-five flight parameters, such as angular rates and ILS errors, were recorded on magnetic tape for later analysis.

Pilots' Experience.- Two pilots were used in the program, and their previous experience is summarized on the next page. Pilot A's 3 hours consisted of two flights in the three-week period prior to the experiment. These flights consisted of some level flight in smooth air at 36 m/sec and 40° of flaps to familiarize the pilot with the Twin Otter's stability and control characteristics, and in addition, some IFR landing approaches at 36 m/sec in moderate turbulence. Pilot B's 1.5 hours were flown one year earlier.

PILOTS' EXPERIENCE

| PILOT | TOTAL NO. OF HOURS | HOURS ACTUAL INSTRUMENT FLYING | HOURS IN SIMULATORS | MAIN TYPES OF AIRCRAFT FLOWN | HOURS IN TWIN OTTER |
|---|---|---|---|---|---|
| Pilot A | 2800 | 45 | 140 | light twin, light single-engine, rotary wing | 3.0 |
| Pilot B | 4000 | 100 | 500 | Convair 340, light single-engine, Lear jet | 1.5 |

## RESULTS

### Results of Turbulence Simulation Development

The development of a non-Gaussian turbulence simulation has been described under "Description of Atmospheric Turbulence" and in Appendix A of this report. It has been shown that, in theory, this new method can closely approximate the patchy nature, non-Gaussian probability distribution, and frequency content of atmospheric turbulence. Furthermore these properties can be varied during operation of the simulation in order to represent changing flight conditions such as vehicle altitude or airspeed.

Digital computer programs modeling the system block diagrams presented in Appendix A have been written and artificial turbulence time histories have been produced. A statistical analysis of these time histories has been carried out and the experimentally obtained results of the analysis of these time histories will now be compared with those expected from the theoretical considerations of Appendix A. The statistical properties of interest in this report are: power spectral density, cross spectral density, probability distribution, and patchiness. Each of these quantities will now be considered in turn. Since similar results were obtained for all three statistical models considered, only the matched non-Gaussian model data will be presented.

Power Spectral Densities.- Figures 18, 19, and 20 compare the power spectral densities of the three gust components at the vehicle center of gravity with the modified Dryden spectra

of figure 3. The fit of the theoretical curves is very good, especially in view of the fact that only one 5-minute data sample was used to produce the experimental curves. Because of the short time history length, spectral estimates below .1 hertz are quite uncertain.

Cross Spectral Densities.- Figure 21 compares the desired cross spectral density of the u and w gust components with the results estimated from a 5-minute sample. The cross spectrum exhibits correct behavior for frequencies above .6 hertz. The large discrepancies below this frequency are attributed to uncertainty caused by the short time history length.

Probability Distribution.- Figures 22 and 23 show typical smoothed cumulative probability and probability density distributions obtained from the simulated turbulence. Both figures show good agreement with theory.

Table 4 compares the estimated fourth and sixth normalized central moments obtained from the analysis of the matched non-Gaussian model time history with the theoretically predicted values.

TABLE 4.- COMPARISON OF THEORETICAL VALUES OF $M_4$ AND $M_6$ WITH THOSE FROM ANALYSIS OF THE MATCHED NON GAUSSIAN MODEL TIME HISTORY

| | $M_4$ | $M_6$ |
|---|---|---|
| From Analysis of Time History | 4.51 | 42.73 |
| Theory (Eq. A-33) | 4.50 | 52.50 |

Agreement is excellent for $M_4$ and fair for $M_6$ . The error in $M_6$ is attributed to the normal difficulty in estimating the higher moments of a random function, and to possible non-Gaussian behavior of the random number generator; it is not thought to indicate a defect in the theory.

Patchy Character.- There is no theoretical model for the patchy nature of turbulence which is to be reproduced by the turbulence simulation, therefore no comparison with theory can be presented here. Instead, the reader's attention is directed to figures 4 and 13, which demonstrate the ability of the non-Gaussian turbulence simulation to model the patchy character of atmospheric turbulence.

## Results of Flight Simulator Experiment

Simulator Fidelity.- The resemblance of the simulator flying characteristics to those of the Twin Otter was considered to be quite close. One pilot thought the roll sensitivity to aileron might be a bit low, however $C_{\ell_{\delta a}}$ had already been increased by 50% from the de Havilland data, and the other pilot was happy with it.

The main criticism of the simulation was the presence of a lot of high-frequency noise, which showed up as a shudder or vibration when simulating smooth air flight. This made the response to turbulence seem quite sharp-edged, as opposed to the wallowing motion felt in the Twin Otter. It is felt that two sources are to blame for this. First and most important, the fact that these vibrations occurred for smooth air conditions suggests that the simulator-drive system and simulator structure, coupled with the compensation network used to improve the high-frequency response (see Appendix C) were to blame. A second factor is probably the neglect of unsteady-aerodynamic effects of the gusts acting at the c.g. and the tail. A sharp gust at the c.g. will immediately become a similar vertical acceleration through the $C_{z_\alpha}$ stability derivative. In real life, the unsteady effects require a finite time for the lift to build up on an aerodynamic surface subjected to an instantaneous change in angle of attack. The pilots felt that this unwanted noise, whatever the source, was sufficient to mask the small differences that the pilots were trying to detect between the various turbulence models.

Another complaint which the pilots felt detracted from the realism was the absence of any drifting in the mean wind. Since the crosswind was set to a constant value for the whole flight, the pilot would just set his heading to correct for this and then wouldn't have to worry about it any more. On a real approach, a pilot flies through a crosswind of varying intensity as he changes altitude, consequently he has to be continually hunting for a bias heading and a bias power-setting in order to stay on the localizer and glideslope. The turbulence model used has the capability of changing the turbulence characteristics with altitude, but it was felt that since the task was a constant-altitude one, the gust parameters should be fixed at those of the altitude flown. Obviously this detracted from the realism.

Results of Pilot Questionnaire.- Answers from the question sheets are shown in figures 24 to 30, and 32 to 34, but for brevity not all the answers are discussed here or shown in these figures. The only plots shown here are those of special interest

or those for which there was a difference between answers for the various turbulence models. Results for the remaining questions are shown in Appendix E.

These plots of the pilots' answers to the questionnaire are to be interpreted as follows. Each individual answer is shown by a small "x" or square. An average of the points for each pilot and model is shown by the large "X" or square. Using the Student's t distribution (ref. 24), and (for the case of turbulence intensity, figure 24) assigning the value 1.0 to the answer "light", 2.0 to "moderate", and 3.0 to "severe", one can calculate the 95% confidence limits for where the true mean must lie for a given pilot and mode. These limits are shown by the vertical bars in the figures. In other words, the data points have a mean denoted by the large "X" or square. Based on these data points, there is 95% confidence that the true mean for a given pilot and model lies somewhere in the region denoted by the vertical bar.

These confidence limits for where the true mean lies give a way to tell whether or not a pilot can readily tell any difference between two turbulence models. One can be 95% confident that the pilot can distinguish between two models if the following two conditions are both met:

(1) The mean for the first model must lie outside the 95% confidence limit for the mean of the second model; and

(2) The mean of the second model must lie outside the 95% confidence limit for the mean of the first model.

An example where the pilot can differentiate (at the 95% confidence level) between models is pilot B's ratings of Gaussian and Real turbulence in figure 24. An example of the pilot being unable to distinguish between two models is shown in figure 28 for pilot A's ratings of Gaussian and Real turbulence. In this case, the mean for Real is outside the confidence limit for Gaussian; however the mean for Gaussian is within the confidence limits for the Real mean.

Turbulence Intensity.- Inspection of the pilot estimates of turbulence intensity shown in figure 24 shows that both pilots were able to distinguish between the Real turbulence and the Gaussian model - the Real one appearing to be the more intense. This is interesting, since the models were all scaled to have the same rms values. Apparently, because of its more continuous nature, the Gaussian turbulence seemed less severe. The pilots were unable to distinguish between any of the other models on the basis of turbulence intensity.

Realism of Turbulence.- Estimates for the turbulence realism are plotted in figure 25. Pilot A found no differences, rating all the models "fair" on the average. Pilot B was able to distinguish between the Real and Gaussian models and between the Real and matched non-Gaussian ones. His mean for the Real turbulence was the highest, being slightly better than "good".

Correctness of Relative Amplitudes of Disturbances.- Plots for the opinion of correctness of roll and yaw amplitudes are shown in figures 26 and 27 respectively. Pilot B generally seemed to think the amplitudes were about right, whereas pilot A (who had the recent Twin Otter time) seemed to feel there was a bit too much yaw and not quite enough roll in all the models. The pilots were happy with the amplitudes of the disturbances in the other axes, except that pilot B thought there was not enough side-force.

Patchy Characteristics.- The patchiness of the turbulence is the one characteristic which is different in the four cases. The Gaussian model turbulence is quite monotonous or continuous in its amplitude, whereas in nature the turbulence tends to have periods of relative quiet followed by relatively noisy bursts. It was hoped that the pilots could distinguish between "patchy" models and a relatively continuous one. The pilots' answers to the question on patchiness are plotted in figure 28. It was hoped the pilots would rate the Gaussian model too continuous, the Real turbulence and the matched non-Gaussian model about right, and the more patchy non-Gaussian perhaps too patchy. As the figure shows, this was not quite the case, although the pilots were able to distinguish between some of the models. The Gaussian one was found to be "a little too continuous", and the other models all bracket being "about right", although their mean values all tend to be slightly towards being continuous.

Statistically, pilot A was able to distinguish that the matched, non-Gaussian and the more patchy non-Gaussian models are patchier than the Gaussian. He was unable to distinguish between the Real and Gaussian, since the Real has such a wide spread on the confidence limits for the mean. Pilot B could tell that the Real and more patchy non-Gaussian models were patchier than the Gaussian. He was unable to distinguish between any of the other cases.

Frequency Content of Turbulence.- Pilot estimates of low and high-frequency content are shown in figures 29 and 30. Both A and B rated the low frequency content as being somewhere between "about right" and "not enough". Although pilot B rated nine of the flights as being about right, he continually remarked that the models lacked what he called "low-low frequency content", which would cause him to have to hunt for the correct directional bias required to stay on the localizer.

(See the discussion on page 49.) For the high frequency criteria, pilot A consistently complained of too much high frequency noise from the simulator drive system. Pilot B, who did not have any recent Twin Otter time, rated the high frequencies as about right. (Pilot B has had considerably more simulator time, and might be more prone to filter out simulator shortcomings.) However a third pilot, who took part in the check-out and who had several hours of recent Twin-Otter time, also complained of too much high-frequency noise.

Cooper Rating.- The pilots were asked to rate the airplane/turbulence/task combination using the Cooper-Harper Pilot Rating Scale shown in figure 31. In figure 32, pilot A's mean ratings were in the 4 1/2 to 5 range, while B rated the combination about a full point lower. Pilot A's means show no statistical difference between models, whereas B rated the Real case higher than the Gaussian and the matched non-Gaussian. This corresponds to the higher rating for turbulence intensity (figure 24) found for the Real turbulence.

Root Mean Square Values of Airplane Motions.- Root-mean-square (rms) values were computed for some of the airplane motions to see if these showed any differences between models. Rms values of the aircraft attitude angles $\theta$ , $\phi$ , and $\psi$ are plotted in Appendix E (figures E-6, E-7, and E-8) and show no consistent differences between the turbulence models. However the rms values of $z_{ILS}$ , the height above the glideslope, shows an interesting result in figure 33. Both pilots show a statistically higher rms value for the Real turbulence than for the Gaussian. This fits in with the estimates of higher intensity for the Real than for Gaussian turbulence, and is significant because the models had the same gust rms values. In comparison, the rms values of displacement from the localizer (fig. 34) show no significant variation between gust cases.

## CONCLUSIONS

This report has described a new method for producing artificial turbulence time histories which is more flexible in its ability to match desired statistical properties than are presently used methods. The use of this method should give improved realism and accuracy when in piloted simulator studies, for aircraft response studies which investigate stability, stability augmentation, guidance, and for studies of aircraft structures as affected by atmospheric turbulence.

The new method was used to produce time histories of turbulence, which were analyzed in order to obtain certain of their important statistical properties. These properties were compared with the properties of actual turbulence.

The conclusions from the analytical studies of the time histories developed by this new method as compared to those developed by other simulation methods are outlined below.

1.) The new method is capable of producing a class of non-Gaussian probability density distributions, which has not been possible with previous turbulence simulations. Using this method one can produce probability distributions which closely match the various probability distributions which are obtained from the analysis of real turbulence data.

2.) The results of the analyses show that the patchy nature of real turbulence is matched by this method. The use of this method in piloted simulators should remove the objection that the use of the Gaussian probability results in turbulence which is too monotonous.

3.) The frequency content of the real turbulence can be matched. Although other methods can do this as well, this important property of turbulence simulation is preserved in this method.

4.) Although not demonstrated experimentally this new method has the capability common to other simulation techniques of simulating the time-varying characteristics.

5.) Since the probability density distribution can be closely matched to that of real turbulence, this method should be capable of predicting the occurrence of large gust velocities more accurately than present methods. This should prove especially valuable in applications in the structures area.

6.) While the mechanization of the proposed method is not as simple as that of the Gaussian model, it is still easily within the capabilities of modern digital or analog computers.

The time histories derived from the non-Gaussian statistical models along with those from real turbulence and from a Gaussian model, were used in a flight simulator experiment in order to compare the realism of these various methods for simulating turbulence. The principal conclusions resulting from the flight simulator experiment are as follows.

1.) The pilots tended to rate the Gaussian model as being "a little to continuous," whereas the two non-Gaussian models and the real time history were rated "about right" with regard to patchiness.

2.) The pilots comparison of intensity indicated that, even though all models were scaled to the same intensities, the non-Gaussian models seemed to be more severe than the Gaussian model. It is concluded that this is due to the fact that there are more large gusts when using the non-Gaussian models. The rms of the glide path errors reinforced this view, as these errors were definitely greater for the real turbulence and the non-Gaussian models than for the Gaussian model.

3.) Although the pilots expressed the impressions discussed above, other impressions and statistical analyses of pilots' performance were not conclusive in differentiating among the various turbulence models. One possible reason for this might be that, even though the non-Gaussian model extended the range of statistical properties matched, pilots may be sensitive to certain properties which are not well matched by this model. A second reason might be that the characteristics of the simulator itself, mainly its high-frequency noise characteristics, tended to mask some of the differences in the turbulence models. Another possible reason might be that the pilots had limited flying time in turbulence in the actual aircraft being simulated.

Department of Aeronautics and Astronautics,
University of Washington,
Seattle, Washington, March 30, 1973.

## REFERENCES


1. Bray, R. S.; and Larsen, W. E.: Simulator Investigation of the Problems of Flying a Swept Wing Transport Aircraft in Heavy Turbulence. Paper presented at Conference on Aircraft Operating Problems, Langley Research Center, May 1965.

2. Hirsch, D. L.; and McCormick, R. L.: Experimental Investigation of Pilot Dynamics in a Pilot Induced Oscillation Situation. Preprint 65-793, Am. Inst. Aeron. and Astronaut., Roy. Aeron. Soc., and Japan Soc. for Aeron. and Space Sci., Aircraft Design and Technology Meeting (Los Angeles, California), Nov. 1965.

3. Seckel, E.; Miller, G. E.; and Nixon, W. B.: Lateral-Directional Flying Qualities for Power Approach. Report 727, Princeton Univ., Sept. 1966.

4. Reeves, P. M.: A Non-Gaussian Turbulence Simulation. Tech. Report AFFDL-TR-69-67, Air Force Flight Dynamics Laboratory, Air Force Systems Command, Wright Patterson Air Force Base, Ohio, Dec. 1969.

5. Dutton, J. A.; and Deaven, D. G.: Some Observed Properties of Atmospheric Turbulence. Statistical Models and Turbulence. Vol. 12 of Lecture Notes in Physics, Springer-Verlag, 1972, pp. 352-383.

6. Frenkiel, F. N.; and Klebanoff, P. S.: Higher Order Correlations in a Turbulent Field. Phys. Fluids, vol. 10, no. 3, Mar. 1967, pp. 507-520.

7. Gault, J. D.; and Gunter, D. E.: Atmospheric Turbulence Considerations for Future Aircraft Designed to Operate at Low Altitudes. Preprint 69-216, Am. Inst. Aeron. and Astronaut., Aircraft Design for 1980 Operations Meeting (Washington, D. C.), Feb. 1968.

8. von Karman, T.: Progress in the Statistical Theory of Turbulence. Turbulence Classic Papers on Statistical Theory, Interstate Publishers, Inc. (New York), 1961.

9. Dryden, H. L.: A Review of the Statistical Theory of Turbulence. Turbulence Classic Papers on Statistical Theory, Interstate Publishers, Inc. (New York), 1961.

10. Elderkin, C. E.: Experimental Investigation of the Turbulence Structure in the Lower Atmosphere. Report BNWL-329, Battelle Northwest, Dec. 1966.

11. Lumley, J. L.; and Panofsky H. A.: Structure of Atmospheric Turbulence. Vol. 12 of Monographs and Texts in Physics and Astronomy, Interscience Publishers (New York), 1964.

12. Skelton, C. B.: Investigation of the Effects of Gusts on V/STOL Craft in Transition and Hover. Tech. Report AFFDL-TR-68-85, Air Force Flight Dynamics Laboratory, Air Force Systems Command, Wright Patterson Air Force Base, Ohio, Oct. 1968.

13. Tomlinson, B. N.: The Simulation of Turbulence and Its Influence on the Pilot. Paper presented at International Conference on Atmospheric Turbulence, Roy. Aeron. Soc. (London, England), May 18-21, 1971.

14. Dutton, J. A., et al.: Statistical Properties of Turbulence at the Kennedy Space Center for Aerospace Vehicles Design. NASA CR-1889, Aug. 1971.

15. Chalk, C. R.; et al.: Background Information and User Guide for MIL-F-8785B(ASG), Military Specification Flying Qualities of Piloted Airplanes. Tech. Report AFFDL-TR-69-72, Air Force Flight Dynamics Laboratory, Air Force Systems Command, Wright Patterson Air Force Base, Ohio, Aug. 1969.

16. Etkin, B.: A Theory of the Response of Airplanes to Random Atmospheric Turbulence. J. Aerospace Sci., vol. 26, no. 1, July 1959.

17. Etkin, B.: Theory of the Flight of Airplanes in Isotropic Turbulence - Review and Extension. AGARD Report 372, April 1961.

18. Eggleston, J. M.; and Diederich, F. W.: Theoretical Calculation of the Power Spectra of the Rolling and Yawing Moments on a Wing in Random Turbulence. NACA Rept. 1321, 1957.

19. Franklin, J. A.: Turbulence and Lateral-Directional Flying Qualities. NASA CR-1718, April 1971.

20. Sears, W. R.: Some Aspects of Non-Stationary Airfoil Theory and Its Practical Applications. J. Aeron. Sci., vol. 8, no. 3, Jan. 1941, pp. 104-108.

21. Etkin, B.: Dynamics of Flight-Stability and Control. John Wiley & Sons, Inc., 1949.

22. Perkins, C. D.; and Hage, R. E.: Airplane Performance Stability and Control. John Wiley & Sons, Inc., 1949.

23. Cooper, G. E.; and Harper, R. P., Jr.: The Use of Pilot Rating in the Evaluation of Aircraft Handling Qualities. NASA TN D-5153, April 1969.

24. Hoel, P. G.; Introduction to Mathematical Statistics. Second ed. John Wiley & Sons, Inc., 1954, p. 226.

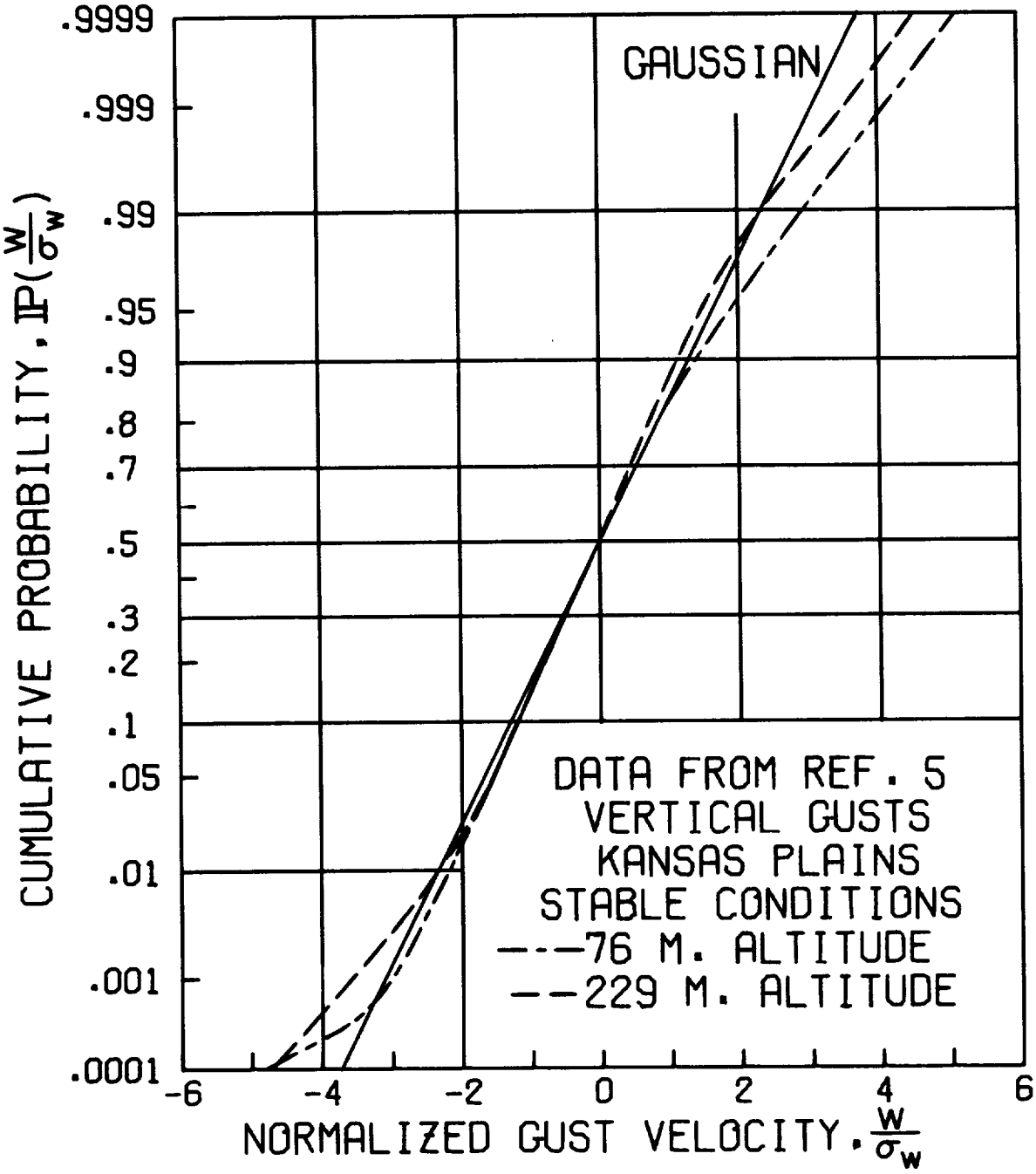


FIGURE 1. TYPICAL CUMULATIVE PROBABILITY DISTRIBUTIONS OF ATMOSPHERIC TURBULENCE

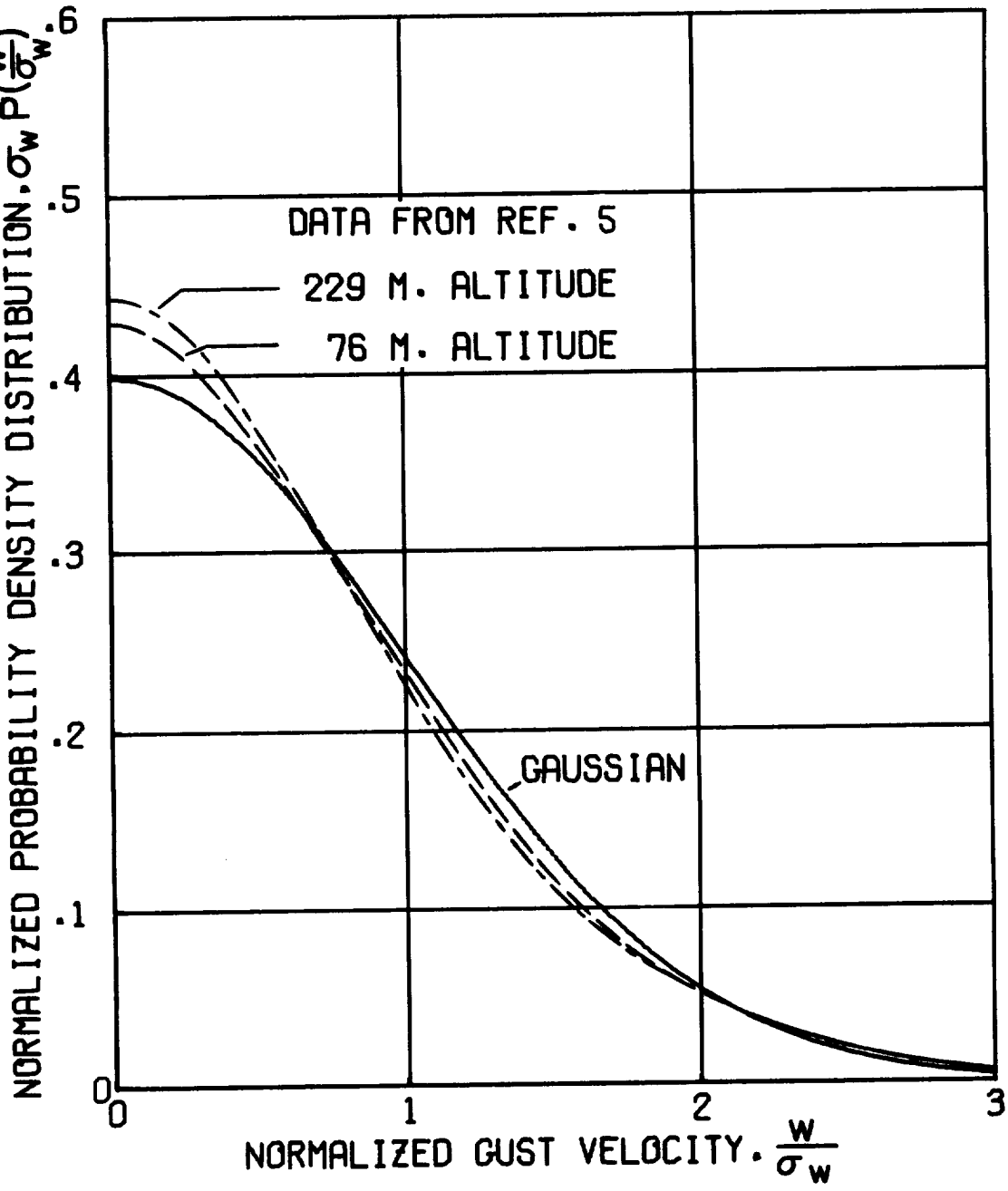


FIGURE 2. TYPICAL PROBABILITY DENSITY DISTRIBUTIONS OF ATMOSPHERIC TURBULENCE

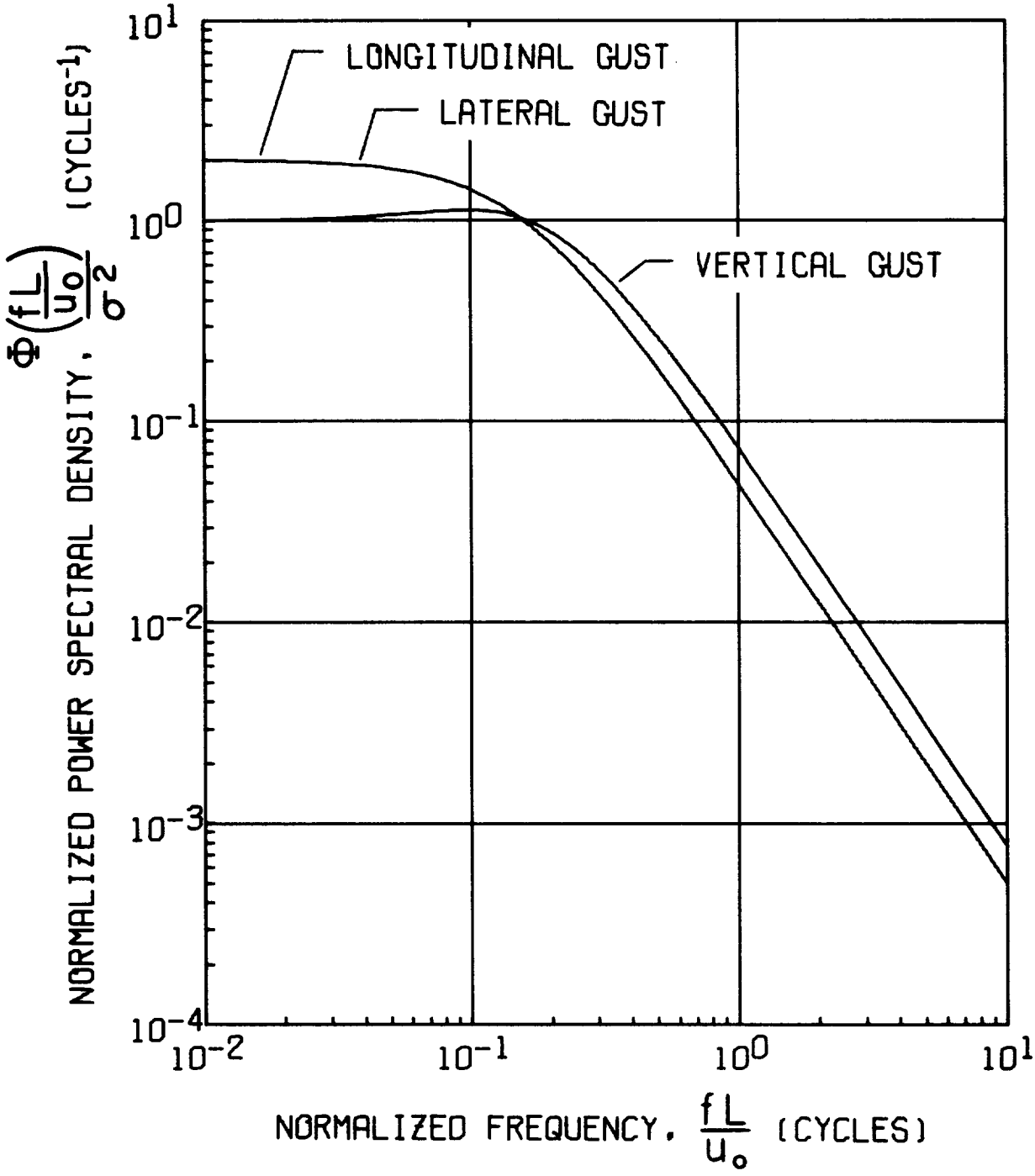


FIGURE 3. NORMALIZED GUST POWER SPECTRAL DENSITIES ASSUMED IN THIS REPORT

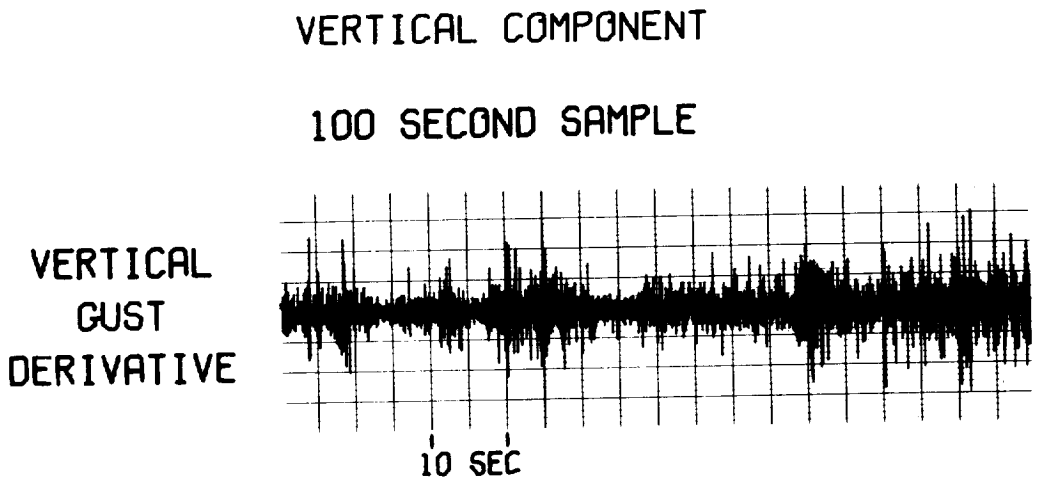


FIGURE 4. TYPICAL PATCHY NATURE OF ATMOSPHERIC TURBULENCE

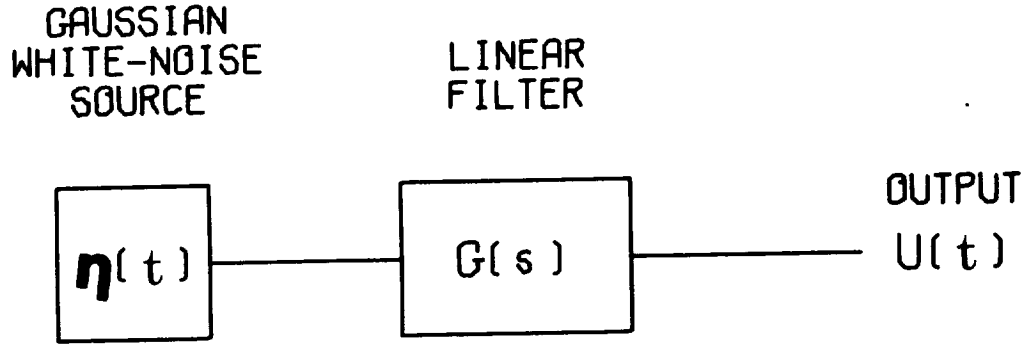


FIGURE 5. LINEARLY-FILTERED GAUSSIAN WHITE-NOISE SIMULATION

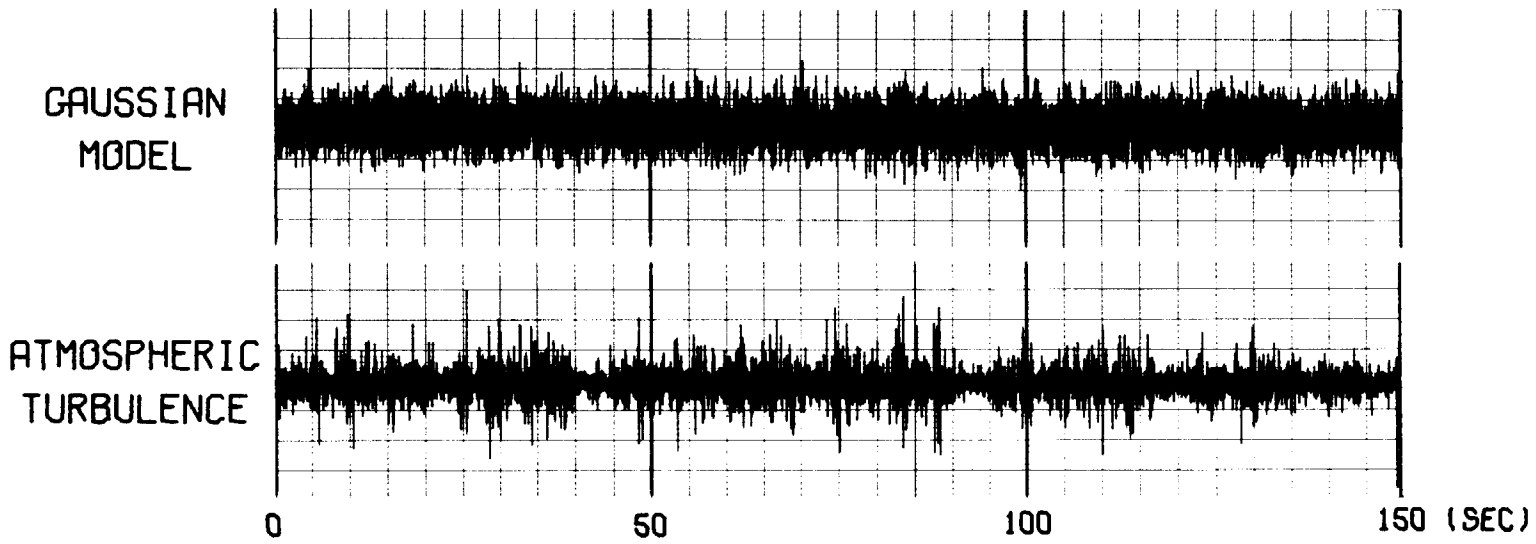


FIGURE 6. PATCHY CHARACTERISTIC OF ACTUAL ATMOSPHERIC TURBULENCE COMPARED WITH THAT PRODUCED BY THE GAUSSIAN TURBULENCE MODEL

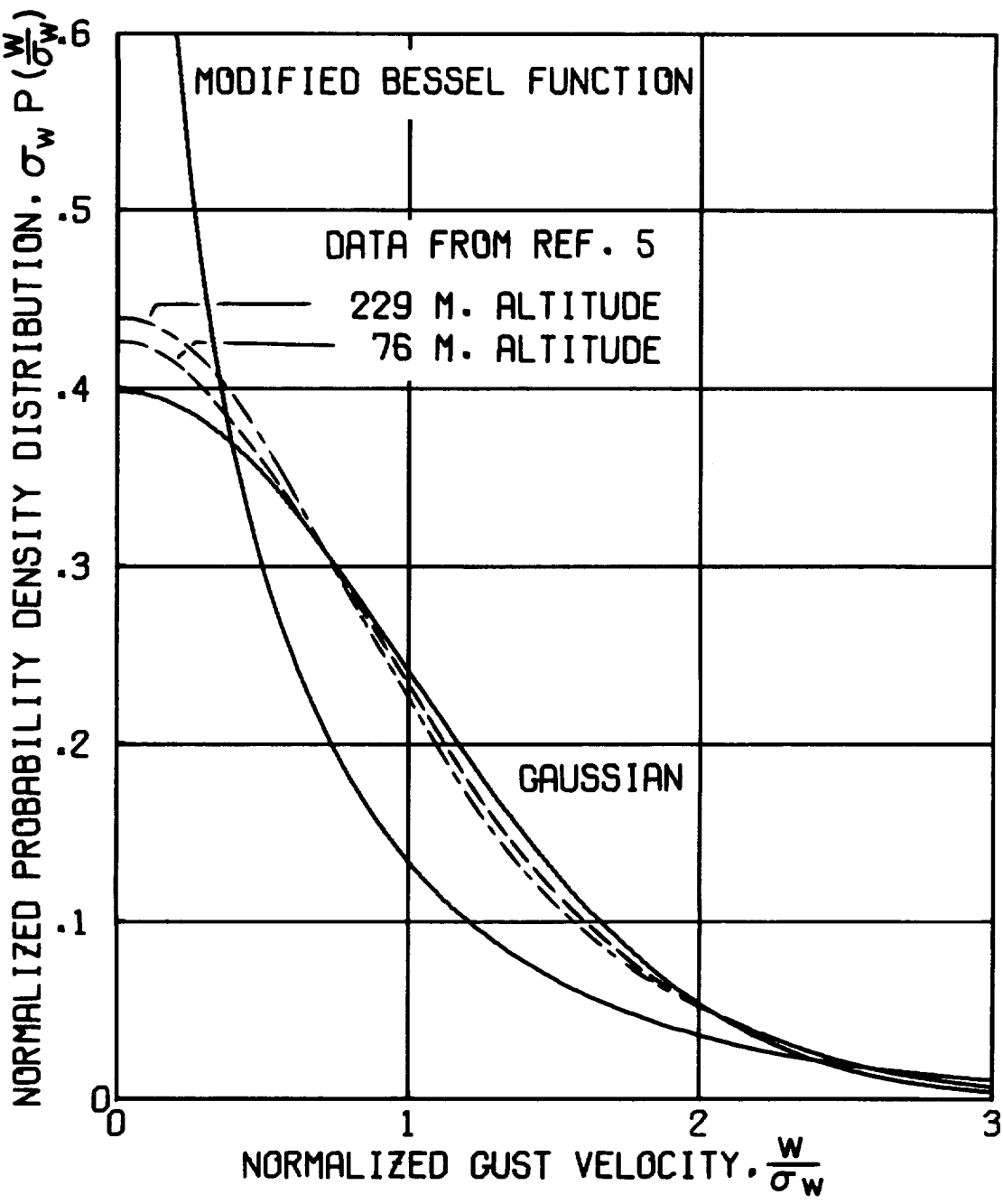


FIGURE 7. COMPARISON OF MODIFIED BESSEL FUNCTION DISTRIBUTION WITH GAUSSIAN AND MEASURED DISTRIBUTIONS

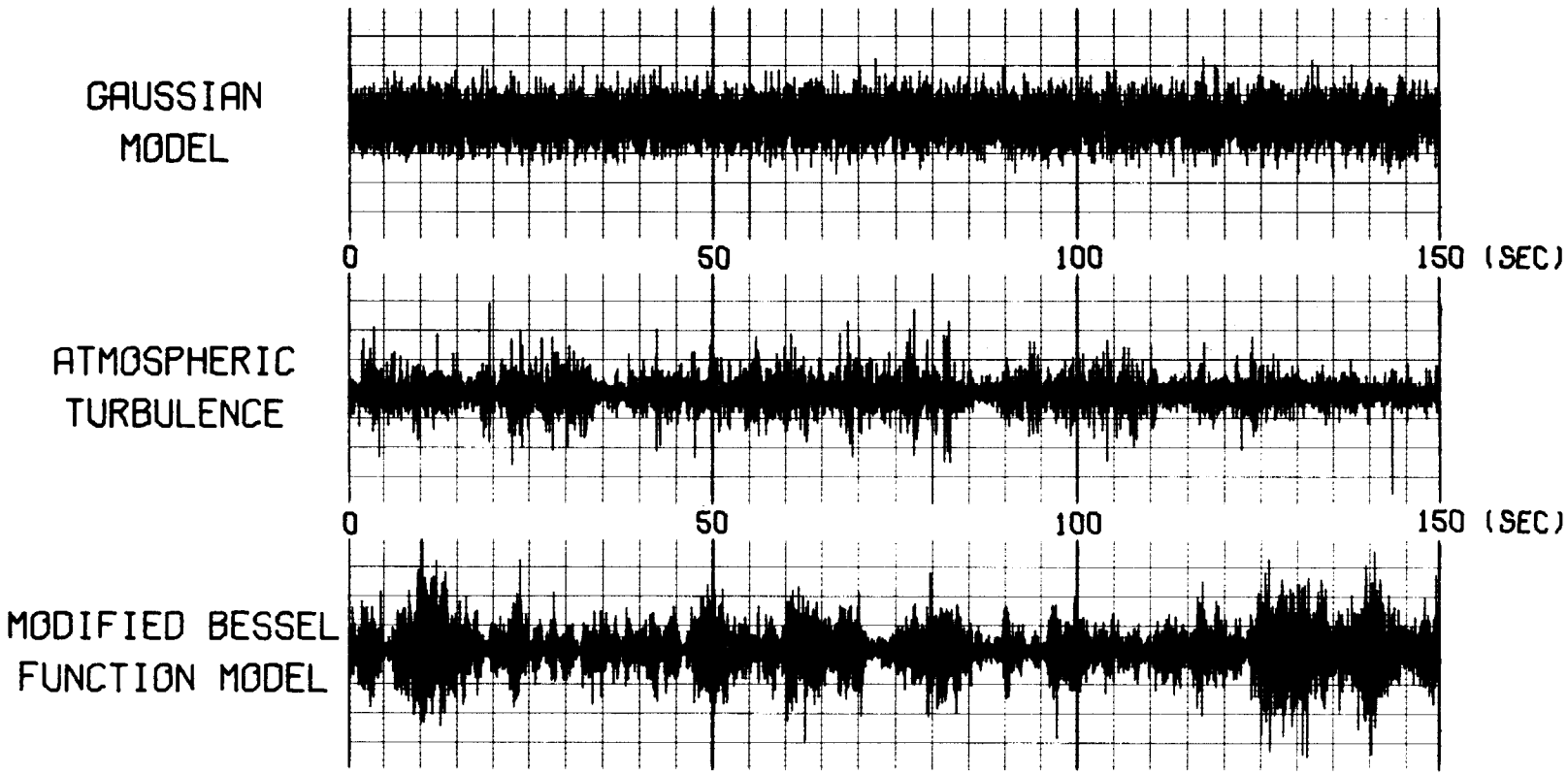


FIGURE 8. PATCHY CHARACTERISTICS OF MODIFIED BESSEL FUNCTION MODEL COMPARED WITH THOSE PRODUCED BY THE GAUSSIAN MODEL AND ACTUAL ATMOSPHERIC TURBULENCE

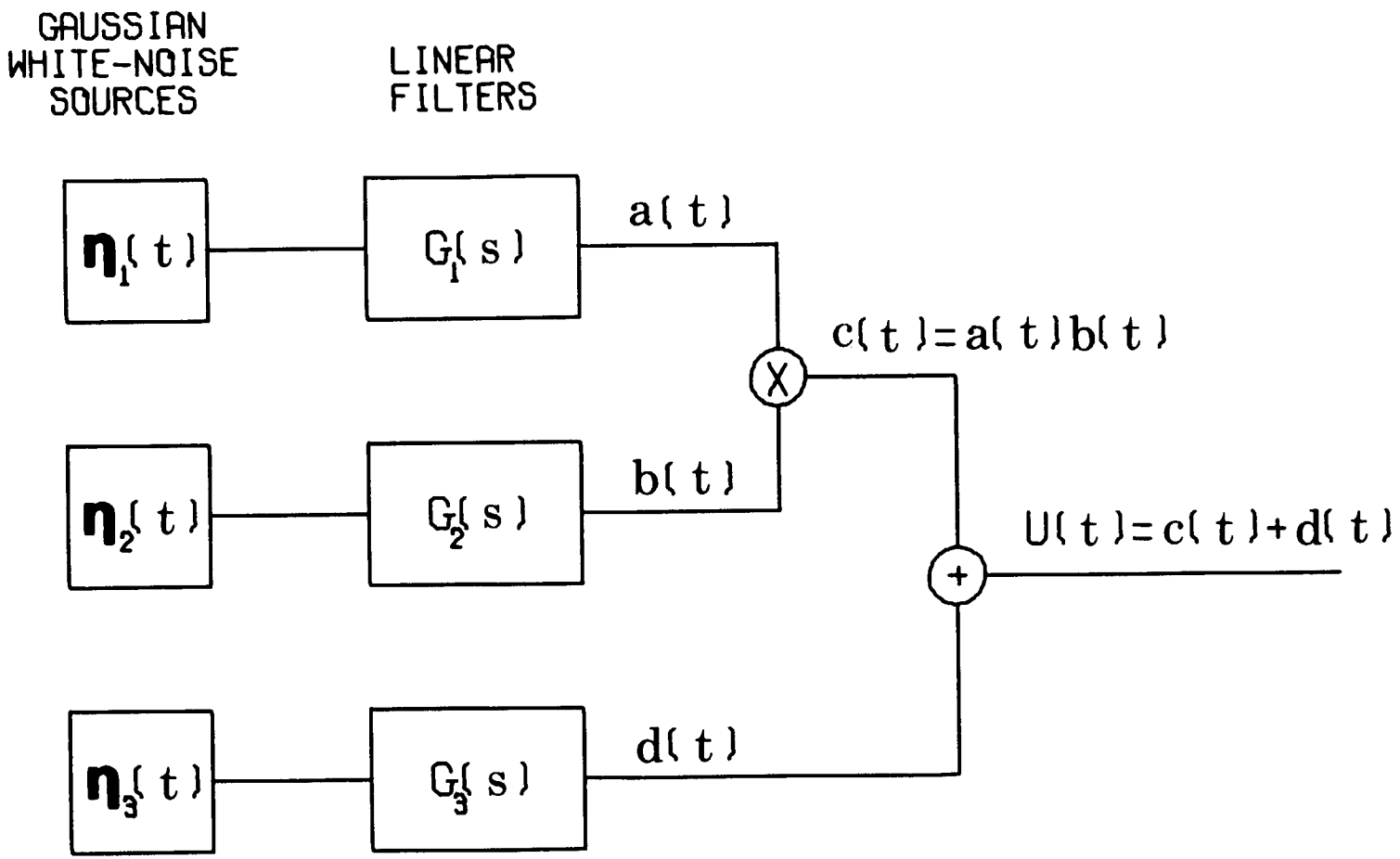


FIGURE 9. PROPOSED NON-GAUSSIAN TURBULENCE SIMULATION

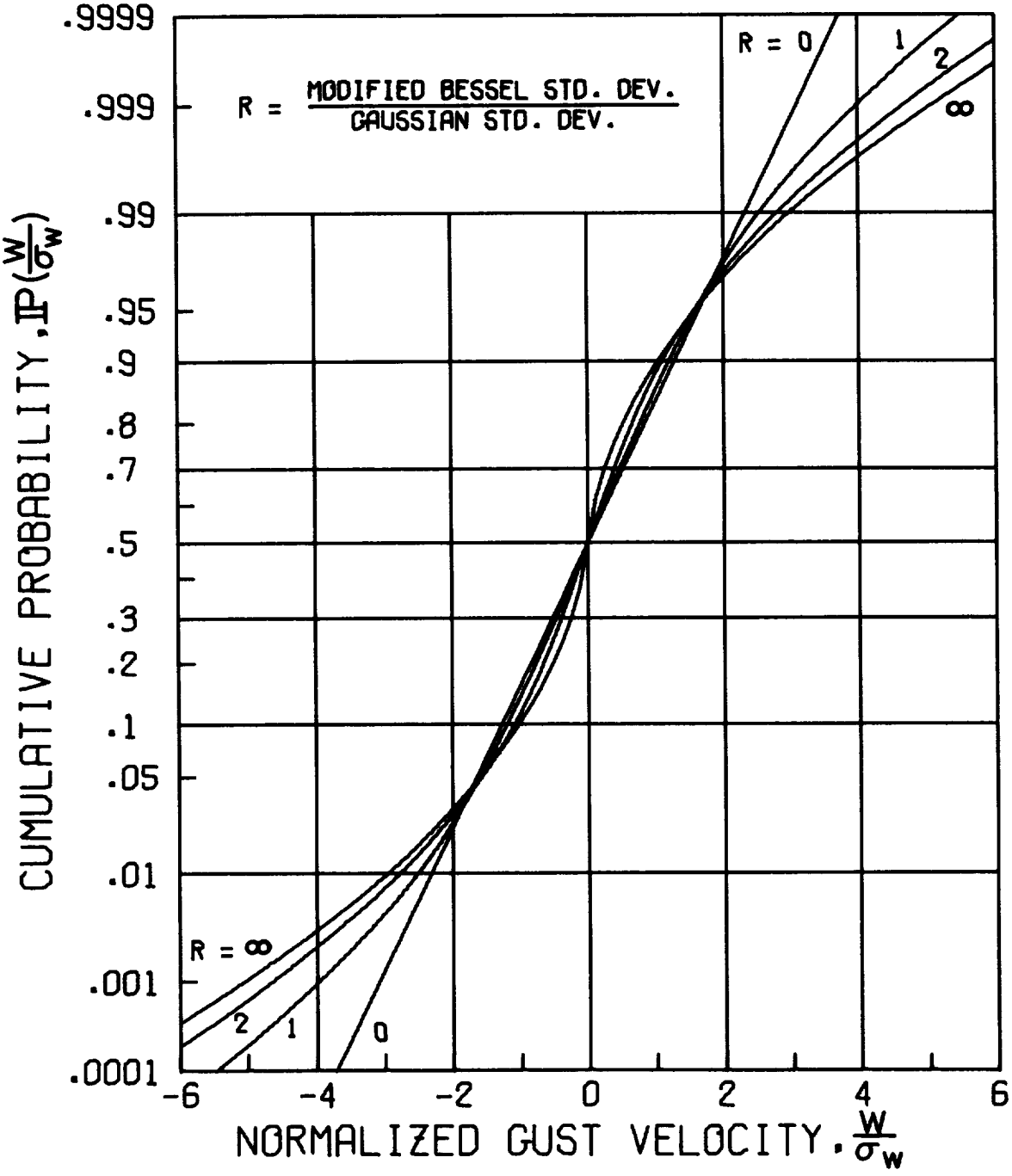


FIGURE 10. COMPARISON OF CUMULATIVE PROBABILITY DISTRIBUTIONS FOR VARIOUS STANDARD DEVIATION RATIOS

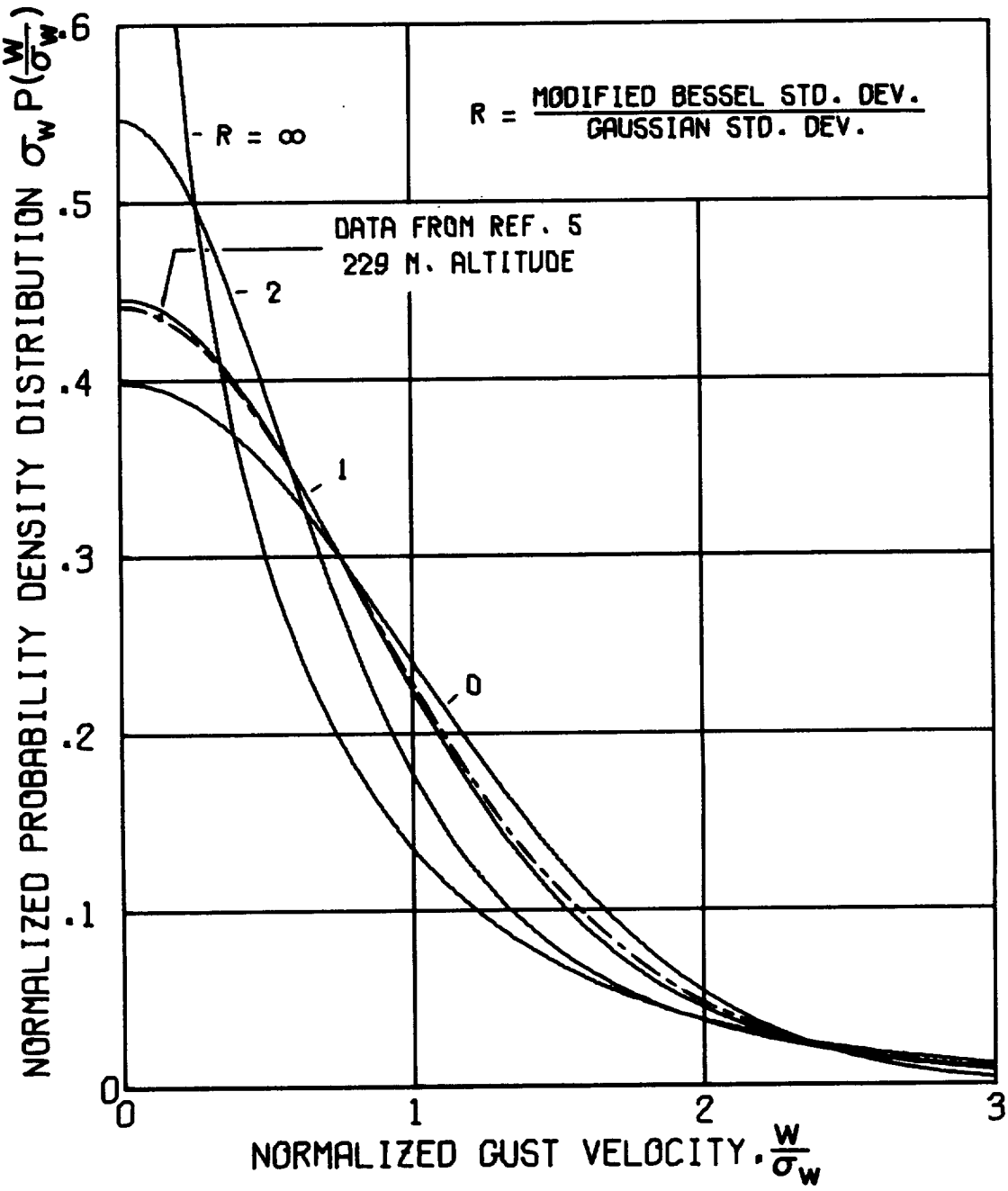


FIGURE 11. COMPARISON OF PROBABILITY DENSITIES FOR VARIOUS VALUES OF THE STANDARD DEVIATION RATIO

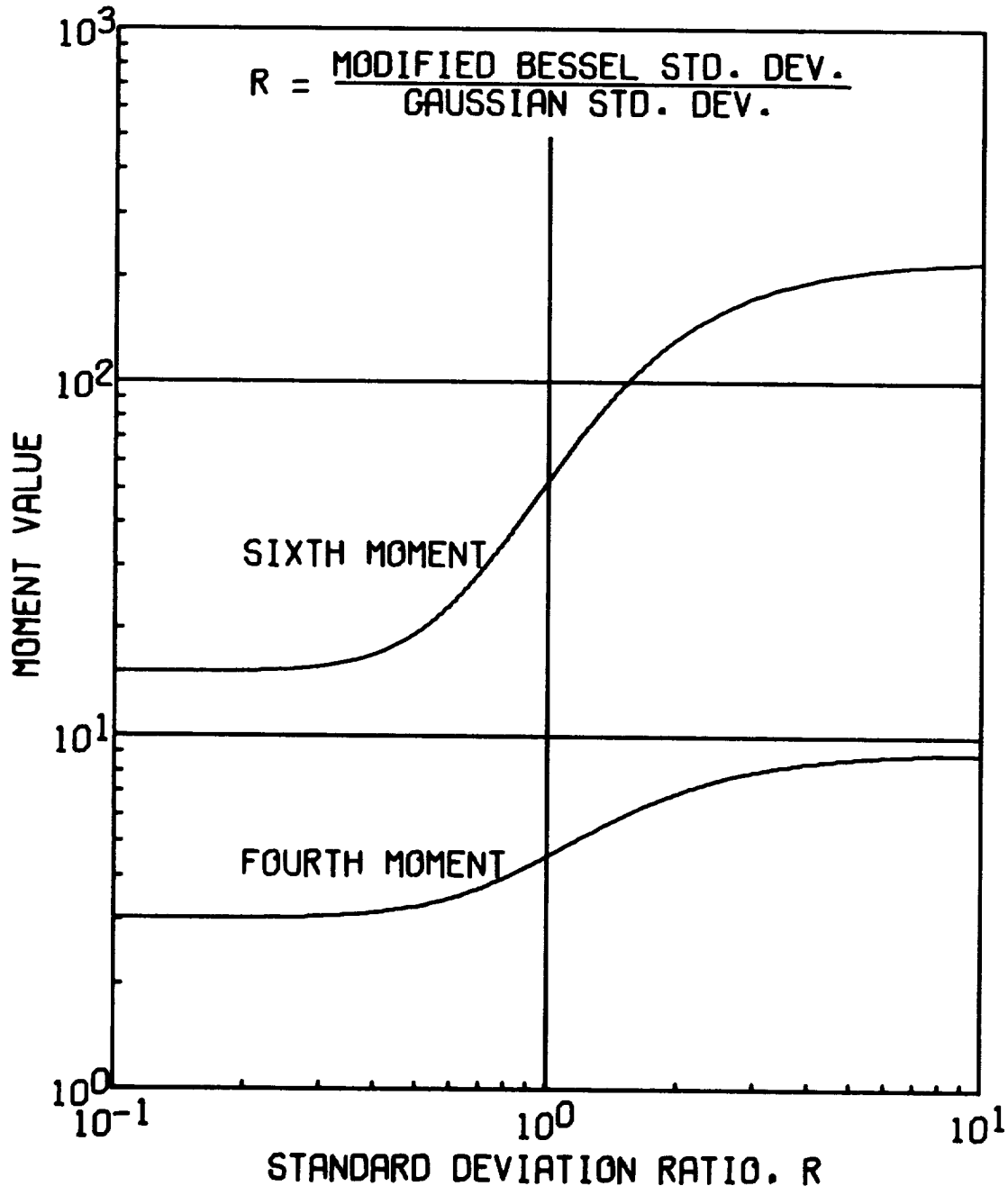


FIGURE 12. DEPENDENCE OF THE FOURTH AND SIXTH NORMALIZED CENTRAL MOMENTS UPON THE STANDARD DEVIATION RATIO

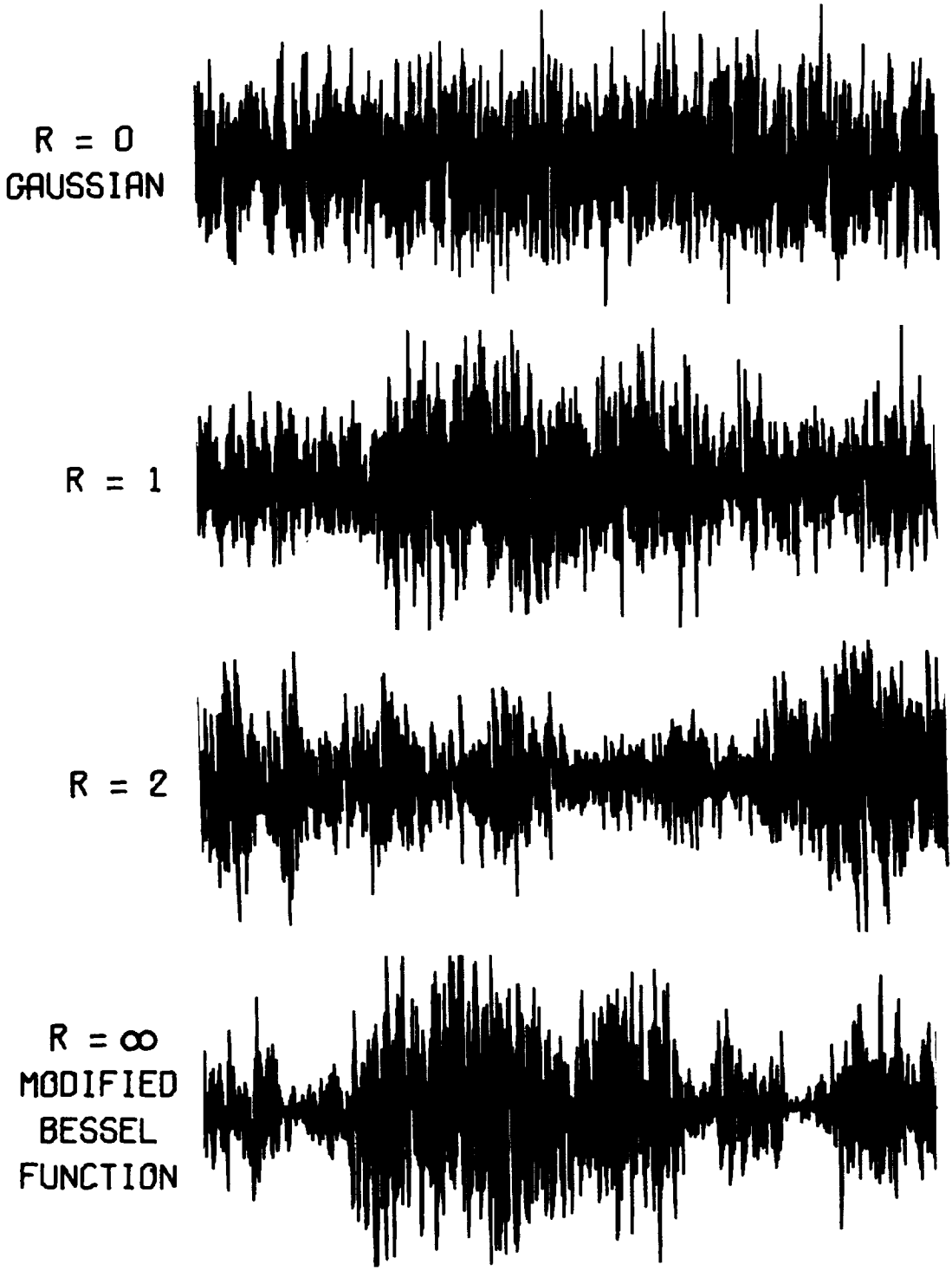


FIGURE 13. DERIVATIVE OF SIMULATED TURBULENCE SHOWING DEPENDENCE OF PATCHY CHARACTERISTIC UPON THE STANDARD DEVIATION RATIO R

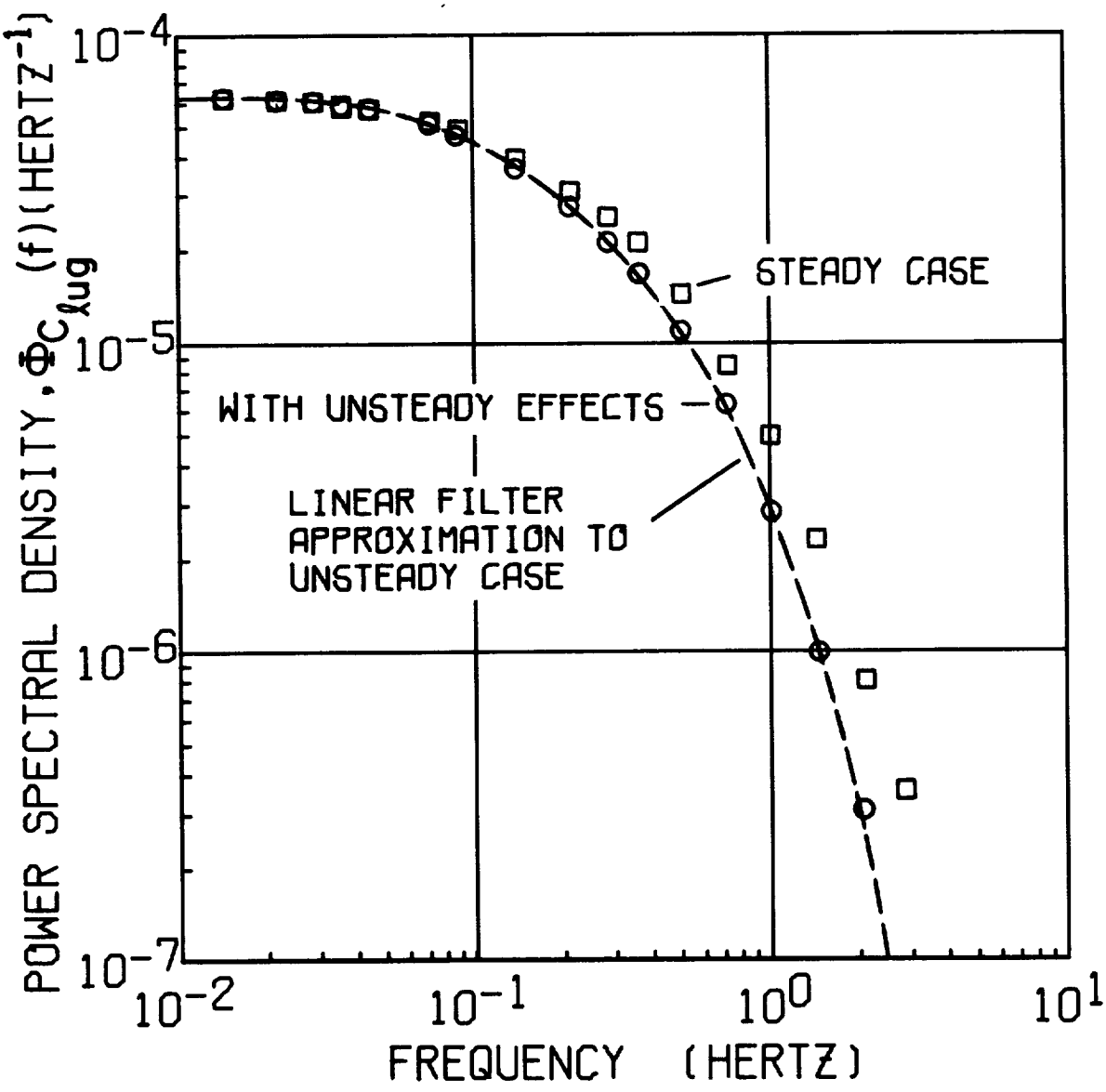


FIGURE 14. POWER SPECTRUM OF ROLLING MOMENT DUE TO DISTRIBUTION OF HEAD-ON GUSTS ACROSS SPAN

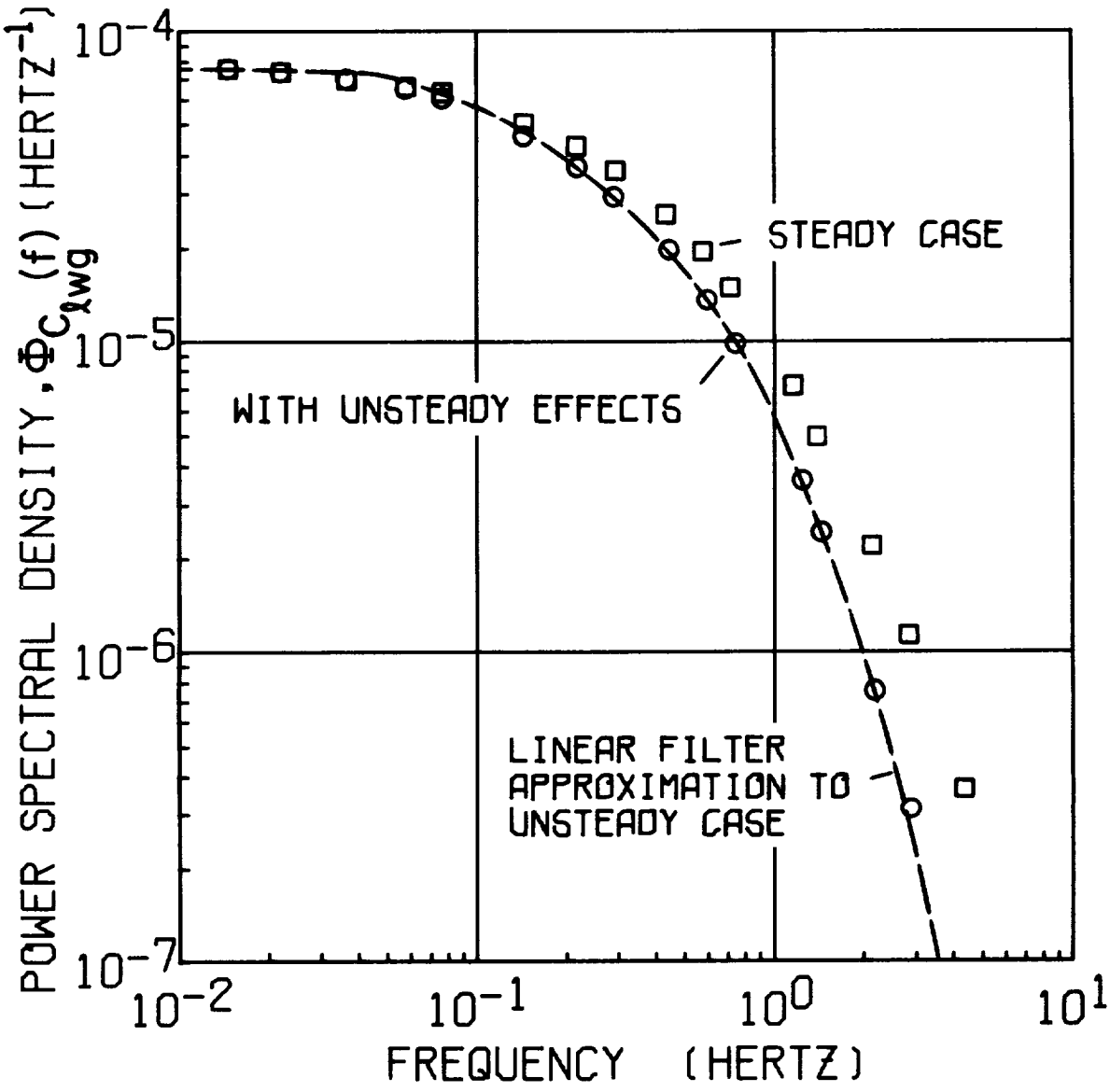


FIGURE 15. POWER SPECTRUM OF ROLLING MOMENT DUE TO DISTRIBUTION OF VERTICAL GUSTS ACROSS SPAN

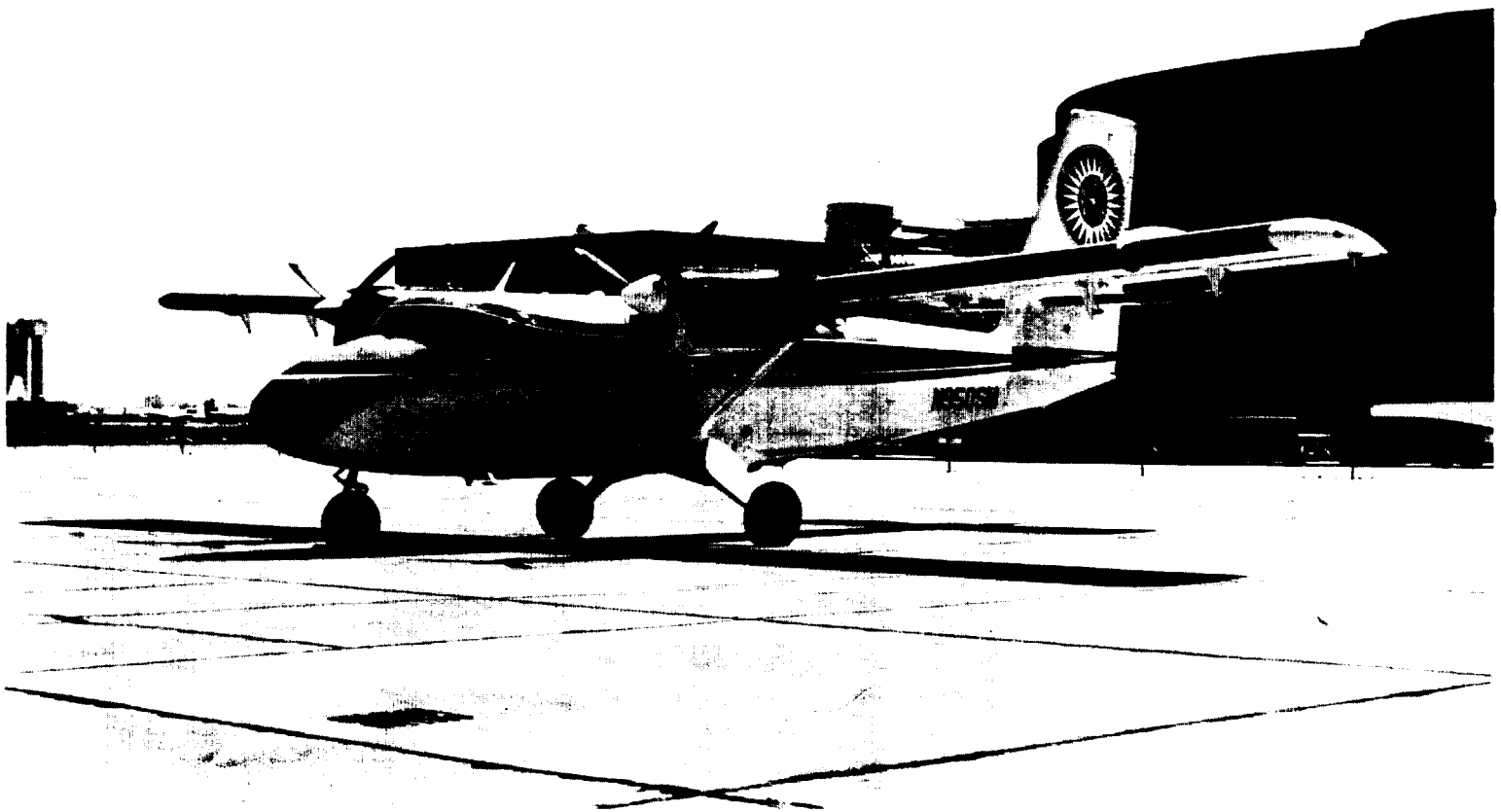

FIGURE 16. DE HAVILLAND DHC-6 TWIN OTTER

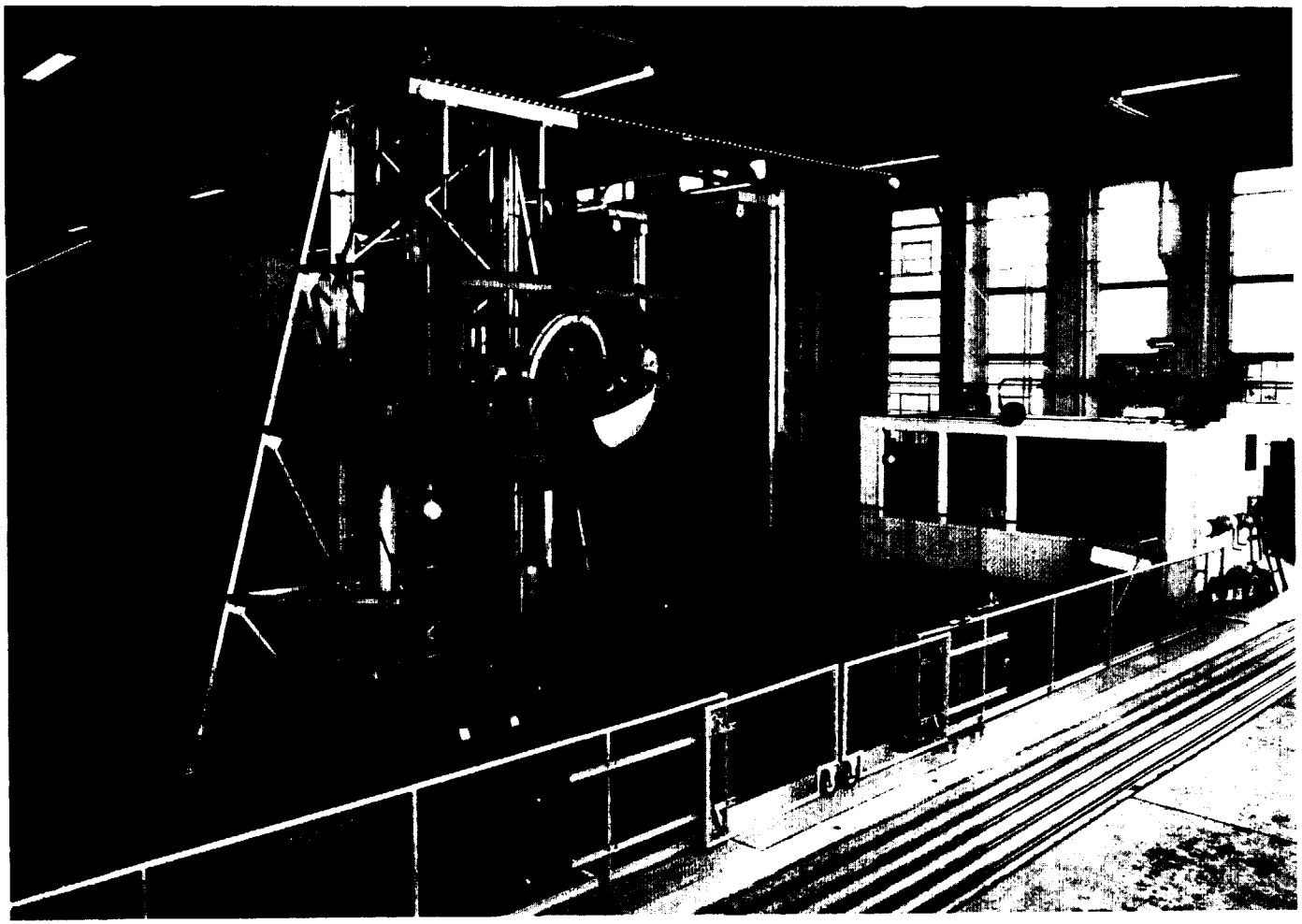

FIGURE 17. NASA-AMES 6-DEGREE FLIGHT SIMULATOR

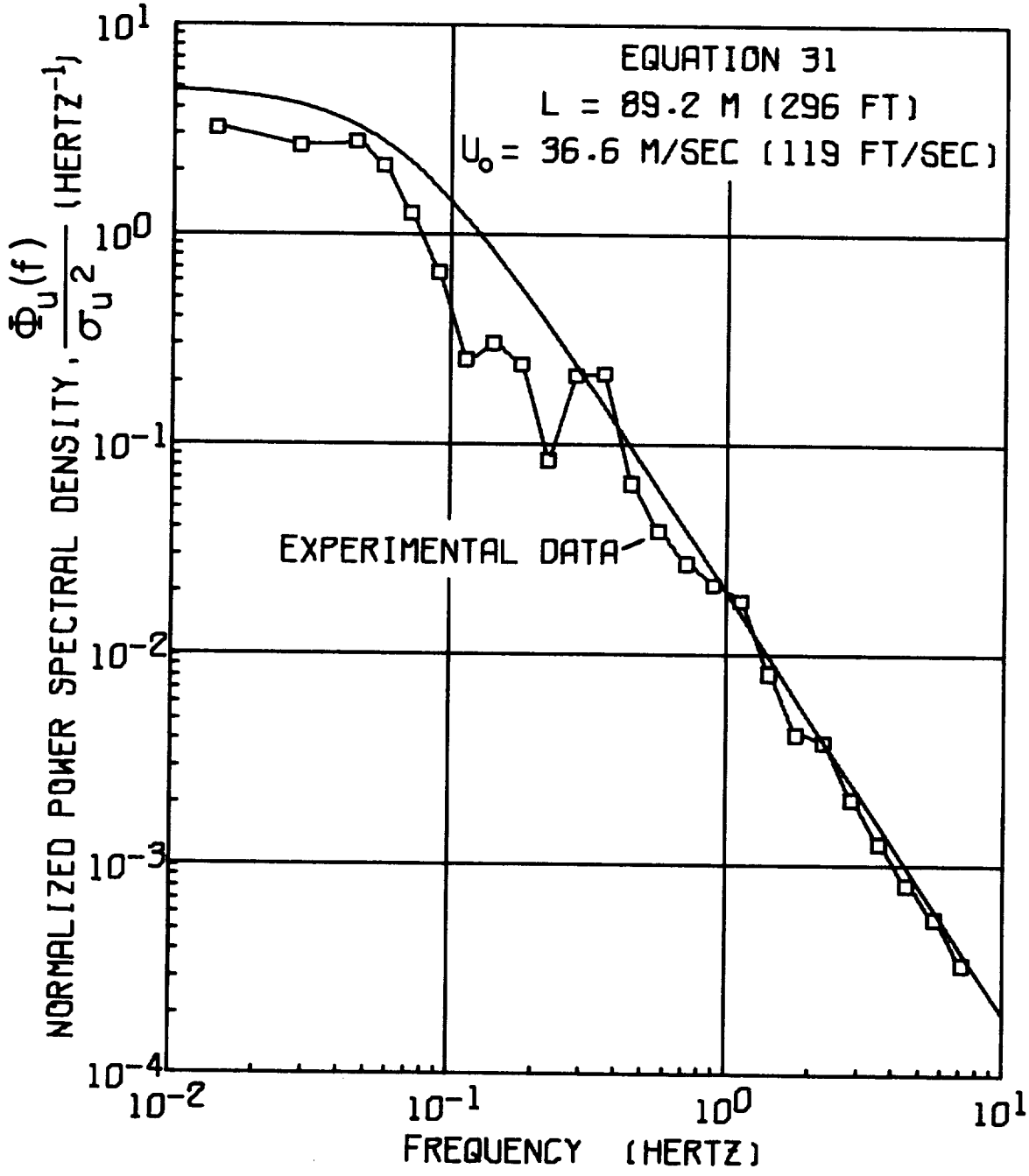


FIGURE 18. POWER SPECTRAL DENSITY OF EXPERIMENTALLY GENERATED LONGITUDINAL GUST COMPONENT

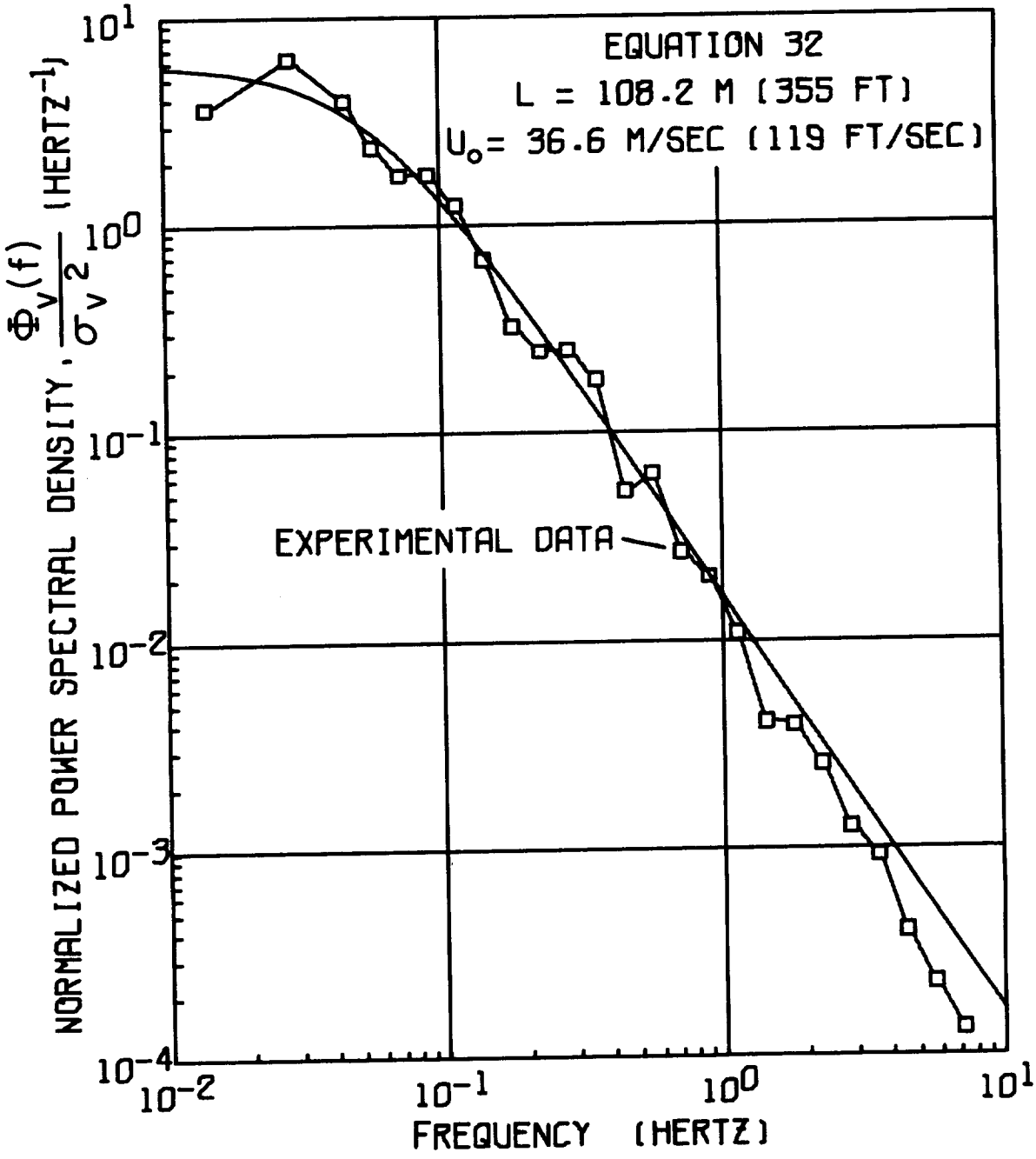


FIGURE 19. POWER SPECTRAL DENSITY OF EXPERIMENTALLY GENERATED LATERAL GUST COMPONENT

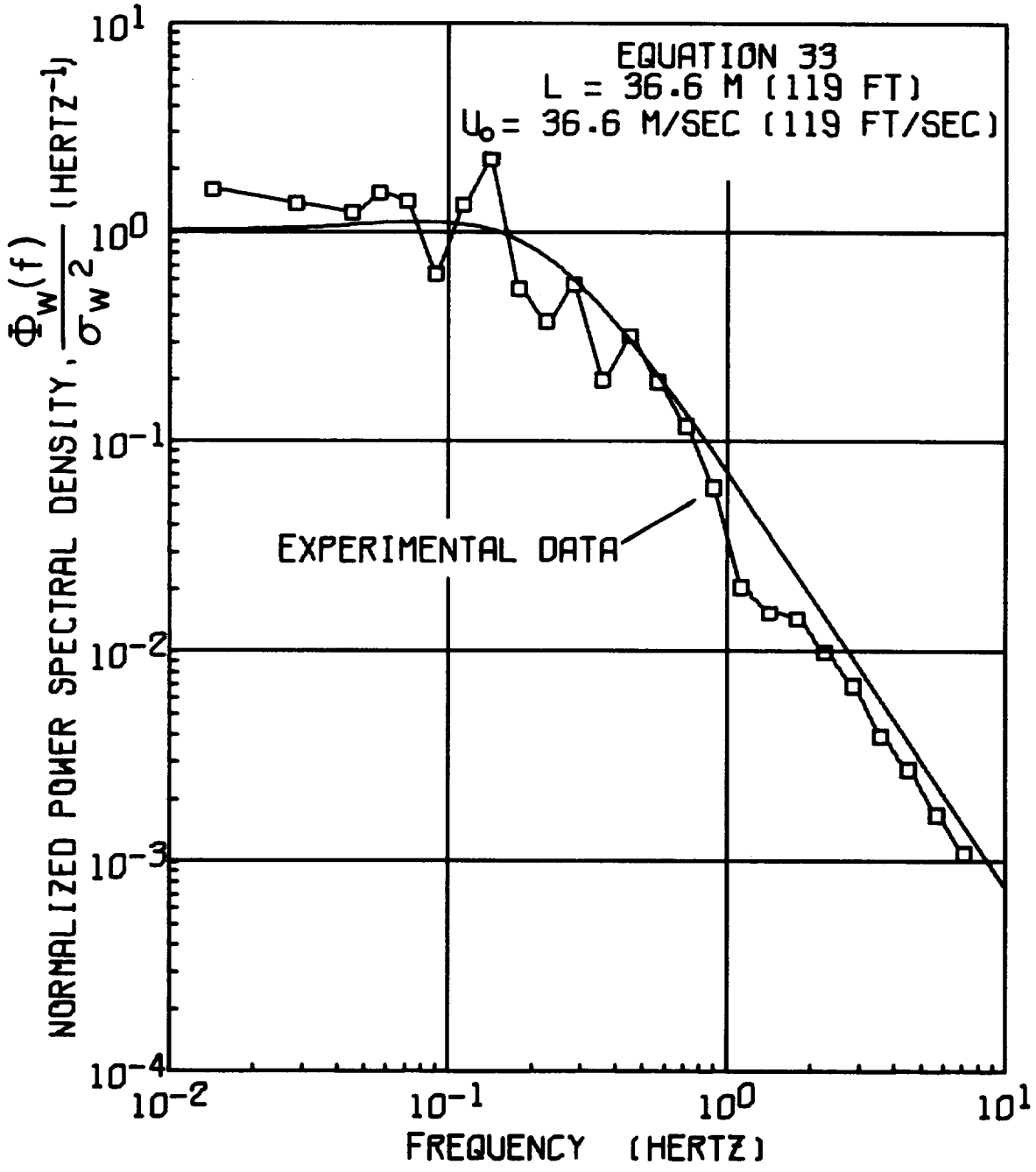


FIGURE 20. POWER SPECTRAL DENSITY OF EXPERIMENTALLY GENERATED VERTICAL GUST COMPONENT

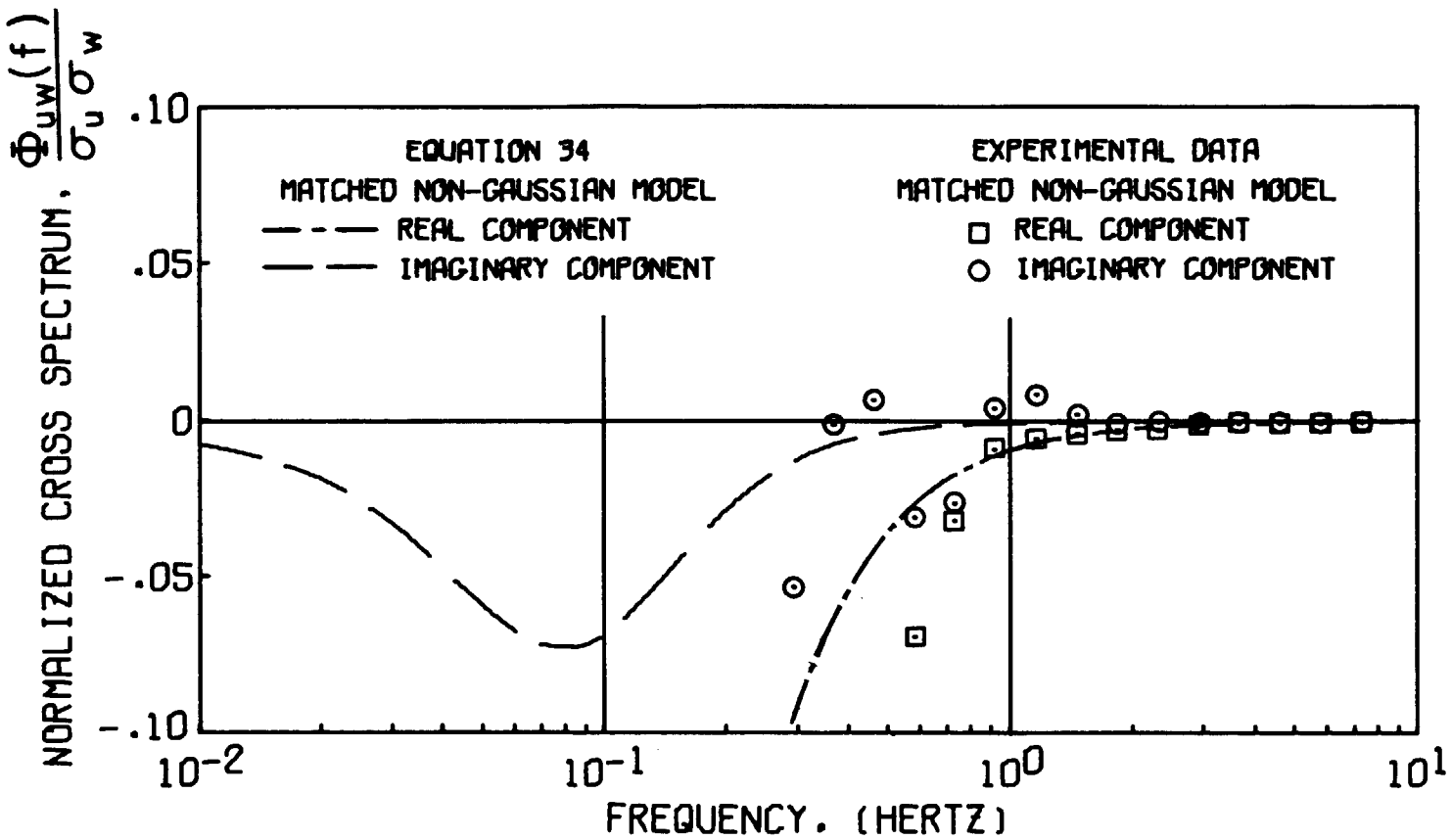


FIGURE 21. CROSS SPECTRAL DENSITY OF EXPERIMENTALLY GENERATED GUSTS (MATCHED NON-GAUSSIAN MODEL)

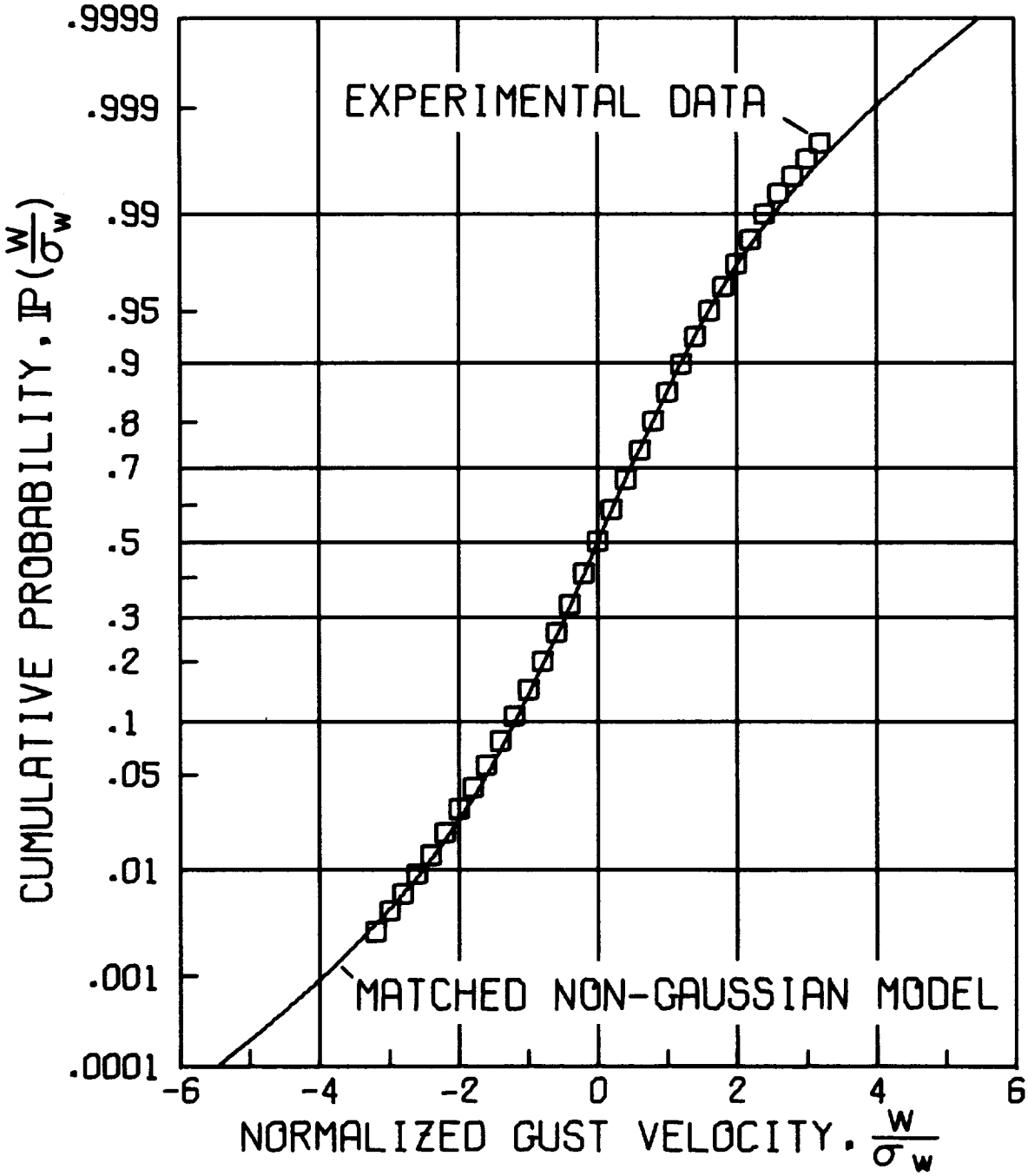


FIGURE 22. CUMULATIVE PROBABILITY DISTRIBUTION OF EXPERIMENTALLY GENERATED TURBULENCE

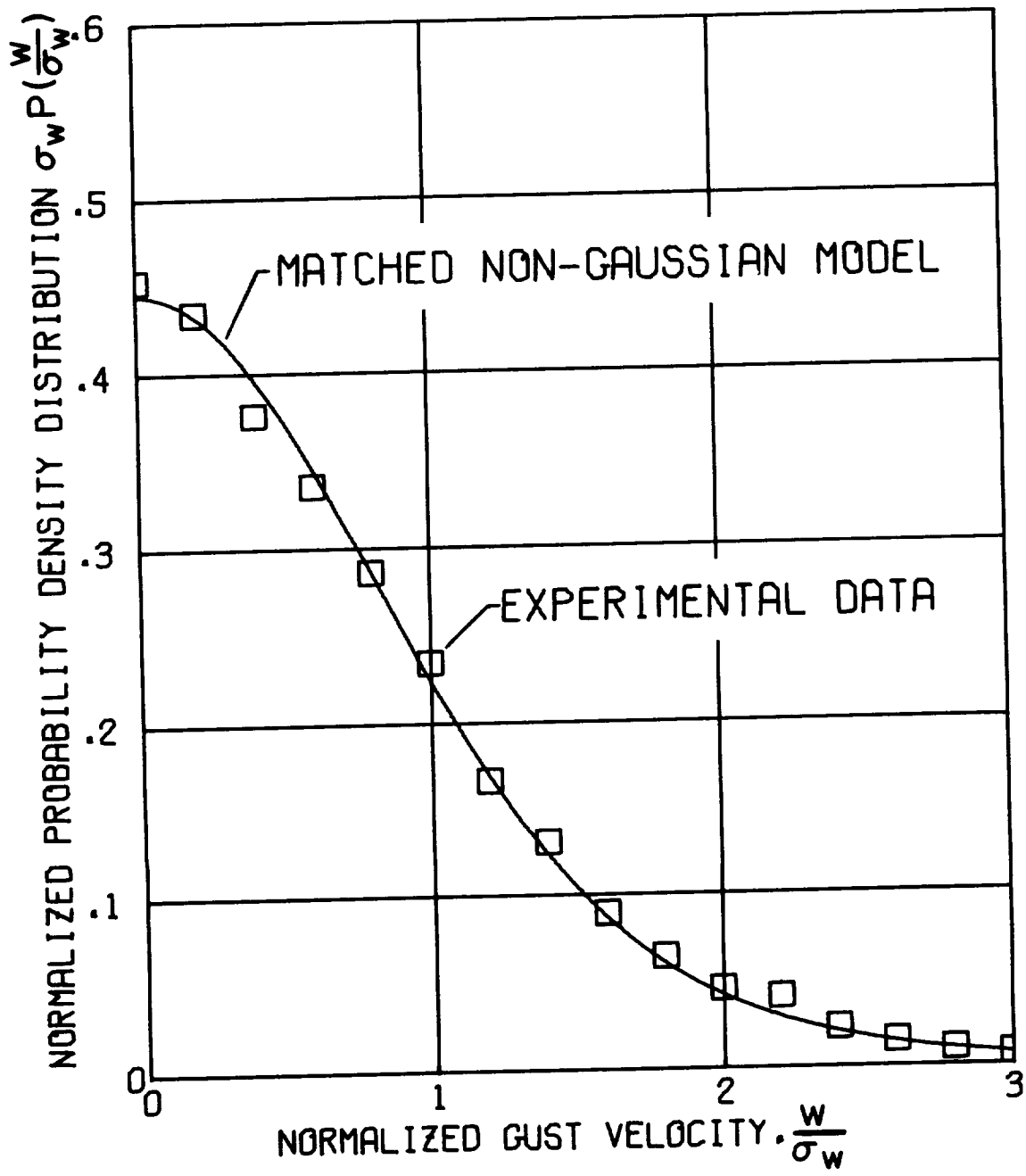


FIGURE 23. PROBABILITY DENSITY DISTRIBUTION OF EXPERIMENTALLY GENERATED TURBULENCE

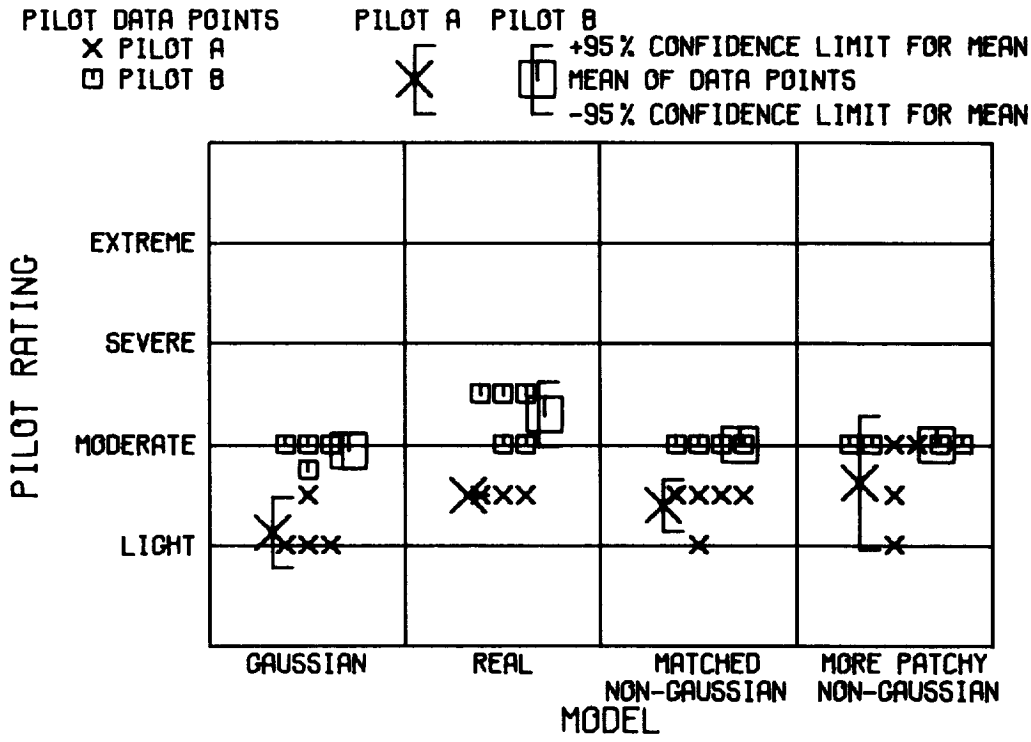


FIGURE 24. TURBULENCE INTENSITY

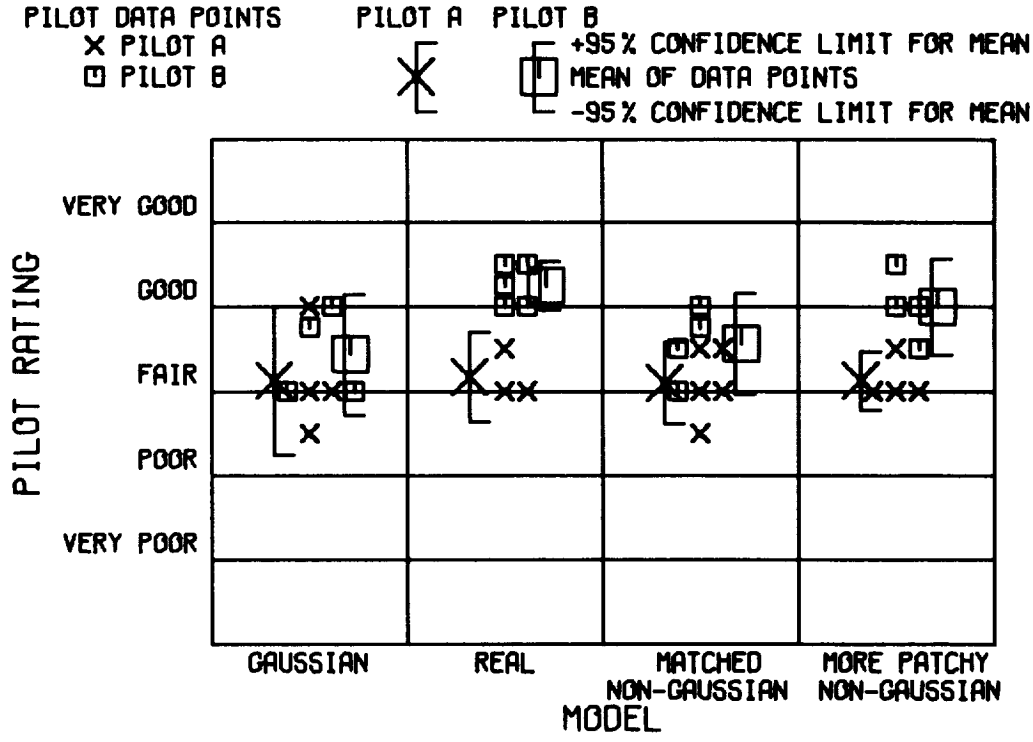


FIGURE 25. REALISM OF TURBULENCE

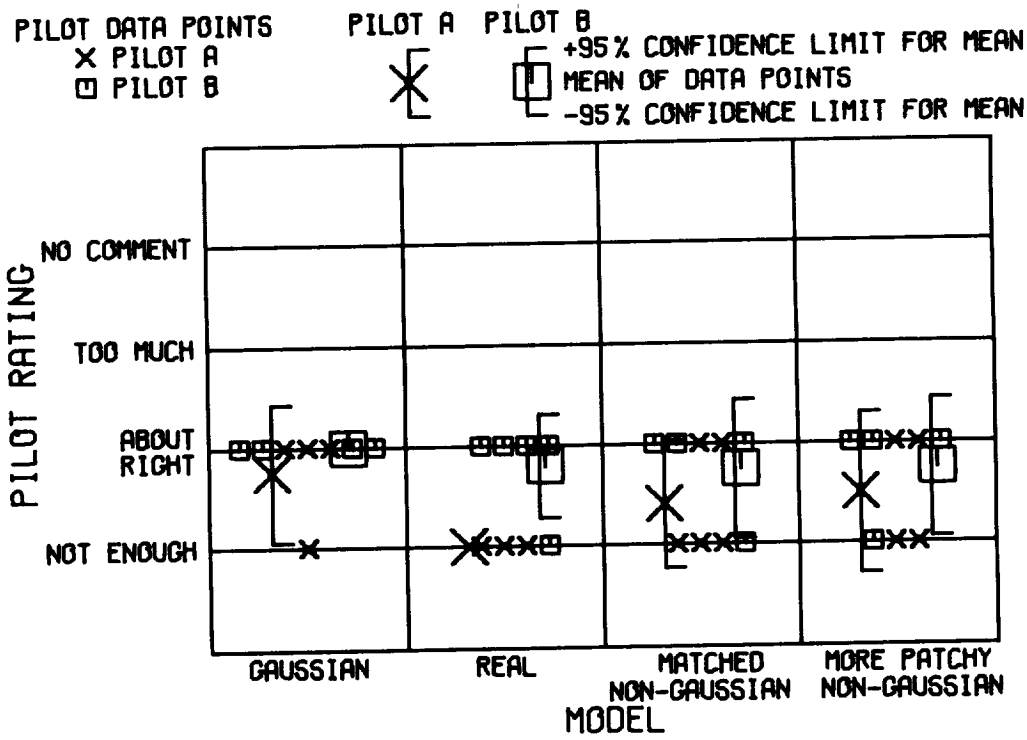


FIGURE 26. CORRECTNESS OF ROLL

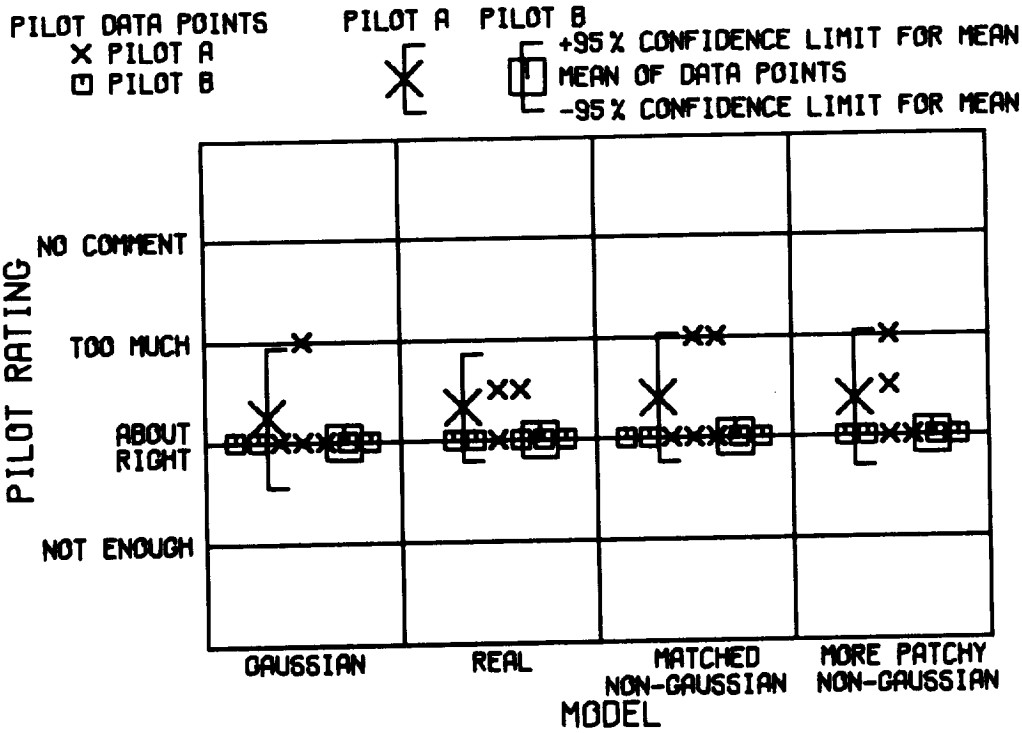


FIGURE 27. CORRECTNESS OF YAW

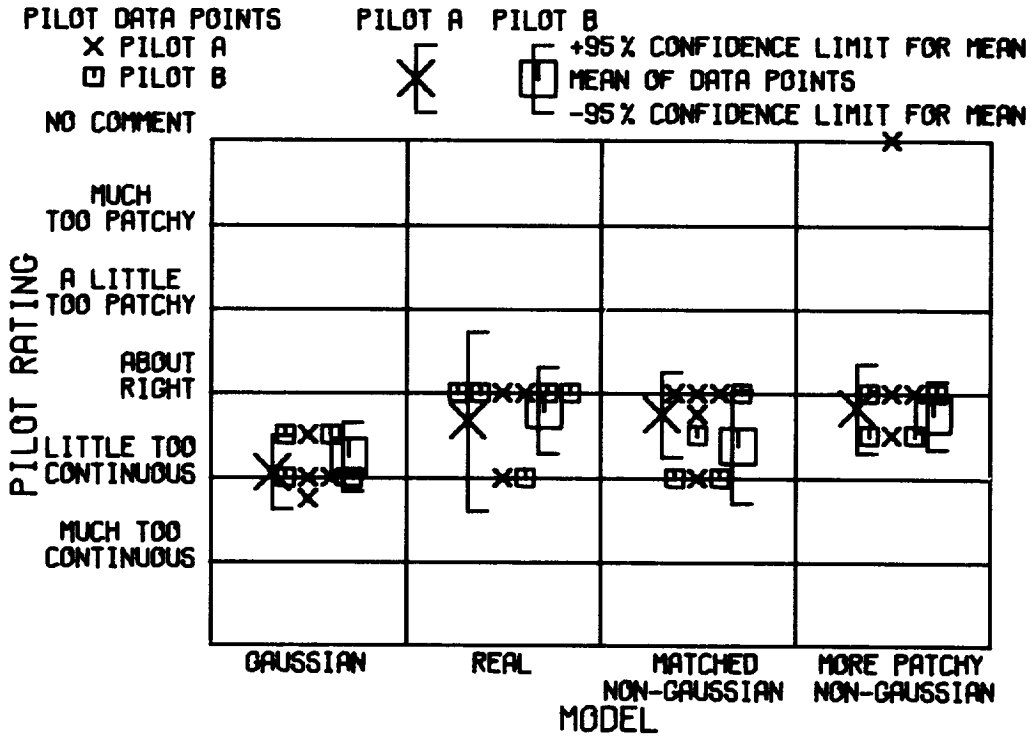


FIGURE 28. PATCHY CHARACTERISTICS

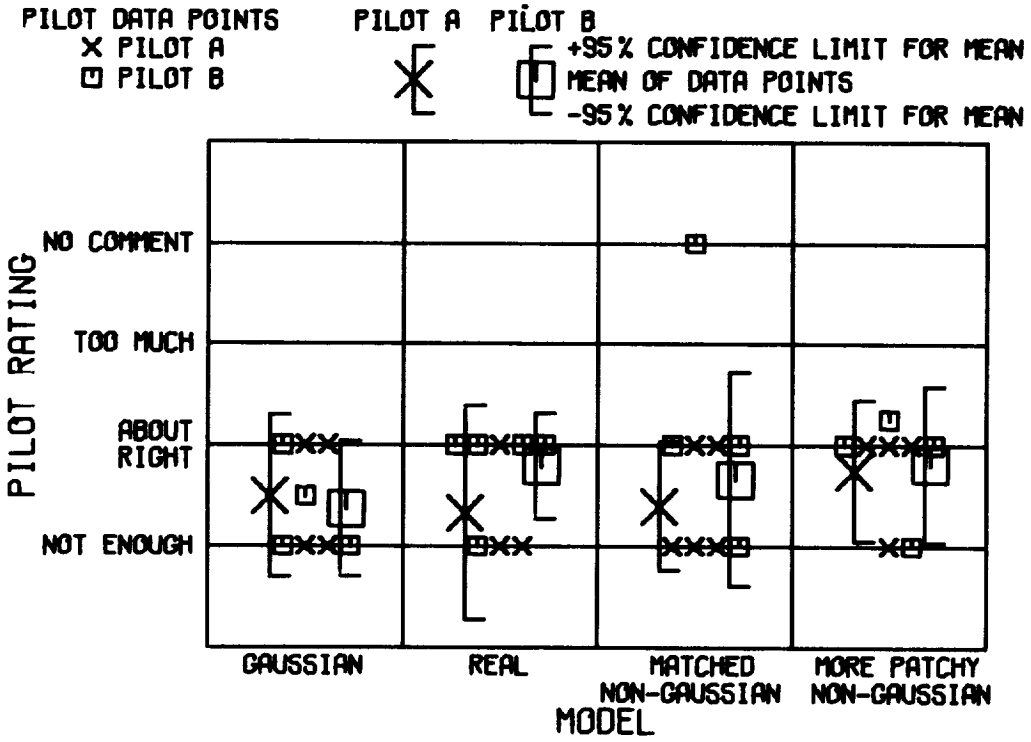


FIGURE 29. LOW FREQUENCY CONTENT

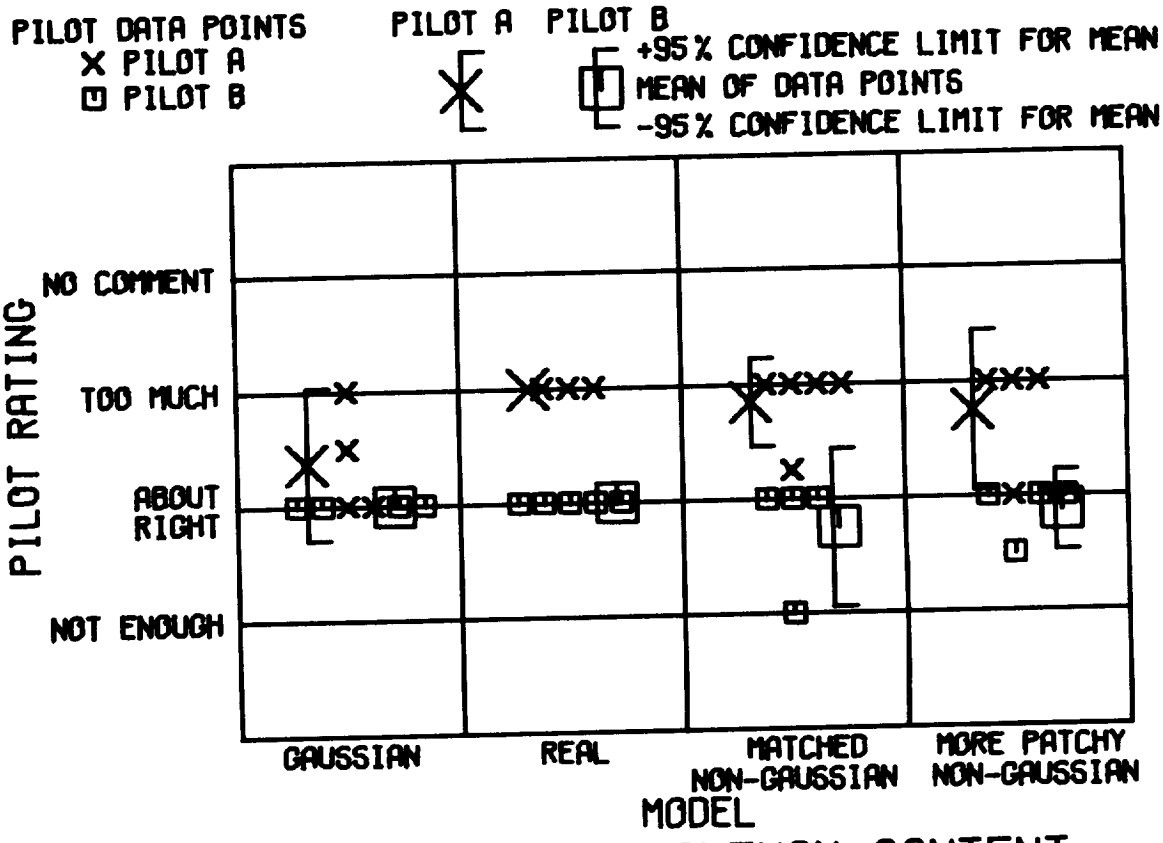


FIGURE 30. HIGH FREQUENCY CONTENT

# HANDLING QUALITIES RATING SCALE

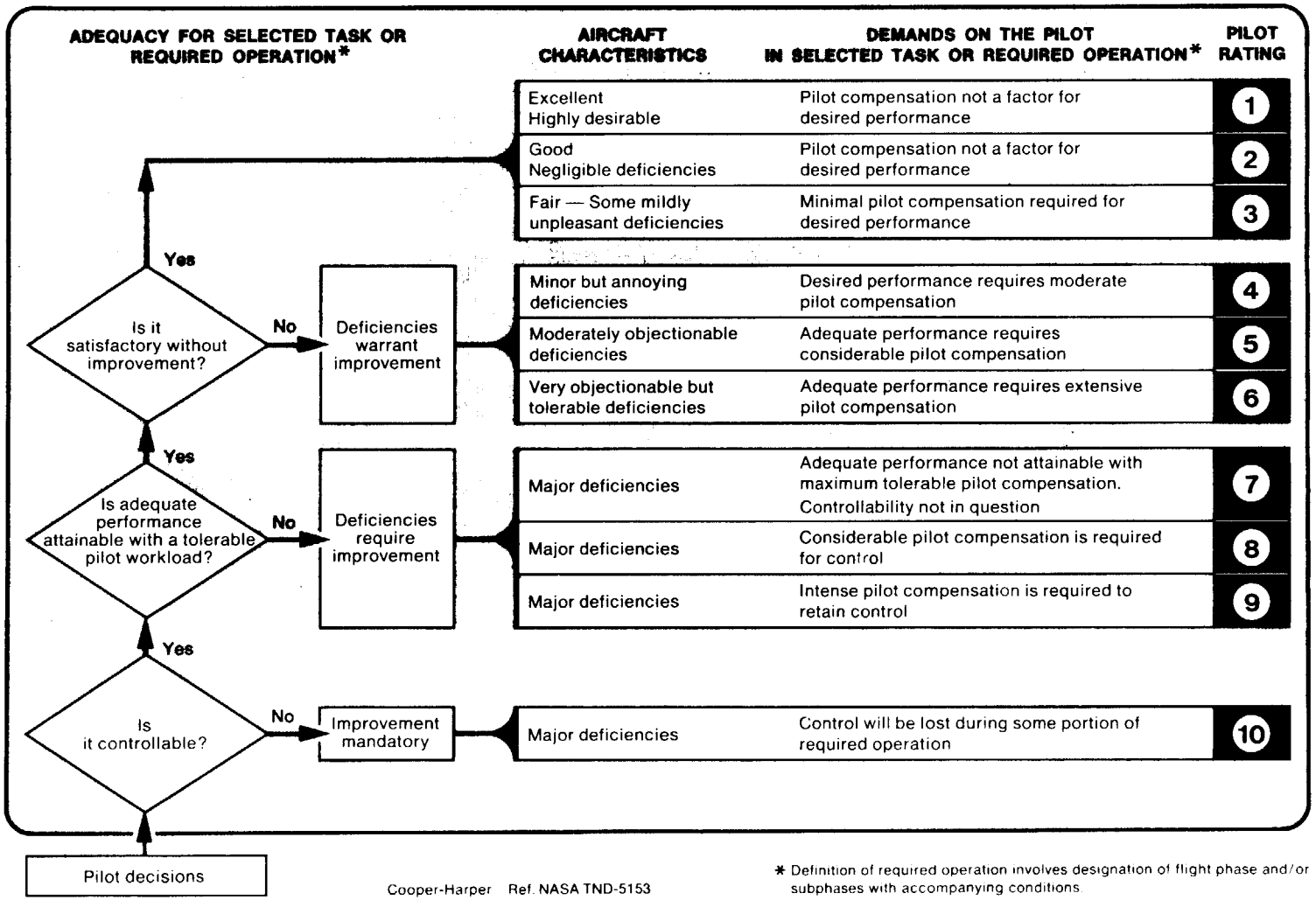


Cooper-Harper Ref. NASA TND-5153

* Definition of required operation involves designation of flight phase and/or subphases with accompanying conditions.

FIGURE 31. COOPER-HARPER PILOT RATING SCALE

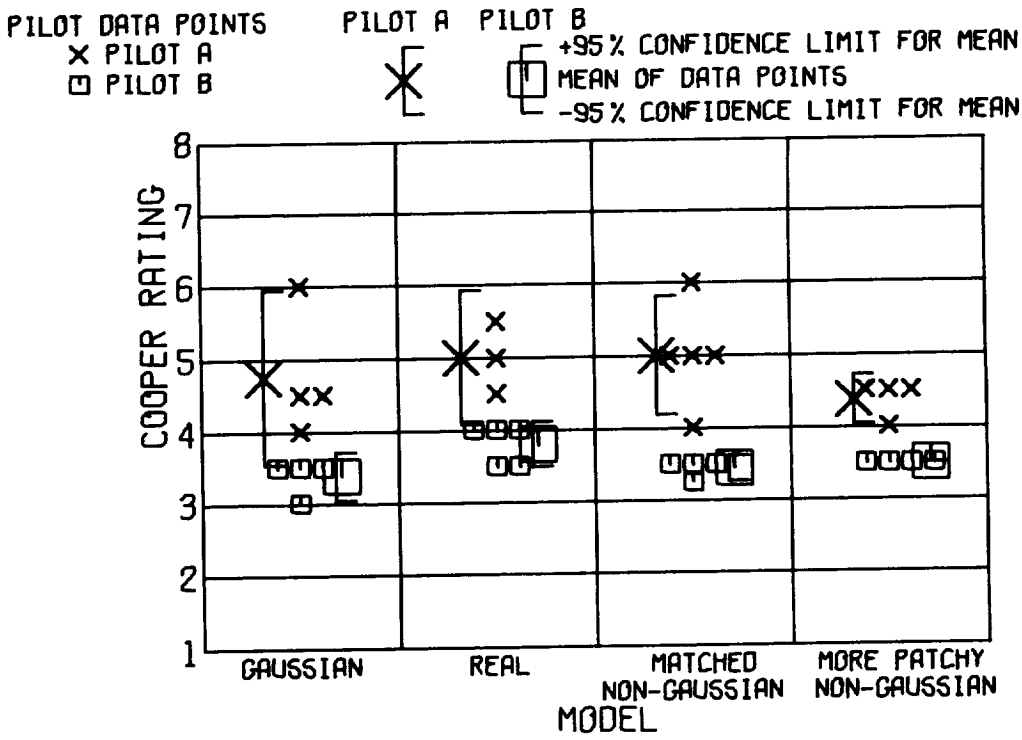


FIGURE 32. COOPER-HARPER RATING

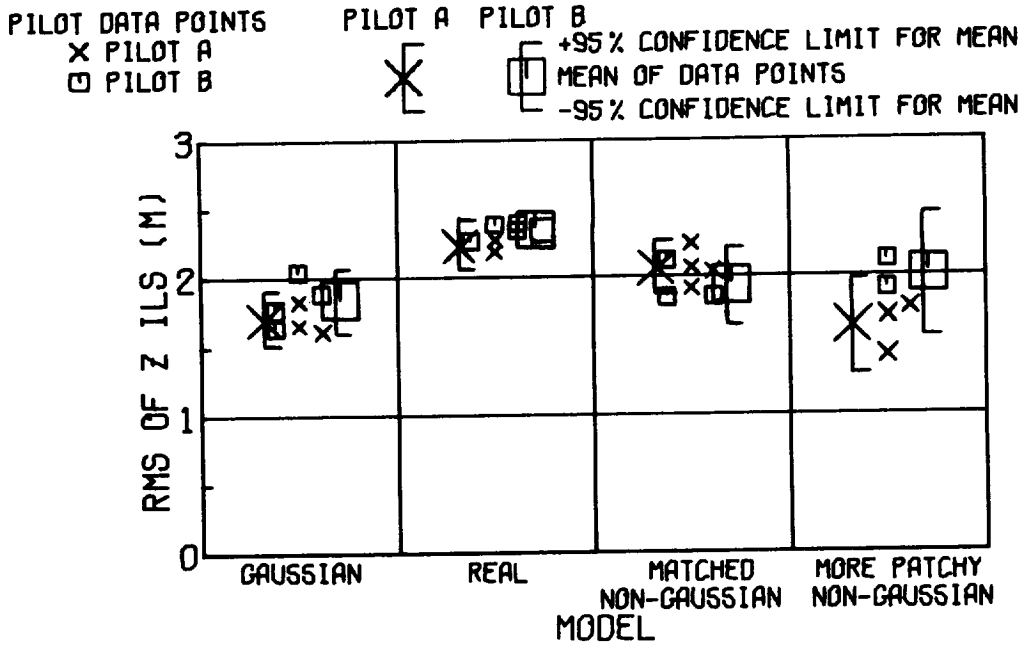


FIGURE 33. RMS OF Z ILS

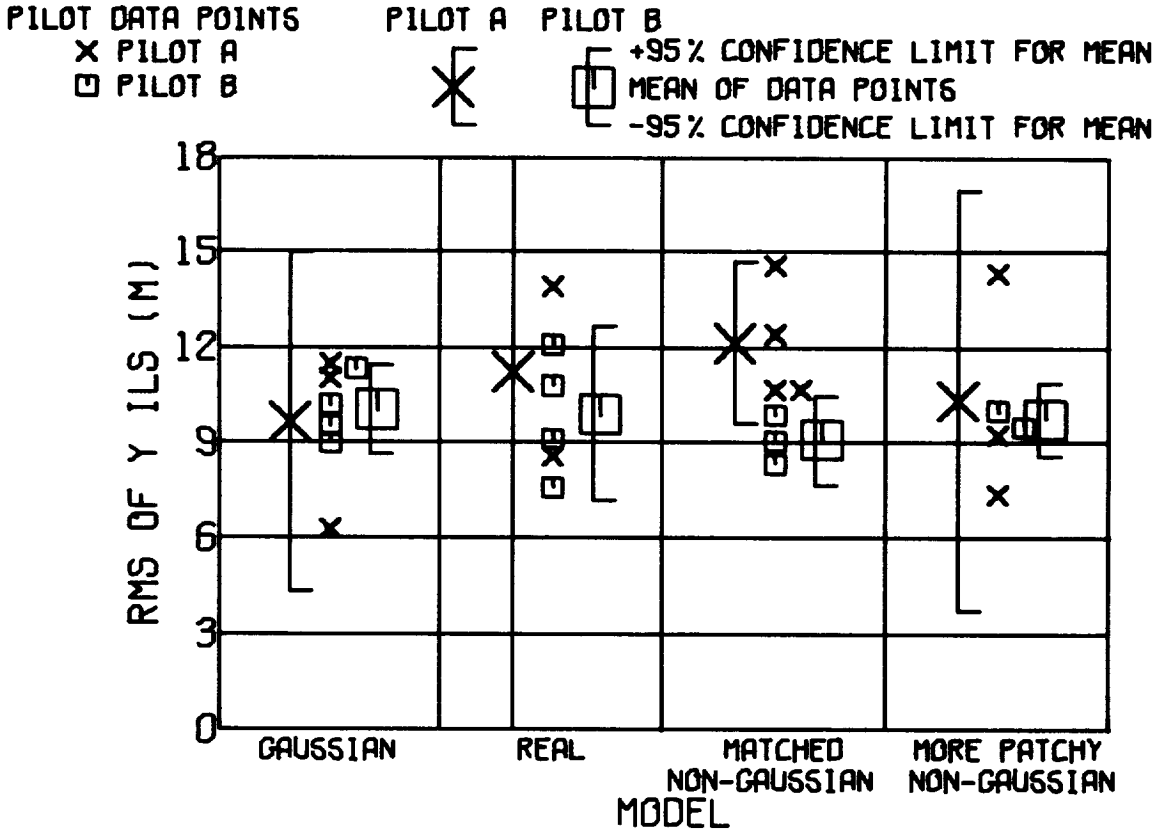


FIGURE 34. RMS OF Y ILS

# APPENDIX A

## DETAILED DESCRIPTION OF TURBULENCE SIMULATION

The purpose of this appendix is to describe in detail the turbulence simulation technique proposed in the main body of the preceding report. This discussion will be divided into six sections.

A brief review of the statistical properties which are to be simulated.

Discussion of turbulence simulation techniques now available and arguments leading to the technique proposed in this report.

A mathematical analysis of the system which generates the uncorrelated components of the turbulence simulation.

Analysis of correlation techniques by which the individual components of the turbulence simulation can be related.

Description of a coordinate rotation scheme by which the specific cross spectral densities needed for the flight simulator experiment of this report were produced.

Construction of a complete block diagram of the proposed turbulence simulation, and specialization of this general system to the three artificial turbulence models used in the flight simulator experiment of this report.

This appendix is intended to function as a self contained description of the proposed non-Gaussian turbulence simulation. It therefore contains symbols, illustrations, and references distinct from those of the preceding report.

## SYMBOLS

| | |
|---|---|
| a | random time history |
| b | random time history |
| c | random time history |
| $C_G$ | Gaussian correlation parameter |
| $C_K$ | modified Bessel Function correlation parameter |
| $C_{\ell_{ug}}$ | non-dimensional rolling moment induced by longitudinal gust component distributed along wing span |
| $C_{\ell_{wg}}$ | non-dimensional rolling moment induced by vertical gust component distributed along wing span |
| $C_{uw}$ | cross correlation of u and w gust components |
| d | random time history |
| erf | error function |
| E | expected value operator |
| f | frequency (hertz) |
| F | Fourier transform operator |
| $g_j$ | impulse response of linear filter $G_j$ |
| $G_j$ | linear filter with transfer function $G_j(s)$ |
| $h_j$ | impulse response of linear filter $H_j$ |
| $H_j$ | linear filter with transfer function $H_j(s)$ |
| i | $\sqrt{-1}$ |
| j | integer |
| $K_j$ | power spectral density of white noise source $\eta_j$ in units of (output variable)$^2$/hertz |
| $K_o$ | modified Bessel function of second type, order zero |

$L_j$ scale length of the $j^{th}$ gust component ( m )

$M_j$ $j^{th}$ normalized central moment of a random process defined by the equation

$$M_j = \lim_{T\to\infty} \frac{1}{2T} \int_{-T}^{T} \left[\frac{x(t)-(\text{mean value of } x)}{\sigma_x}\right]^j dt$$

n integer

$N_i$ Gaussian white noise process

P probability density distribution

$\mathbb{P}$ cumulative probability distribution

R ratio of modified Bessel process standard deviation to Gaussian process standard deviation (see eq. A-30)

s Laplace variable

t time (sec)

u gust component in direction of mean wind relative to surface ( m /sec), also denotes simulated turbulence time history

u´ longitudinal gust component in vehicle coordinates ( m /sec)

$u_o$ mean true airspeed of vehicle ( m /sec)

v lateral gust component in earth-fixed coordinates ( m /sec) forming right hand system with u and w ( m /sec)

v´ lateral gust component in vehicle coordinates ( m /sec)

w vertical gust component in earth-fixed coordinates positive downward ( m /sec)

w´ vertical gust component in vehicle coordinates ( m /sec)

x random time history

$y$ random time history

$z$ random time history

$\gamma$ variable of integration

$\delta$ Dirac delta function

$\eta$ Gaussian white noise

$\lambda$ variable of integration

$\xi$ variable of integration

$\sigma_x$ standard deviation of the random process $x(t)$ (units of x)

$\tau$ correlation time increment (sec)

$\phi_x$ power spectral density of the random function $x(t)$ (units of $x^2$/hertz), $\phi_x$ is an even function of frequency, related to $\sigma_x$ by the equation

$$\sigma_x^2 = \int_{-\infty}^{\infty} \phi_x(f)\, df$$

$\phi_{xy}$ cross spectral density of random processes $X(t)$ and $Y(t)$ (units of XY/hertz), $\phi_{xy}$ is the Fourier transform of the cross correlation of X and Y

$\psi$ heading angle of vehicle relative to the mean wind in earth-fixed coordinates

$\binom{\eta}{\kappa}$ binomial coefficient

Operators:

$*$ convolution (see eq. A-45), the free variable of the convolution is denoted by a subscript

$\underline{\ }$ (underbar) complex conjugate

## Statistical Properties to be Simulated

The turbulence simulation described here consists of a linear filter array driven by Gaussian white noise generators. The output of this system consists of five simultaneously generated random time histories which are to be inputs to a flight simulator. These five time histories can be physically interpreted as follows.

1.) The longitudinal gust component (in earth-fixed coordinates, parallel to the mean wind) occurring at the vehicle center of gravity.

2.) The lateral gust component (in earth-fixed coordinates) occurring at the vehicle center of gravity.

3.) The vertical gust component (in earth-fixed coordinates) occurring at the vehicle center of gravity.

4.) The non-dimensional rolling moment of the vehicle (in body axes) due to the distribution of longitudinal gusts along the wing.

5.) The non-dimensional rolling moment of the vehicle (in body axes) due to the distribution of vertical gusts along the wing.

In addition to these five time histories, the vehicle yawing moments and gusts occurring at the tail surfaces are also required for a realistic flight simulation. Yawing moments due to the distribution of gusts along the wing are assumed to be directly proportional to the rolling moments (inputs 4 and 5 above) and therefore need not be explicitly generated by the turbulence simulation. Furthermore, it is assumed that some means is available to delay the gust components (inputs 1, 2, and 3 above) in order to provide gusts at the vehicle tail surfaces.

The time histories produced by the turbulence simulation are to model turbulence and its effects in a statistical sense. The statistical properties of interest in this report are the following.

1.) Power spectral density, the average frequency content.

2.) Cross spectral density, the average phase relationship between the frequency components of two time histories.

3.) Probability distribution, a description of the values assumed by a random time history and the probability of their occurrence.

4.) Patchiness, the tendency of turbulence to occur as patches of activity separated by regions of less intense motion.

Each of these four properties will now be discussed in detail.

Power Spectral Density of Artificial Turbulence.- The power spectral densities of the gusts at the vehicle center of gravity are a modified form of those suggested by H. L. Dryden (reference A-1).

$$\phi_u(f) = \frac{\sigma_u^2 L_u}{u_o} \frac{2}{\left[1 + \left(\frac{2\pi L_u f}{u_o}\right)^2\right]} \qquad \text{(A-1)}$$

$$\phi_v(f) = \frac{\sigma_v^2 L_v}{u_o} \frac{2}{\left[1 + \left(\frac{2\pi L_v f}{u_o}\right)^2\right]} \qquad \text{(A-2)}$$

$$\phi_w(f) = \frac{\sigma_w^2 L_w}{u_o} \frac{\left[1 + 3\left(\frac{2\pi L_w f}{u_o}\right)^2\right]}{\left[1 + \left(\frac{2\pi L_w f}{u_o}\right)^2\right]^2} \qquad \text{(A-3)}$$

These equations differ from those of Dryden in that the form of the lateral gust spectrum has been changed to a form similar to that describing the longitudinal component, and independent scale lengths have been assumed for each component. It is important to note that Dryden's equations were intended to represent only stationary, isotropic, homogeneous, and ergodic turbulence. The equations represented above are, in general, intended to represent non-stationary, non-isotropic, and non-homogeneous turbulence. In order to allow this generality the scale lengths, $L$, and standard deviations, $\sigma$, of equations (A-1) through (A-3) must be functions of altitude, atmospheric stability, vehicle heading relative to the mean wind, mean wind velocity, and any other variables which may affect the power spectra. Since the turbulence considered in this report is assumed to be stationary, homogeneous and ergodic, $L$ and $\sigma$ are taken to be constants in the particular turbulence models described here.

The power spectral densities of the rolling moments induced by the distribution of gusts along the wing are dependent upon the geometry of the vehicle as well as the characteristics of turbulence. Different spectra will be required for each vehicle to be simulated. (A technique for deriving these spectra is presented in reference A-2.) The particular spectra suitable for simulating the DHC-6 "Twin Otter" aircraft flying at an altitude of 76.2 m (250 ft.) above the surface in the landing configuration is

$$\Phi_{C_{\ell_{ug}}} = \frac{\sigma_u^2 (.004842)^2 [1 + .5513(2\pi f)^2][1 + .0515(2\pi f)^2]}{[1 + 1.5798(2\pi f)^2][1 + .0180(2\pi f)^2][1 + .0704(2\pi f)^2]^2}$$

$$\Phi_{C_{\ell_{wg}}} = \frac{\sigma_w^2 (.006331)^2 [1 + .5349(2\pi f)^2][1 + .0133(2\pi f)^2]}{[1 + 1.5401(2\pi f)^2][1 + .004628(2\pi f)^2][1 + .03894(2\pi f)^2]^2}$$

The dependence of these spectra upon the gust scale length and the vehicle airspeed has not been given as in equations (A-1) through (A-3) because these spectra were sufficient for the flight simulator experiment described in this report and further generalization was considered unnecessary. The simulation of a different vehicle or different operating conditions will require the derivation of new rolling moment spectra.

Cross Spectral Densities.- The cross correlation of gust components is typically neglected in turbulence simulations because explicit forms for cross spectra are usually not known and because the generation of cross spectra greatly complicates the simulation process. Cross spectra were considered necessary for the flight simulator experiment described in the main body of this report because its object was to compare the realism of turbulence simulations which differed only in their probability distributions and patchy characteristics. The matching of cross spectra was necessary in order to eliminate the correlation of turbulence components as a variable of the experiment.

The turbulence simulation described here produces a non-zero cross spectrum between the longitudinal and vertical gust components at the vehicle center of gravity. All other cross spectra are identically zero. The decision to correlate only the longitudinal and vertical gusts is based upon evidence presented by Elderkin (reference A-3) which indicates that only these components are correlated. It should be noted that

Elderkin's data were obtained from tower measurements. Different results might be obtained from airborne measurements taken while flying across the mean wind.

The cross spectral density chosen to relate the u and w gust components is based upon only a qualitative analysis of the data presented in reference A-3. The mathematical form is suggested by the method of cross correlation used.

$$\phi_{uw} = \frac{\sigma_u \sigma_w \sqrt{2}}{R^2+1} \left\{ \frac{2R^2}{C_K^2} \left(\frac{L_w}{u_o}\right) \left(\frac{L_u}{u_o}\right) \left[ \frac{[1+3(\pi C_K f)^2 - i(2\pi C_K f)]}{[1+(\pi C_K f)^2]^2} \right] \right.$$

$$\left. + \sqrt{\frac{L_u L_w}{u_o^2}} \left[ \frac{[1+i\sqrt{3}\ (2\pi \frac{L_w}{u_o})\ f]}{[1+i(2\pi \frac{L_w}{u_o} f)][1+(2\pi C_G f)^2]} \right] \right\} \qquad \text{(A-6)}$$

where $R$ , $C_K$ , and $C_G$ are arbitrary parameters satisfying the inequalities.

$$R > 0 \qquad \text{(A-7)}$$

$$C_K > \frac{2L_w}{u_o} \quad C_K > \frac{2L_u}{u_o} \qquad \text{(A-8)}$$

$$C_G > \frac{L_w}{u_o} \quad C_G > \frac{L_u}{u_o} \qquad \text{(A-9)}$$

The physical significance of these parameters in the simulation system will be described in a later section of this appendix.

Probability Distribution.- In this report, three methods of characterizing the probability distributions of turbulence will be used.

1.) Cumulative probability distribution.

2.) Probability density distribution.

3.) Normalized central moments.

Figures A-1 and A-2 present typical cumulative probability and probability density distributions of atmospheric turbulence from reference A-4. In both cases the result expected of a Gaussian process is also given for comparison. Note that atmospheric turbulence has more large and small gusts than a Gaussian process.

Another way to consider the probability distribution of a random process is through its moments. Table A-1 below compares the fourth and sixth normalized central moments of a typical turbulence time history with those expected from a Gaussian process. The higher values measured in real turbulence indicate an increased probability of large gusts. The real turbulence time history used in Table A-1 was a five minute sample from the LO-LOCAT data collection project (LO-LOCAT Phase 3, Test 1141).

TABLE A-1.- COMPARISON OF THE FOURTH AND SIXTH NORMALIZED CENTRAL MOMENTS OF ATMOSPHERIC TURBULENCE WITH THOSE OF A GAUSSIAN PROCESS

| | $M_4$ | $M_6$ |
|---|---|---|
| Atmospheric turbulence | 3.5 | 21.7 |
| Gaussian process | 3.0 | 15.0 |

The data presented above indicate, at least qualitatively, the non-Gaussian behavior of atmospheric turbulence. In view of the limited data available, no explicit form for the probability distribution will be suggested here. However, the turbulence simulation to be proposed in the next section of this appendix will be required to have a distribution with the general characteristics described above.

So far nothing has been said about the probability distribution of vehicle rolling moments, or possible differences in the distributions of the three gust components. In view of the limited data describing the gust distributions and the complete absence of data describing the rolling moments, all components of the turbulence simulation will be assumed to have the same probability distribution.

Patchy Characteristics.- There is no easily formulated statistical quantity representing the patchy nature of atmospheric turbulence. However, the existence of a patchy character can easily be observed in recordings of the gust time derivative. Figure A-3 compares a typical gust derivative time history with

that resulting from two of the artificial turbulence generation methods to be considered presently. Note that the turbulence time history has a clearly discernable patchy nature.

Not only should each component of the turbulence simulation have this characteristic, but examination of measured data shows that the patchiness is correlated for all three components. This correlation of patches will be discussed further below.

## Turbulence Simulation Techniques

In this section various methods of producing time histories with the statistical properties described above will be considered.

The Gaussian Simulation.- By far the most widely used turbulence simulation is the linearly filtered Gaussian white noise method. A block diagram of this system is shown in figure A-4. The technique is quite simple and consists of passing Gaussian white noise through a linear filter. The filter transfer function is chosen so as to produce an output with the power spectral density of turbulence. Proper choice of the transfer function allows virtually any power spectrum of practical interest to be produced. The spectra proposed in this report, equations (A-1) through (A-5), are easily generated. It is also possible to produce cross spectra between two or more components of the simulated turbulence. Thus the linearly filtered Gaussian white noise turbulence simulation can be used to accurately model the frequency characteristics of turbulence.

Unfortunately, this technique cannot reproduce the probabalistic nature of turbulence because the time histories which it produces are always Gaussian. As shown in figures A-1 and A-2 atmospheric turbulence is clearly non-Gaussian. Therefore the Gaussian model is unrealistic. The linearly filtered Gaussian white noise method also cannot model the patchy nature of turbulence. Figure A-3 compares the patchy characteristics of a Gaussian process with those of real turbulence. Note the complete absence of patches in the Gaussian time history. The frequency content of both time histories is the same, the different character of the Gaussian process is due entirely to the fact that it is Gaussian.

The Modified Bessel Simulation.- The patchy nature of atmospheric turbulence suggests that a simulation based upon the multiplication of two Gaussian processes may provide a realistic representation. The first process would represent constant intensity turbulence and the second would represent its time varying standard deviation. Figure A-5 presents a block diagram of such a system.

A turbulence simulation of this type has already been studied in reference A-5 where it is shown that this technique is capable of modeling the frequency content of turbulence just as is the Gaussian model described above. From the standpoint of probability distribution and patchy characteristics, however, the product of Gaussian processes appears to be too extreme. Figures A-6 and A-7 present the cumulative probability and probability density produced by this simulation. (The probability density function is proportional to the modified Bessel function of second type and order zero, hence the name "modified Bessel simulation.") Figure A-3 compares the patchy characteristics to those of the Gaussian simulation and real turbulence.

Notice that in all three figures (A-3, A-6, and A-7) the Gaussian and modified Bessel processes appear to "bracket" the behavior of real turbulence. The modified Bessel simulation produces more large gusts, more small gusts, and more severe patches than are found in real turbulence while the Gaussian simulation underestimates each of these. It therefore seems reasonable to propose a turbulence simulation which combines both the Gaussian and modified Bessel simulations. Figure A-8 shows the block diagram of such a system.

The statistical properties produced by the system of figure A-8 will be developed in the next section of this appendix. However, certain characteristics are immediately apparent and will be discussed here.

The random process $c(t)$ in figure A-8 is produced by the same system shown in figure A-5; it is therefore a modified Bessel process. Similarly, $d(t)$ is produced by the same system shown in figure A-4 and is therefore a Gaussian process. If the standard deviation of the Gaussian process is made much less than that of the modified Bessel process, $u(t)$ will become essentially modified Bessel in nature. On the other hand, if the standard deviation of $c(t)$ is made small relative to that of $d(t)$, the system output will become Gaussian. It is clear, therefore, that the proposed turbulence simulation is capable of producing either the Gaussian or the modified Bessel simulations as special cases. In general the system output will lie somewhere between these extremes.

## Statistical Analysis of Turbulence Simulation

A statistical analysis of one component of the proposed simulation (figure A-8) will now be presented. Expressions for the power spectral density and probability distributions of the system output will be derived. In figure A-8 recall that $\eta_1$, $\eta_2$, and $\eta_3$ are statistically independent Gaussian

white noise sources, and $G_1$ , $G_2$ , and $G_3$ are linear filters with transfer functions $G_1(s)$ , $G_2(s)$ , and $G_3(s)$ respectively. The time histories $a(t)$ and $b(t)$ are multiplied to produce $c(t)$ which is then summed with $d(t)$ to give the overall system output.

Power Spectral Density.- In order to derive an expression for $\Phi_u(f)$ it will first be necessary to consider the power spectra of $a(t)$ , $b(t)$ , $c(t)$ , and $d(t)$ . The well known relationship between the input and output power spectral densities of a linear filter with transfer function $G(s)$ is

$$\Phi_y(f) = |G(i2\pi f)|^2 \Phi_x(f) \qquad \text{(A-10)}$$

where $y(t)$ is the system output and $x(t)$ is the system input. If $x(t)$ is a white noise process then $\Phi_x$ is a constant, independent of $f$ . In this case the shape of $\Phi_y$ is determined entirely by the filter transfer function. In figure A-8, $a$ , $b$ , and $d$ are the responses of linear systems to white noise inputs. Denote the power spectral constants of the white noise sources $\eta_1$ , $\eta_2$ , and $\eta_3$ by $K_1$ , $K_2$ , and $K_3$ respectively. Then by application of equation (A-10) the power spectral densities of $a$ , $b$ , and $d$ are:

$$\Phi_a(f) = |G_1(i2\pi f)|^2 K_1 \qquad \text{(A-11)}$$

$$\Phi_b(f) = |G_2(i2\pi f)|^2 K_2 \qquad \text{(A-12)}$$

$$\Phi_d(f) = |G_3(i2\pi f)|^2 K_3 \qquad \text{(A-13)}$$

Next consider the power spectral density of $c(t)$ . It is proven in reference A-5 that if $z(t)$ is the product of statistically independent random processes $x(t)$ and $y(t)$ then the power spectral density of $z(t)$ is

$$\Phi_z(f) = \int_{-\infty}^{\infty} \Phi_x(\lambda)\ \Phi_y(f-\lambda)d\lambda \qquad \text{(A-14)}$$

In the present case $c(t)$ is the product of $a(t)$ and $b(t)$ .

Furthermore $a(t)$ and $b(t)$ are statistically independent because they are derived from statistically independent noise sources. Therefore the power spectral density of $c(t)$ is

$$\Phi_c(f) = \int_{-\infty}^{\infty} \Phi_a(\lambda)\ \Phi_b(f-\lambda)d\lambda \tag{A-15}$$

An expression for $\Phi_u$, the power spectral density of the system output, can now be given. The process $u(t)$ is the sum of $c(t)$ and $d(t)$. These two random time histories must be statistically independent because they are generated by statistically independent white noise sources. The power spectral density of a sum of independent random processes is merely the sum of their respective power spectra. Therefore

$$\Phi_u(f) = \Phi_c(f) + \Phi_d(f) \tag{A-16}$$

Substitution for $\Phi_c$ from eq. (A-15) and for $\Phi_a$, $\Phi_b$, $\Phi_d$ from eq. (A-11) through (A-13) gives

$$\Phi_u(f) = K_1K_2 \int_{-\infty}^{\infty} |G_1(i2\pi\lambda)|^2 |G_2[i2\pi(f-\lambda)]|^2 d\lambda + K_3|G_3(i2\pi f)|^2 \tag{A-17}$$

Equation (A-17) is a general expression for the power spectral density of the system output. Considerable simplification results if the filter transfer functions $G_1$, $G_2$, and $G_3$ are required to satisfy the condition

$$\frac{K_3|G_3(i2\pi f)|^2}{\sigma_d^2} = \frac{K_1K_2}{\sigma_a^2\sigma_b^2} \int_{-\infty}^{\infty} |G_1(i2\pi\lambda)|^2 |G_2(i2\pi(f-\lambda)|^2\, d\lambda \tag{A-18}$$

In this case the power spectral shape becomes invariant with respect to the standard deviations $\sigma_a$, $\sigma_b$, and $\sigma_d$. The expression for $\Phi_u$ becomes

$$\Phi_u(f) = (\sigma_a^2\sigma_b^2 + \sigma_d^2)\ \frac{K_3|G_3(i2\pi f)|^2}{\sigma_d^2} \tag{A-19}$$

Note that the shape of $\Phi_u$ is now determined entirely by the choice of $G_3$ just as in the linearly filtered Gaussian white noise turbulence simulation.

In the following it will always be assumed that the condition expressed by equation (A-18) is satisfied. Hence, equation (A-19) gives the power spectral density of the system output, $u(t)$ .

Probability Distribution.- When the linear filters of the system have been chosen so that condition (A-18) is satisfied, the shape of the output power spectral density is not influenced by changing the standard deviations of $c(t)$ or $d(t)$ . However, the probability distribution of the output is affected. Expressions for $P_u$ , $\mathbb{P}_u$ , and $M_n$ will now be derived.

1.) Probability Density Distribution, $P_u$ .

Consider again figure A-8. The white noise time histories $\eta_1$ , $\eta_2$ , and $\eta_3$ are, by definition, Gaussian. It is well known that when a Gaussian process is passed through a linear system it remains Gaussian. Therefore $a(t)$ , $b(t)$ , and $d(t)$ are Gaussian and the probability density of each is the familiar normal distribution.

$$P_a(x) = \frac{1}{\sigma_a\sqrt{2\pi}} \exp\left[-\frac{1}{2}\left(\frac{x}{\sigma_a}\right)^2\right] \qquad \text{(A-20)}$$

$$P_b(x) = \frac{1}{\sigma_b\sqrt{2\pi}} \exp\left[-\frac{1}{2}\left(\frac{x}{\sigma_b}\right)^2\right] \qquad \text{(A-21)}$$

$$P_d(x) = \frac{1}{\sigma_d\sqrt{2\pi}} \exp\left[-\frac{1}{2}\left(\frac{x}{\sigma_d}\right)^2\right] \qquad \text{(A-22)}$$

Now consider $P_c(x)$ . The time history $c(t)$ is the product of $a(t)$ with $b(t)$ . A derivation of the probability density distribution of a product is presented in reference A-5. The result is

$$P_c(x) = \int_0^\infty \left[P_a(\gamma)\ P_b\left(\frac{x}{\gamma}\right) + P_a(-\gamma)\ P_b\left(-\frac{x}{\gamma}\right)\right] \frac{d\gamma}{\gamma} \qquad \text{(A-23)}$$

In deriving an expression for $P_u(x)$ it is convenient to first find $\mathbb{P}_u(x)$, then obtain $P_u(x)$ by differentiation. By definition

$$\mathbb{P}_u(x) = \text{PROBABILITY } [u(t) \leq x] \tag{A-24}$$

In this case

$$u(t) = c(t) + d(t)$$

Therefore $\mathbb{P}_u(x)$ can be expressed symbolically as

$$\mathbb{P}_u(x) = \int_{-\infty}^{\infty} \text{PROBABILITY}\left[\text{AND } \begin{matrix} d(t) = \lambda \\ \text{SIMULTANEOUSLY} \\ c(t) \leq x-\lambda \end{matrix}\right] d\lambda \tag{A-25}$$

Since $c(t)$ and $d(t)$ are statistically independent, $\mathbb{P}_u(x)$ can be written

$$\mathbb{P}_u(x) = \int_{\lambda=-\infty}^{\infty} P_d(\lambda) \int_{\gamma=-\infty}^{x-\lambda} P_c(\gamma)\, d\gamma\, d\lambda \tag{A-26}$$

Differentiation of equation (A-26) with respect to $x$ gives $P_u(x)$

$$P_u(x) = \int_{-\infty}^{\infty} P_d(\lambda) P_c(x-\lambda)\, d\lambda \tag{A-27}$$

Substitution for $P_c$ from equation (A-20) gives

$$P_u(x) = \int_{\lambda=-\infty}^{\infty} \int_{\gamma=0}^{\infty} P_d(\lambda) \left[P_a(\gamma) P_b\left(\frac{x-\lambda}{\gamma}\right) + P_a(-\gamma) P_b\left(\frac{\lambda-x}{\gamma}\right)\right] \frac{d\gamma}{\gamma}\, d\lambda \tag{A-28}$$

Now substitute the expressions for $P_a$, $P_b$, and $P_c$ from equations (A-17), (A-18), and (A-19). Integrate with respect to $\lambda$ and make the substitutions

$$\xi = \frac{\gamma}{\sigma_a \sqrt{2}} \tag{A-29}$$

$$R = \frac{\sigma_a \sigma_b}{\sigma_d} \tag{A-30}$$

$$\sigma_u = [(\sigma_a \sigma_b)^2 + \sigma_d^2]^{1/2} \tag{A-31}$$

where $\sigma_u$ is the standard deviation of $u(t)$ and $R$ is the ratio of $\sigma_c$ to $\sigma_d$. The final result is

$$\sigma_u P_u \left(\frac{x}{\sigma_u}\right) = \frac{(1+R^2)^{1/2}}{\pi} \int_0^\infty \left[\frac{2}{1+2\xi^2 R^2}\right]^{1/2} \exp\left[-\xi^2 - \frac{1}{2}\left(\frac{x}{\sigma_u}\right)^2 \frac{(1+R^2)}{(1+2\xi^2 R^2)}\right] d\xi \tag{A-32}$$

This result is presented in normalized form so that the choice of $\sigma_u$ has no influence on the resulting curve. Note the presence of $R$ as a parameter of the equation and the absence of any dependence upon the filter transfer functions other than through $R$. Equation (A-29) is easily evaluated numerically, and results for various values of the standard deviation ratio $R$ are presented in figure A-9.

Note that $R$ is the ratio of $\sigma_c$ to $\sigma_d$ and recall that $d(t)$ is a Gaussian process while $c(t)$ is the product of Gaussian processes. It is shown in reference A-5 that the probability density of $c(t)$ is characterized by the modified Bessel function of second type and order zero, it is therefore called a Bessel function process. $R$ is the ratio of the "amounts" of these two processes used to generate $u(t)$. When $R$ is very large, $u(t)$ is composed almost entirely of the Bessel function process. Similarly, when $R$ is very small $u(t)$ is composed almost entirely of the Gaussian process. The curves of figure A-9 reflect this result.

2.) Cumulative Probability Distribution, $\mathbb{P}_u$

The cumulative probability distribution of the system output can be obtained from equation (A-32) by integration.

$$\mathbb{P}_u\left(\frac{x}{\sigma_u}\right) = .5 + \int_0^{x/\sigma_u} P_u\left(\frac{\gamma}{\sigma_u}\right) d\gamma \qquad \text{(A-33)}$$

Substitute for $P_u$ from equation (A-32), interchange the order of integration, and make the substitution for $\gamma$

$$\lambda = \gamma \frac{(1+R^2)^{1/2}}{(1+2\xi^2R^2)^{1/2}} \qquad \text{(A-34)}$$

The result is

$$\mathbb{P}_u\left(\frac{x}{\sigma_u}\right) = .5 + \frac{2}{\pi}\int_{\xi=0}^{\infty}\int_{\lambda=0}^{\frac{x}{\sigma_u}\left[\frac{1+R^2}{1+2\xi^2R^2}\right]^{1/2}} \exp(-\lambda^2)\exp(-\xi^2)\,d\lambda\,d\xi \qquad \text{(A-35)}$$

Integrate with respect to $\lambda$ and obtain the final result.

$$\mathbb{P}_u\left(\frac{x}{\sigma_u}\right) = .5 + \frac{1}{\sqrt{\pi}}\int_0^{\infty}\exp(-\xi)^2\ \mathrm{erf}\left[\frac{x\left(\frac{1+R^2}{2}\right)^{1/2}}{\sigma_u(1+2R^2\xi^2)^{1/2}}\right] d\xi \qquad \text{(A-36)}$$

where erf denotes the error function. Equation (A-36) is easily evaluated by standard numerical techniques. Results for various values of R are given in figure A-10.

3.) Normalized Central Moments, $M_n$.

The normalized central moments of the system output can be obtained from equation (A-32) by integration. Since the average value of u(t) is zero, its nth normalized central moment is given by

$$M_n = \int_{-\infty}^{\infty}\left(\frac{x}{\sigma_u}\right)^n P_u\left(\frac{x}{\sigma_u}\right) dx \qquad \text{(A-37)}$$

Substitute for $P_u$ from equation (A-32). Interchange the order of integration and integrate by parts to obtain

$$M_{n\ (n\ \text{even})} = \frac{2[(1)(3)\cdots(n-1)]}{\sqrt{\pi}\ (1+R^2)^{n/2}} \int_0^\infty [2\xi^2R^2+1]^{n/2} \exp(-\xi^2)\, d\xi \qquad \text{(A-38)}$$

$$M_{n\ (n\ \text{odd})} = 0 \qquad \text{(A-39)}$$

Integrate equation (A-38) to obtain

$$M_{n\ (n\ \text{even})} = \frac{[(1)(3)\cdots(n-1)]}{(1+R^2)^{n/2}} \sum_{j=0}^{n/2} \binom{n/2}{j} R^{n-2j} [(1)(3)\cdots(n-2j-1)] \qquad \text{(A-40)}$$

where $\binom{n/2}{j}$ denotes the binomial coefficient. The dependence of $M_n$ upon $R$ is illustrated for $M_4$ and $M_6$ in figure A-11.

Summary of Results for Individual Components.- Expressions defining the power spectral density and probability distribution of the suggested turbulence simulation components have been derived and are presented as equations (A-18), (A-19), (A-32), (A-36), and (A-40). The last three of these are also presented graphically in figures A-9, A-10, and A-11.

It is important to note that the shape of each component's power spectral density is determined only by the transfer functions of the filters used to generate that component. Similarly, the probability distribution is determined only by the standard deviation ratio $R$.

If it is not necessary to introduce cross correlations between the various components, the results presented above are sufficient to permit construction of a complete turbulence simulation. Each of the five components listed at the beginning of this appendix would be generated by a system of the type shown in figure A-8. The power spectrum and probability distribution of each would be determined by the above mentioned equations.

## Correlation of Components

The problem of correlating the components of the proposed turbulence simulation will now be considered. Two types of correlation are required, cross spectral densities and patch correlation.

Cross Spectral Densities.- This section discusses a technique by which a non-zero cross spectral density relating the u and w components of the turbulence simulation can be introduced. The method is taken from reference A-5 and consists essentially of generating these two time histories from statistically dependent white noise sources. It will be shown that this can be accomplished without altering the probability distribution or power spectral density of either component.

Consider the system of figure A-12. Note that the right hand side, enclosed by dashed lines, consists of two systems of the type shown in figure A-8. However, the Gaussian white noise sources have been replaced by the linear filters $H_i$ and noise sources $\eta_i$ appearing on the left of figure A-12. It is the purpose of these $H_i$ and $\eta_i$ to produce statistically dependent white noise time histories. If a set of transfer functions can be found such that the time histories denoted by $N_i(t)$ are Gaussian white noise, then all statements made in the previous section on Statistical Analysis regarding the two systems on the right hand side of figure A-12 remain true. In particular, the probability distributions and power spectral densities are unchanged. However, because the noise sources $\eta_1$ , $\eta_3$ , and $\eta_5$ are used in the generation of both $u(t)$ and $w(t)$ , these two time histories will now be correlated. It will first be shown that non-trivial choices of the filters $H_i$ are possible, then an expression for the resultant cross spectral density will be derived.

1.) Construction of Gaussian White Noise from Non-White Noise Processes

Consider the block diagram of figure A-13 which is taken from the top left corner of figure A-12. In that figure, $\eta_1$ and $\eta_2$ are independent Gaussian white noise sources. $H_1$ and $H_2$ are linear filters. Certain conditions must be placed on $H_1$ and $H_2$ such that $N_1(t)$ will be Gaussian white noise.

Recall that a Gaussian process remains Gaussian when passed through a linear filter. Furthermore, a sum of independent Gaussian processes is Gaussian. Hence $N_1(t)$ must be Gaussian.

Next consider the power spectral density of $N_1(t)$. Recall the expression relating the power spectral densities of the input and output of a linear system and note that the noise $\eta_1$ and $\eta_2$ are independent. Then the expression for $\Phi_{N_1}$ is

$$\Phi_{N_1}(f) = |H_1(i2\pi f)|^2 K_1 + |H_2(i2\pi f)|^2 K_2 \qquad \text{(A-41)}$$

where $K_1$ and $K_2$ are the power spectral constants of $\eta_1$ and $\eta_2$ respectively. Now require $N_1(t)$ to be white noise so that $\Phi_{N_1}$ is a constant

$$\Phi_{N_1} = K_{N_1} \qquad \text{(A-42)}$$

For simplicity require $K_1$ to equal $K_2$.

$$K_1 = K_2 \qquad \text{(A-43)}$$

Then (A-41) becomes

$$|H_1(i2\pi f)|^2 + |H_2(i2\pi f)|^2 = \frac{K_{N_1}}{K_1} \qquad \text{(A-44)}$$

The time history $N_1(t)$ will be Gaussian white noise if equations (A-43) and (A-44) are satisfied. Requiring each of the white noise sources of figure A-12 and each of the filter pairs $H_1 - H_2$ through $H_{11} - H_{12}$ to satisfy equations (A-43) and (A-44) will cause all of the $N_i(t)$ to be Gaussian white noise.

2.) Cross Spectral Density

The cross spectral density of $w(t)$ and $u(t)$ will now be computed. This will be done by first finding an expression for the cross correlation of $w$ and $u$, then Fourier transforming to obtain the cross spectral density.

In the time domain the response time history of a linear system is given by the convolution of its impulse response function with the input time history. In this report the convolution operator is denoted by an asterisk. Therefore the response of linear filter $H_1$ to the input $\eta_1(t)$ is given by

$$(\eta_1 * h_1)_t = \int_{-\infty}^{\infty} \eta_1(t-\lambda) h_1(\lambda) d\lambda \tag{A-45}$$

Note that convolution is associative.

$$[(\eta_1 * h_1) * g_1]_t = [\eta_1 * (h_1 * g_1)]_t = [\eta_1 * h_1 * g_1]_t \tag{A-46}$$

From figure A-12, expressions for $u(t)$ and $w(t)$ are:

$$w(t) = (\eta_1 * h_1 * g_1)_t + (\eta_2 * h_2 * g_2)_t + [(\eta_3 * h_3 * g_2)_t + (\eta_4 * h_4 * g_2)_t][(\eta_5 * h_5 * g_3)_t + (\eta_6 * h_6 * g_3)_t] \tag{A-47}$$

$$u(t) = (\eta_1 * h_7 * g_4)_t + (\eta_8 * h_8 * g_4)_t + [(\eta_3 * h_9 * g_5)_t + (\eta_{10} * h_{10} * g_5)_t][(\eta_5 * h_{11} * g_6)_t + (\eta_{12} * h_{12} * g_6)_t] \tag{A-48}$$

Now consider the cross correlation of these two time histories

$$C_{uw}(\tau) = E\{u(t)w(t+\tau)\} \tag{A-49}$$

Substitition of equations (A-47) and (A-48) into (A-49) leads to a lengthy expression containing many convolutions. This equation will not be reproduced here, but the method to be followed in reducing it to the final result will be explained. Write each convolution involving a white noise function in the same form as equation (A-45). Then each $\eta$ has a $t$ appearing in its argument. Now interchange the order of integration and

apply the expected value operator directly to the integrand. The expected value operates only on the time variable which appears only in the arguments of the white noise functions. Recall that

$$E\{\eta_i(t+A)\,\eta_j(t+B)\} = \begin{cases} 0 & \text{if } i \neq j \\ K_i\,\delta(A-B) & \text{if } i = j \end{cases} \qquad \text{(A-50)}$$

where $A$ and $B$ are arbitrary constants, $\delta$ is the Dirac delta function, and $K_i$ is the power spectral constant of the white noise source $\eta_i$. Finally, take the Fourier transform with respect to $\tau$, recalling the Fourier identities

$$F\{\int_{-\infty}^{\infty} x(t-\lambda)y(\lambda)d\lambda\} = X(f)Y(f) \qquad \text{(A-51)}$$

$$F\{\int_{-\infty}^{\infty} x(t+\lambda)y(\lambda)d\lambda\} = X(f)\underline{Y}(f) \qquad \text{(A-52)}$$

where $\underline{\ }$ denotes complex conjugate. The final result for $\Phi_{uw}(f)$ is

$$\begin{aligned}\Phi_{uw}(f) = {} & K_1[\underline{H_7}(i2\pi f)\underline{G_4}(i2\pi f)H_1(i2\pi f)G_1(i2\pi f)] \\ & + K_3K_5[H_3(i2\pi f)G_2(i2\pi f)\underline{H_9}(i2\pi f)\underline{G_5}(i2\pi f)]^* \\ & [H_5(i2\pi f)G_3(i2\pi f)\underline{H_{11}}(i2\pi f)\underline{G_6}(i2\pi f)]\end{aligned} \qquad \text{(A-53)}$$

This is the required expression for $\Phi_{uw}$. Note that of the 12 H filters present in the generating system of figure A-12 only the odd indexed $H_i$ appear in equation (A-53). These filters can be chosen subject only to the condition (A-44). Hence considerable generality has been obtained in the specification of a cross spectral density. It is of course quite difficult to find the appropriate $H_i$ such that $\Phi_{uw}$ matches some particular function which is of interest. This report follows the method of reference A-5 in selecting $H_i$ involving

arbitrary constants. The resulting expression for $\Phi_{uw}$ is not as general as equation (A-53), but does provide a relatively simple cross spectral shape with continuously adjustable parameters. This approach to the problem of cross spectra was completely adequate for the flight simulator experiment described in this report.

Patch Correlation.- In addition to the conventional cross spectral density discussed in the preceding section, another type of correlation called "patch correlation" must be considered. If the simulated turbulence is to have a patchy character, observed time histories show that when a patch is encountered the increased activity should appear in all of the turbulence components at the same time. In an effort to obtain this sort of correlation without altering the probability distribution, power spectral density, or cross spectral density of the components, the following approach was used. Only the u and w gust components will be discussed here, but a similar method can be applied to all components of the simulated turbulence. Unfortunately, this technique is only useful in the case of a digitally generated simulation.

Figure A-14 shows the cross correlated u and w gust components of the turbulence generator as in figure A-12, but with the noise sources $\eta_8$, $\eta_{10}$, and $\eta_{12}$ replaced by signal paths from $\eta_2$, $\eta_4$, and $\eta_6$. As before, the $\eta_i$ are independent Gaussian white noise sources. In a digital system these noise sources produce not continuous functions of time but uncorrelated, normally distributed random numbers. The $\pm 1$ operators represent random sign functions which take on the gain values plus unity or minus unity as each sample of turbulence is computed. Since successive samples of a white noise process are uncorrelated, these random sign functions alter neither the Gaussian nor the white noise nature of the inputs to $H_8$, $H_{10}$, and $H_{12}$. Furthermore, if $\eta_x$ and $\eta_y$ denote respectively the input and output of a random sign function, then $\eta_x$ and $\eta_y$ are independent in the sense that

$$E\{\eta_x \eta_y\} = E\{\eta_x\}E\{\eta_y\} = 0 \tag{A-54}$$

However, they are correlated in the sense that

$$E\{\eta_x^2 \eta_y^2\} = E\{\eta_x^4\} = E\{\eta_y^4\} \tag{A-55}$$

Equation (A-54) implies that the cross spectral density of u(t) and w(t) remains unchanged by this patch correlation technique. However, in view of equation (A-55), it is possible that large excursions of w(t) will tend to be accompanied by large excursions of u(t) . This has not been proven, but examination of sample time histories produced by the proposed turbulence simulation reveals that patches of activity do tend to appear on all components at the same time. It will be shown later how the above described procedure was extended to include all components of the simulation.

### Rotation of Coordinates to Provide Cross Spectra Relating Components Other Than u and w

The object of the flight simulator experiment described in the main body of this report was to compare the realism of several artificial turbulence models with that of actual atmospheric turbulence. The artificial models were to differ from the real turbulence only in their probability distributions, therefore it was necessary to eliminate as many other differences as possible. One of these was the cross spectra of the turbulence components.

The problem of cross spectra has already been discussed in the previous section of this appendix. However, the remarks made at that time referred to the gust components measured in an earth fixed coordinate system. Unfortunately, the real turbulence time histories used in the flight simulator experiment were all obtained in a vehicle fixed coordinate system. Since the data collecting aircraft could be flying at any heading relative to the mean wind direction, non-zero cross spectra relating components other than the longitudinal and vertical are possible.

There are two ways to match the cross spectra of the artificial models to those of the real time histories:

(1) fly the simulated vehicle at various headings relative to the mean wind, essentially modeling the manner in which the real turbulence data were obtained;

(2) rotate the coordinates in which the artificial models are generated so that the simulated vehicle heading remains constant.

The first of these methods would simplify the turbulence generation scheme, but would require different vehicle headings for each time history tested. This is undesirable from the standpoint of providing a uniform flight task for all models.

The second approach complicates the turbulence simulation but permits the same flight task to be used for evaluating each model. It is therefore the method adopted in this report.

Equations describing the influence of a coordinate rotation in the $u-v$ plane upon the spectra and cross spectra observed by the simulated vehicle will now be derived. Figure A-15 shows the geometry of the rotation. The gust components in the vehicle coordinate system are:

$$u' = u \cos \psi + v \sin \psi \tag{A-56}$$

$$v' = v \cos \psi - u \sin \psi \tag{A-57}$$

$$w' = w \tag{A-58}$$

The spectra and cross spectra of these components are:

$$\Phi_{u'} = \Phi_u \cos^2\psi + \Phi_v \sin^2 \psi \tag{A-59}$$

$$\Phi_{v'} = \Phi_v \cos^2\psi + \Phi_u \sin^2 \psi \tag{A-60}$$

$$\Phi_{w'} = \Phi_w \tag{A-61}$$

$$\Phi_{u'v'} = [\Phi_v - \Phi_u] \frac{\sin(2\psi)}{2} \tag{A-62}$$

$$\Phi_{u'w'} = \Phi_{uw} \cos \psi \tag{A-63}$$

$$\Phi_{v'w'} = -\Phi_{uw} \sin \psi \tag{A-64}$$

Using equations (A-59) through (A-64) it is possible to work backward from the known spectra and cross spectra of the real turbulence time histories in vehicle coordinates to a suitable set of spectra and a $u-w$ cross spectra in earth-fixed coordinates. Exact solutions are generally impossible because the six equations involve only five unknowns, but reasonable results may be obtained for certain spectra shapes, and this was possible

for the time histories used in this report. It should be emphasized that this procedure was necessary only because the objective of the flight simulation was to evaluate the realism of various turbulence models. The coordinate rotation used here would not be necessary in a typical flight simulator experiment.

## System Diagram and Specialization to Produce Specific Turbulence Models

The equations and techniques of the preceding sections have been applied to produce the complete system of figure A-16 and Table A-2. The results of reference A-5 have been used extensively.

The system shown is suitable only for digital generation techniques because of the random sign functions required by patch correlation. If these are eliminated the system could be used with an analog computer, but additional noise generators would be required in order to prevent unwanted cross correlations.

The coordinate rotation applied to the u and v gust components follows the method suggested in the previous section on "Rotation of Coordinates". This rotation is necessary only for the specific experiment described in this report and is not required for a typical flight simulation.

The proposed turbulence simulation can be simplified greatly if the $u-w$ cross correlation is not required. In this case only the filters enclosed by the dashed lines in figure A-16 are required.

The five output time histories of the complete system have the frequency and probability characteristics described previously in this appendix. However the scale lengths, cross correlation parameters, and coordinate rotation angles required to model the real time histories used in the flight simulator experiment have not been specified. These parameters are tabulated in Table A-3 for the two LO-LOCAT time histories used in this report.

TABLE A-2.- TRANSFER FUNCTIONS OF FIGURE A-16

$$G_1(s) = \frac{\sqrt{\frac{A_3}{K_3}} \quad (1 + \frac{2L_w s}{u_o})}{(1 + C_K s)}$$

$$G_2(s) = \frac{s\sqrt{\frac{A_3}{K_4}\left[C_K^2 - (\frac{2L_w}{u_o})^2\right]}}{(1 + C_K s)}$$

$$G_3(s) = \frac{\frac{\sigma_w R \pi}{\sqrt{1+R^2}} (\frac{L_w}{u_o})^2 \quad 16\sqrt{\frac{2}{C_1 A_3}}}{(1 + \frac{2L_w s}{u_o})}$$

$$G_4(s) = \frac{-\sqrt{\frac{A_6}{K_5}} (1 + \frac{2L_w s}{u_o})^2}{(1 + C_K s)^2}$$

$$G_5(s) = \frac{s\sqrt{\frac{A_6}{K_6}}\{\sqrt{2\ C_K^2 - (\frac{2L_w}{u_o})^2} + s\sqrt{C_K^4 - (\frac{2L_w}{u_o})^4}\}}{(1 + C_K s)^2}$$

$$G_6(s) = \frac{\frac{s}{2\pi}\sqrt{\frac{C_1}{A_6}}}{(1 + \frac{2L_w s}{u_o})^2}$$

$$G_7(s) = \frac{s\sqrt{\frac{A_9}{K_2}\left[C_G^2 - \left(\frac{L_w}{u_o}\right)^2\right]}}{(1 + C_G s)}$$

$$G_8(s) = \frac{-\sqrt{\frac{A_9}{K_1}}\left(1 + \frac{L_w s}{u_o}\right)}{(1 + C_G s)}$$

$$G_9(s) = \frac{\sigma_w\sqrt{\frac{L_w}{A_9 u_o (1+R^2)}}\left(1 + \sqrt{3}\,\frac{L_w s}{u_o}\right)}{\left(1 + \frac{L_w s}{u_o}\right)^2}$$

$$G_{10}(s) = \frac{\sqrt{\frac{A_{12}}{K_1}}\left(1 + \frac{L_u s}{u_o}\right)}{(1 + C_G s)}$$

$$G_{11}(s) = \frac{s\sqrt{\frac{A_{12}}{K_2}\left[C_G^2 - \left(\frac{L_u}{u_o}\right)^2\right]}}{(1 + C_G s)}$$

$$G_{12}(s) = \frac{\sigma_u\sqrt{\frac{2L_u}{A_{12} u_o (1+R^2)}}}{\left(1 + \frac{L_u s}{u_o}\right)}$$

$$G_{13}(s) = \frac{\sqrt{\frac{A_{15}}{K_3}}\left(1 + \frac{2L_u s}{u_o}\right)}{(1 + C_K s)}$$

$$G_{14}(s) = \frac{s\sqrt{\frac{A_{15}}{K_4}\left[C_K^2 - \left(\frac{2L_u}{u_o}\right)^2\right]}}{(1 + C_K s)}$$

$$G_{15}(s) = \frac{\frac{4\sigma_u R L_u}{u_o}\sqrt{\frac{1}{C_2 A_{15}(1+R^2)}}}{\left(1 + \frac{2L_u s}{u_o}\right)}$$

$$G_{16}(s) = \frac{\sqrt{\frac{A_{18}}{K_5}}\left(1 + \frac{2L_u s}{u_o}\right)}{(1 + C_K s)}$$

$$G_{17}(s) = \frac{s\sqrt{\frac{A_{18}}{K_6}\left[C_K^2 - \left(\frac{2L_u}{u_o}\right)^2\right]}}{(1 + C_K s)}$$

$$G_{18}(s) = \frac{\sqrt{\frac{C_2}{A_{18}}}}{\left(1 + \frac{2L_u s}{u_o}\right)}$$

$$G_{19}(s) = \frac{\sigma_v\sqrt{\frac{2L_v}{K_1 u_o (1+R^2)}}}{\left(1 + \frac{L_v s}{u_o}\right)}$$

$$G_{20}(s) = \frac{4\sigma_v R \frac{L_v}{u_o}\sqrt{\frac{C_3}{(K_3+K_4)(1+R^2)}}}{\left(1 + \frac{2L_v s}{u_o}\right)}$$

$$G_{21}(s) = \frac{\sqrt{\frac{1}{C_3(K_5+K_6)}}}{\left(1 + \frac{2L_v s}{u_o}\right)}$$

$$G_{22}(s) = \frac{\sigma_u\ (0.004842)\,(1+0.7425s)\,(1+0.2270s)}{\sqrt{K_1(1+R^2)}\ (1+1.2569s)\,(1+0.1341s)\,(1+0.2653s)^2}$$

$$G_{23}(s) = \frac{\sigma_u R\sqrt{C_4}\ (.016219)}{\sqrt{(K_3+K_4)(1+R^2)}\ (1+4.3993s)}$$

$$G_{24}(s) = \frac{(1+0.2391s)\,(1+0.9324s)}{\sqrt{C_4(K_5+K_6)}\ (1+1.7596s)\,(1+0.1383s)\,(1+0.2823s)^2}$$

$$G_{25}(s) = \frac{\sigma_w\ (0.006331)\,(1+0.7314s)\,(1+0.1154s)}{\sqrt{K_1(1+R^2)}\ (1+1.2410s)\,(1+0.06803s)\ \ (1+.19733s)^2}$$

$$G_{26}(s) = \frac{\sigma_w R\sqrt{C_5}\ (.021162)}{\sqrt{(K_3+K_4)(1+R^2)}\ (1+4.3993s)}$$

$$G_{27}(s) = \frac{(1+0.1171s)\,(1+0.9166s)}{\sqrt{C_5(K_5+K_6)}\ (1+1.7286s)\,(1+0.0691s)\,(1+0.2065s)^2}$$

TABLE A-3.- FILTER COEFFICIENTS FOR SPECIFIC TURBULENCE SIMULATIONS

$A_i$ are arbitrary scaling factors, may be set equal to unity if desired

$K_i$ must be set equal to power spectral constant of corresponding white noise source $\eta_i$

$u_o$ = 36.02 m/sec (118 ft/sec) in all cases

$\sigma_u$ = .765 m/sec (2.51 ft/sec) in all cases

$\sigma_v$ = .832 m/sec (2.73 ft/sec) in all cases

$\sigma_w$ = .579 m/sec (1.90 ft/sec) in all cases

Models Based on Real Turbulence Sample from LO-LOCAT Test 1140, Condition 21, Category 412112

| | GAUSSIAN | MATCHED NON-GAUSSIAN | MORE PATCHY NON-GAUSSIAN |
|---|---|---|---|
| $L_u$ | 170.7 m (560 ft) | 170.7 m (560 ft) | 170.7 m (560 ft) |
| $L_v$ | 141.7 m (465 ft) | 141.7 m (465 ft) | 141.7 m (465 ft) |
| $L_w$ | 141.7 m (465 ft) | 141.7 m (465 ft) | 141.7 m (465 ft) |
| $C_G$ | 1.9 | 1.7 | 1.6 |
| $C_K$ | --- | 3.6 | 3.1 |
| $\psi$ (deg.) | 45 | 45 | 45 |

Models Based on Real Turbulence Sample from LO-LOCAT Test 1141, Condition 21, Category 413212

| | GAUSSIAN | MATCHED NON-GAUSSIAN | MORE PATCHY NON-GAUSSIAN |
|---|---|---|---|
| $L_u$ | 90.2 m (296 ft) | 90.2 m (296 ft) | 90.2 m (296 ft) |
| $L_v$ | 108.2 m (355 ft) | 108.2 m (355 ft) | 108.2 m (355 ft) |
| $L_w$ | 36.0 m (118 ft) | 36.0 m (118 ft) | 36.0 m (118 ft) |
| $C_G$ | 2.9 | 2.55 | 2.55 |
| $C_K$ | --- | 5.05 | 5.05 |
| $\psi$ (deg.) | 0 | 0 | 0 |

## REFERENCES


A-1. Dryden, H. L.: A Review of the Statistical Theory of Turbulence. Turbulence Classic Papers on Statistical Theory, Interstate Publishers, Inc. (New York), 1961.

A-2. Eggleston, J. M.; and Diederich, F. W.: Theoretical Calculation of the Power Spectra of the Rolling and Yawing Moments on a Wing in Random Turbulence. NACA Rept. 1321, 1957.

A-3. Elderkin, C. E.: Experimental Investigation of the Turbulence Structure in the Lower Atmosphere. Report BNWL-329, Battelle Northwest, Dec. 1966.

A-4. Dutton, J. A.; and Deaven, D. G.: Some Observed Properties of Atmospheric Turbulence. Statistical Models and Turbulence. Vol. 12 of Lecture Notes in Physics, Springer-Verlag, 1972, pp. 352-383.

A-5. Reeves, P. M.: A Non-Gaussian Turbulence Simulation. Tech. Report AFFDL-TR-69-67, Air Force Flight Dynamics Laboratory, Air Force Systems Command, Wright Patterson Air Force Base, Ohio, Dec. 1969.

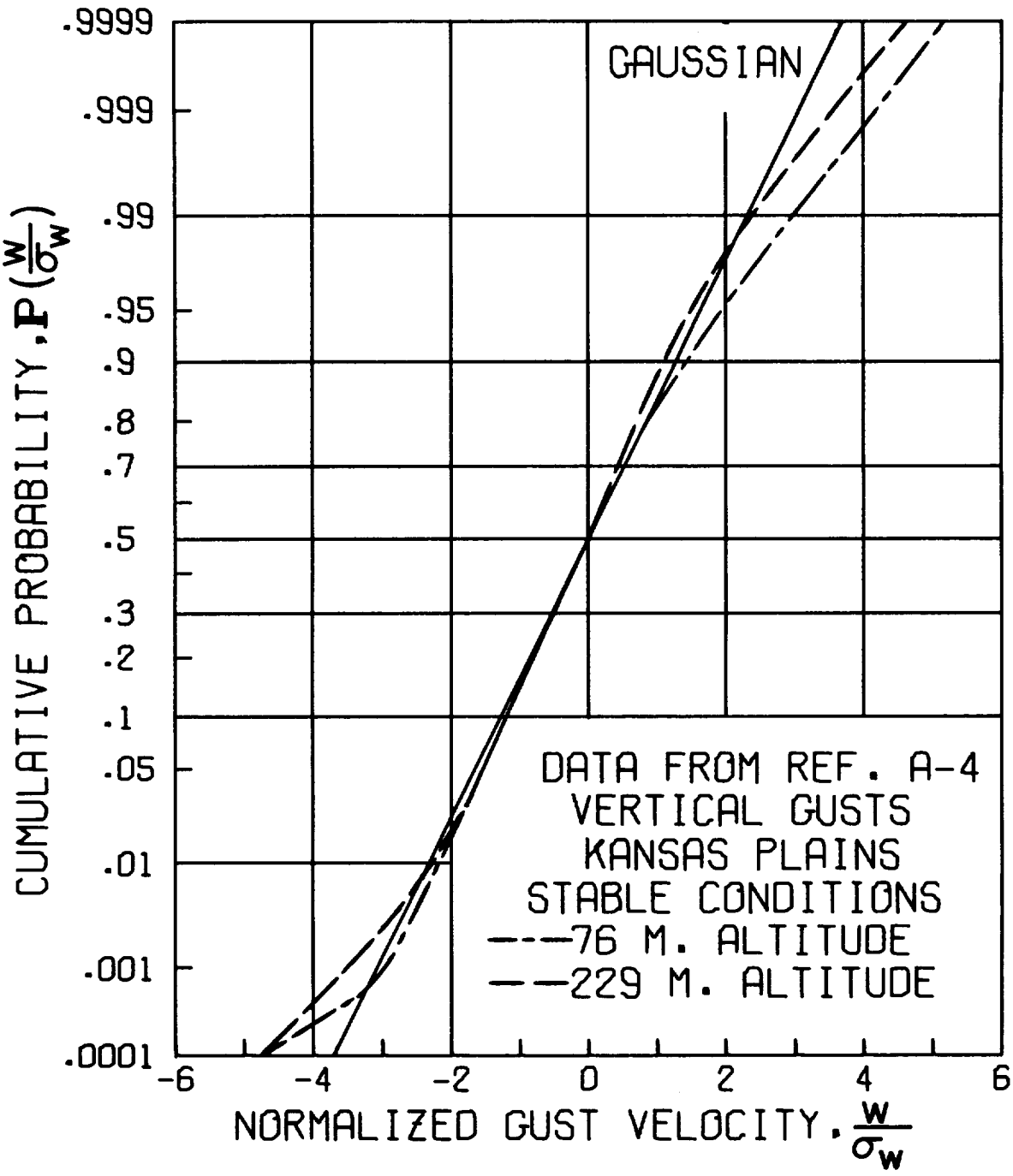


FIGURE A-1. TYPICAL CUMULATIVE PROBABILITY DISTRIBUTIONS OF ATMOSPHERIC TURBULENCE

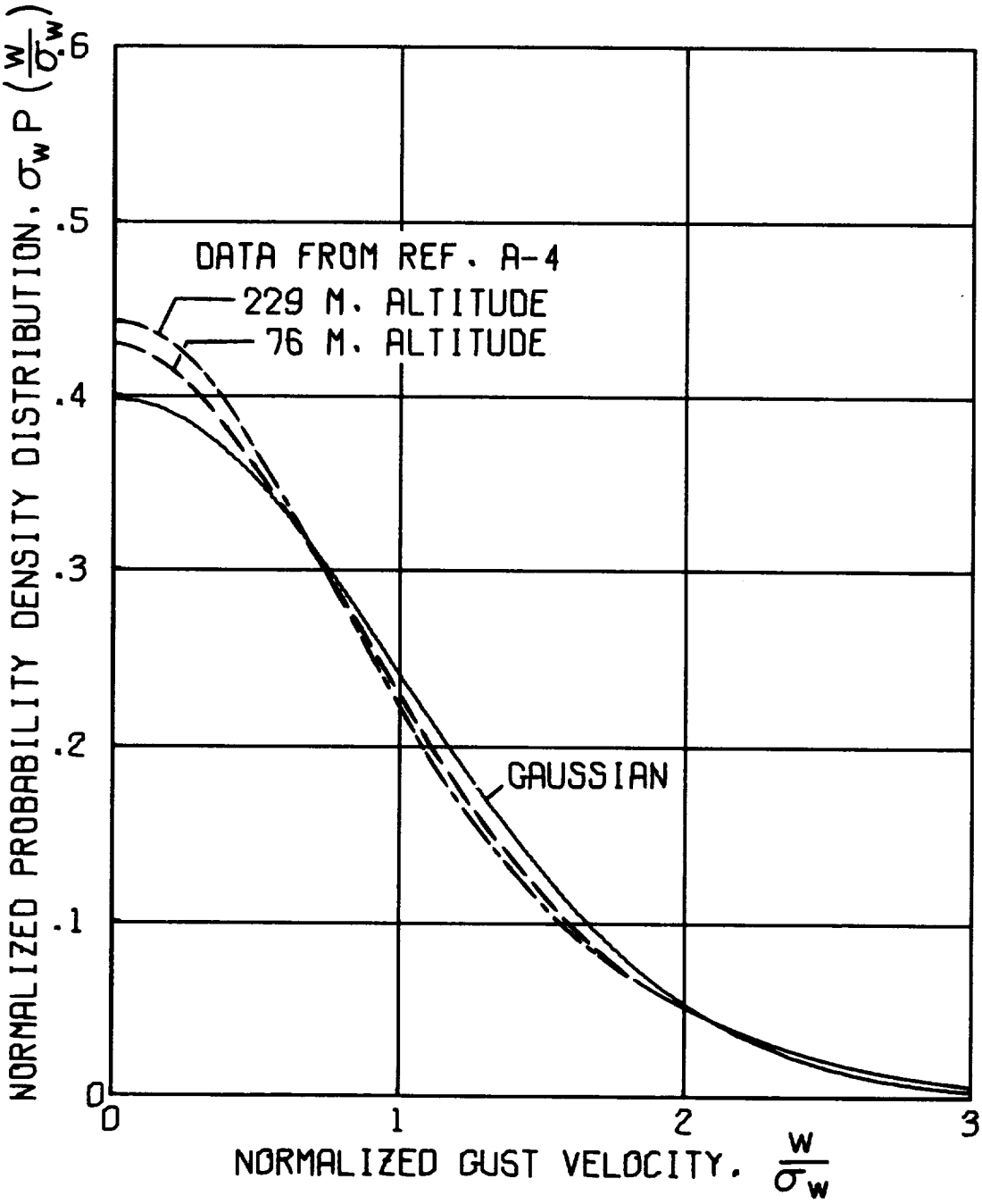


FIGURE A-2. TYPICAL PROBABILITY DENSITY DISTRIBUTIONS OF ATMOSPHERIC TURBULENCE

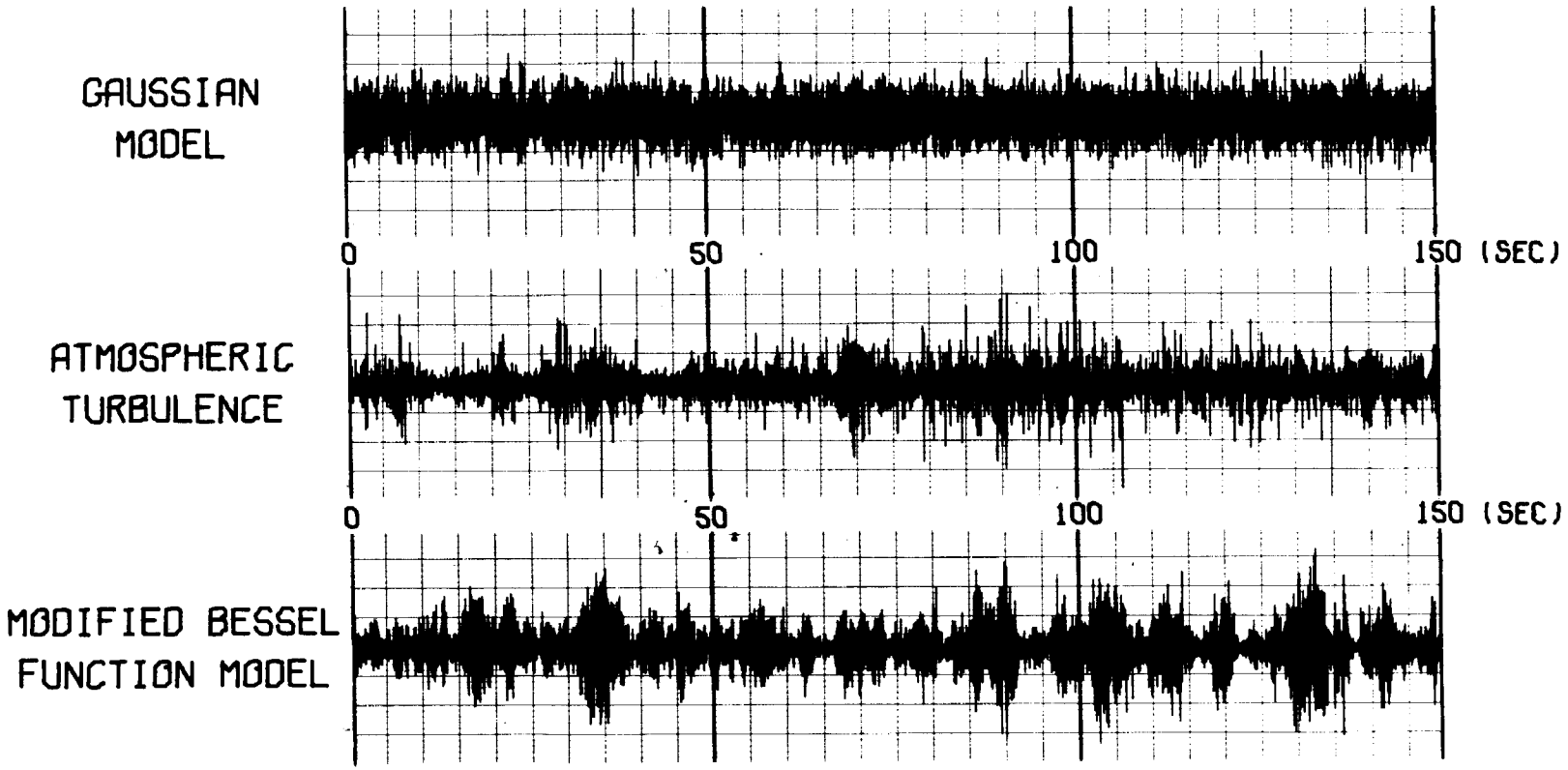


FIGURE A-3. PATCHY CHARACTERISTICS OF MODIFIED BESSEL FUNCTION MODEL COMPARED WITH THOSE PRODUCED BY THE GAUSSIAN MODEL AND ACTUAL ATMOSPHERIC TURBULENCE

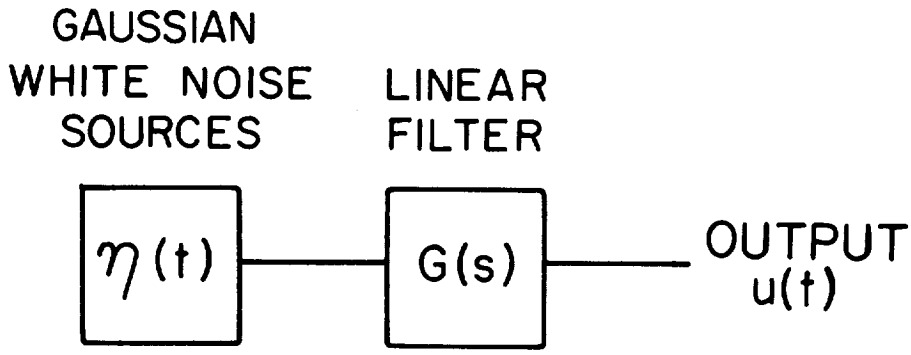


FIGURE A-4. LINEARLY FILTERED GAUSSIAN WHITE NOISE TURBULENCE SIMULATION

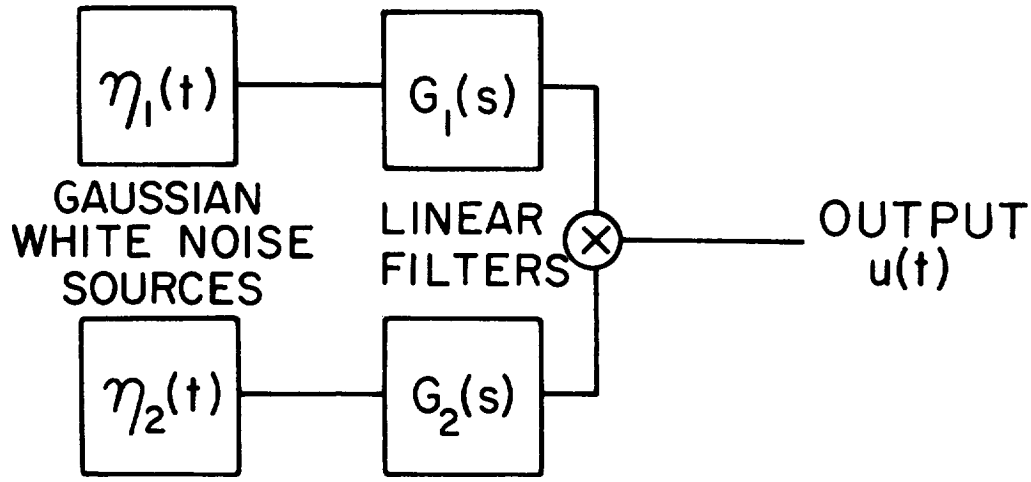


FIGURE A-5. A NON-GAUSSIAN SIMULATION BASED UPON THE MULTIPLICATION OF TWO GAUSSIAN PROCESSES

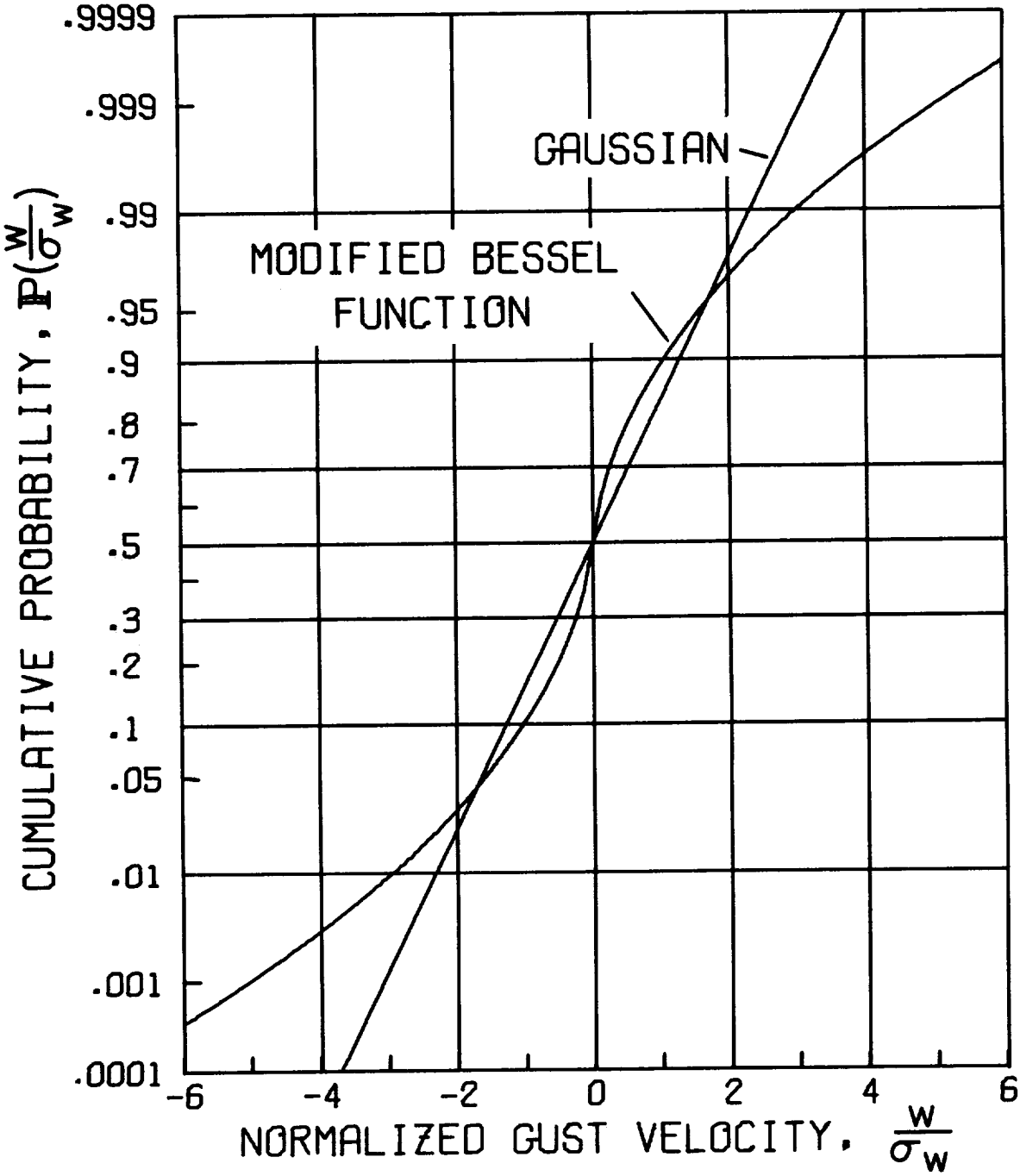


FIGURE A-6. COMPARISON OF GAUSSIAN AND MODIFIED BESSEL FUNCTION CUMULATIVE PROBABILITY DISTRIBUTIONS

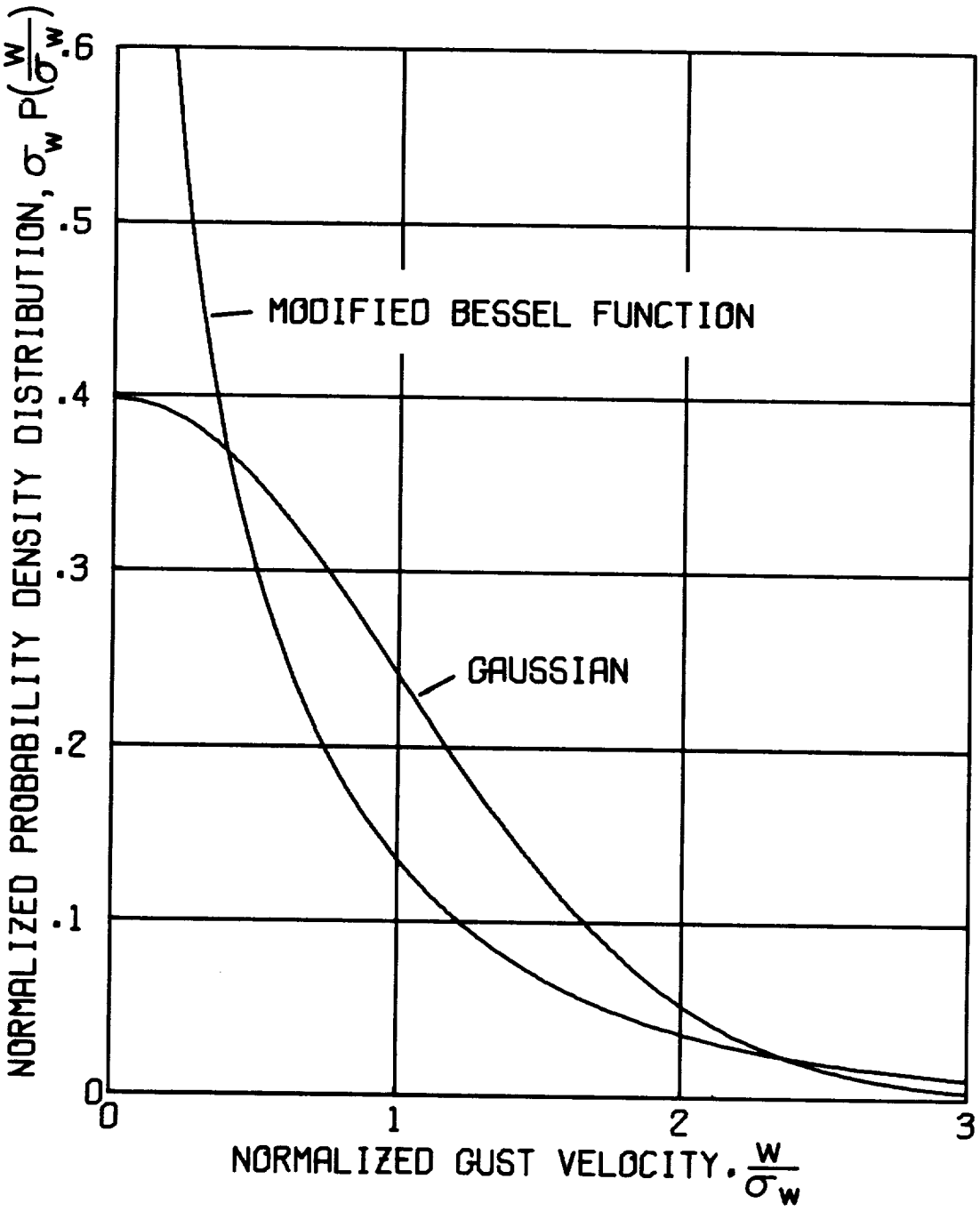


FIGURE A-7. COMPARISON OF GAUSSIAN AND MODIFIED BESSEL FUNCTION PROBABILITY DENSITIES

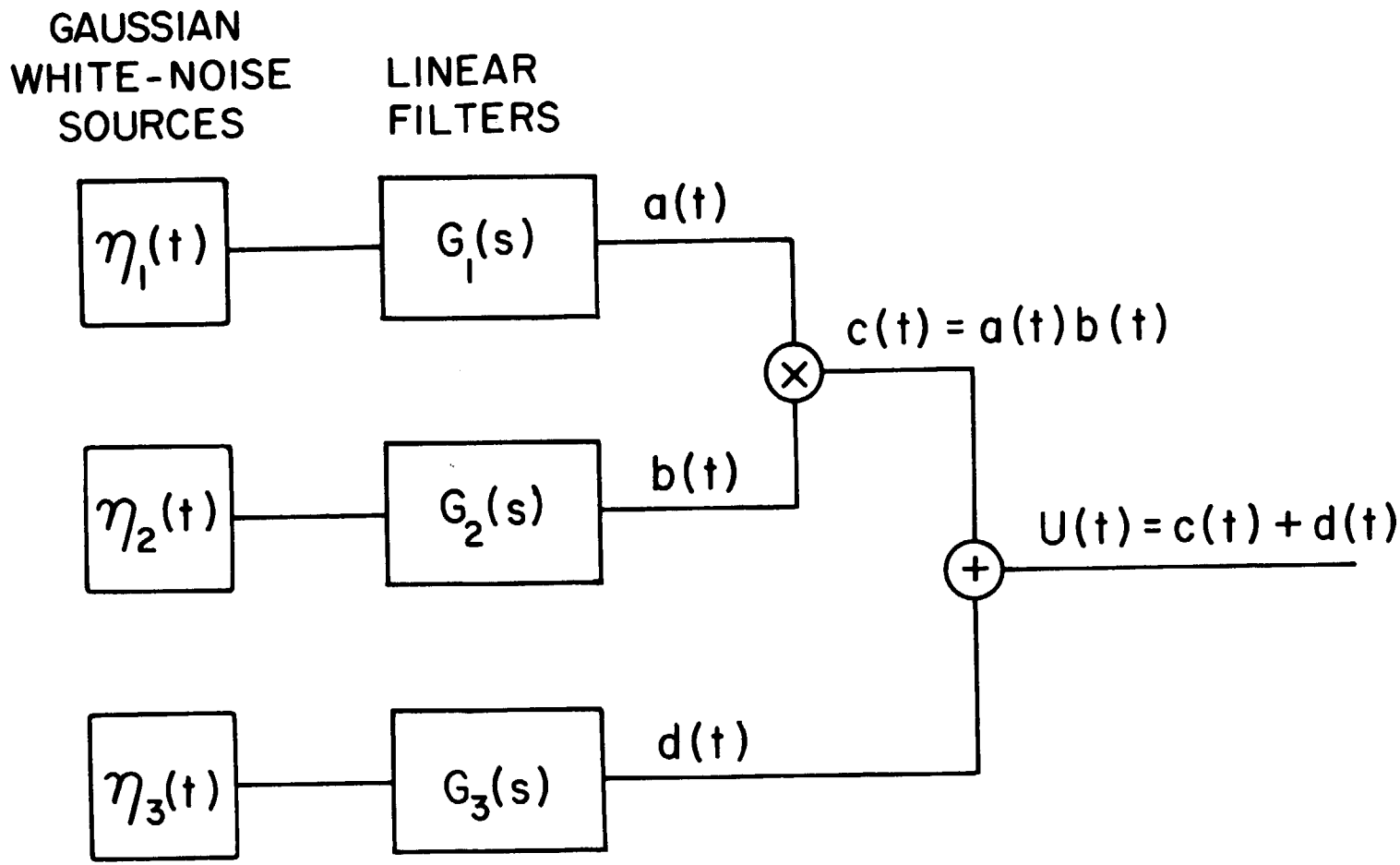


FIGURE A-8. PROPOSED NON-GAUSSIAN TURBULENCE SIMULATION

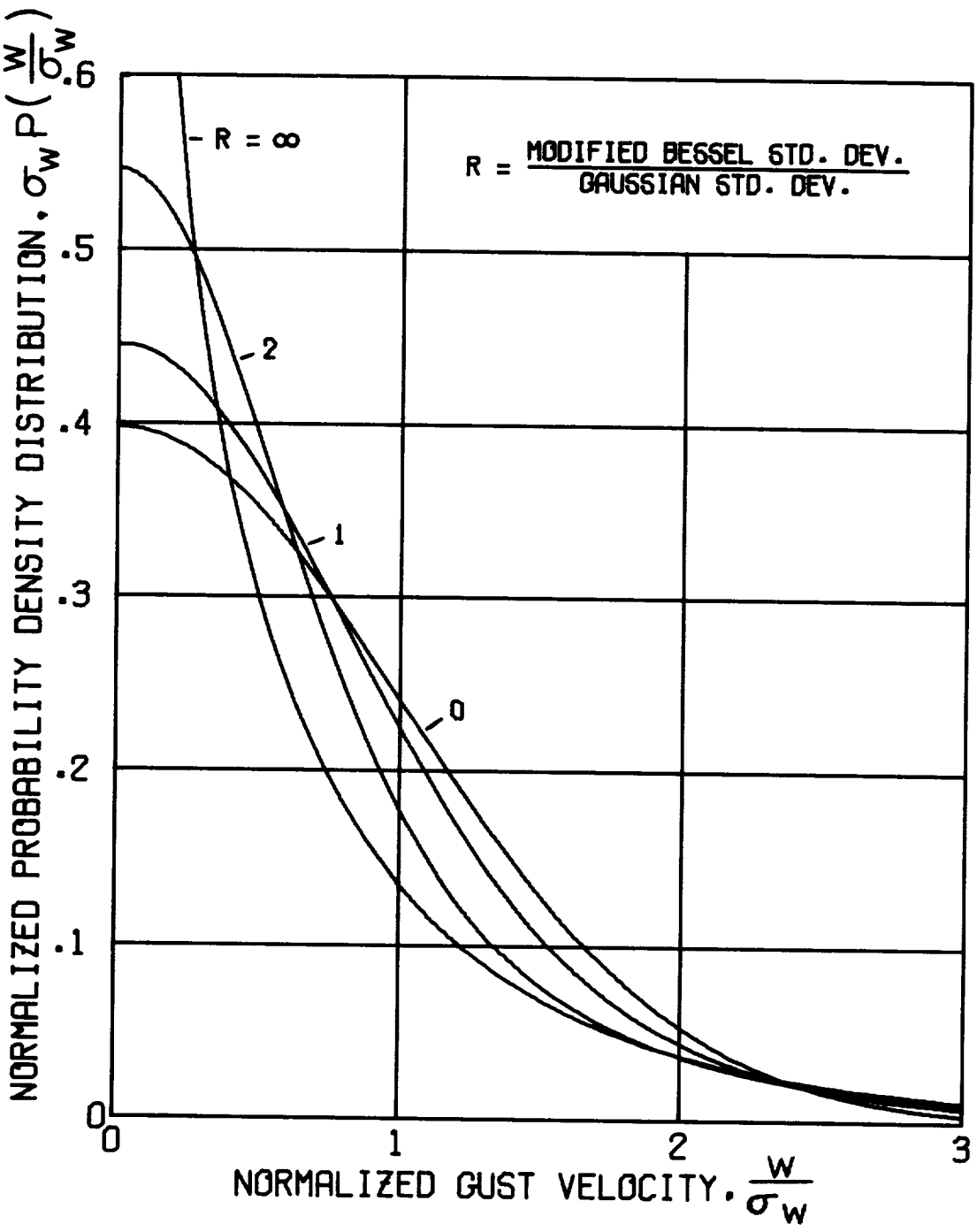


FIGURE A-9. COMPARISON OF PROBABILITY DENSITIES FOR VARIOUS VALUES OF THE STANDARD DEVIATION RATIO

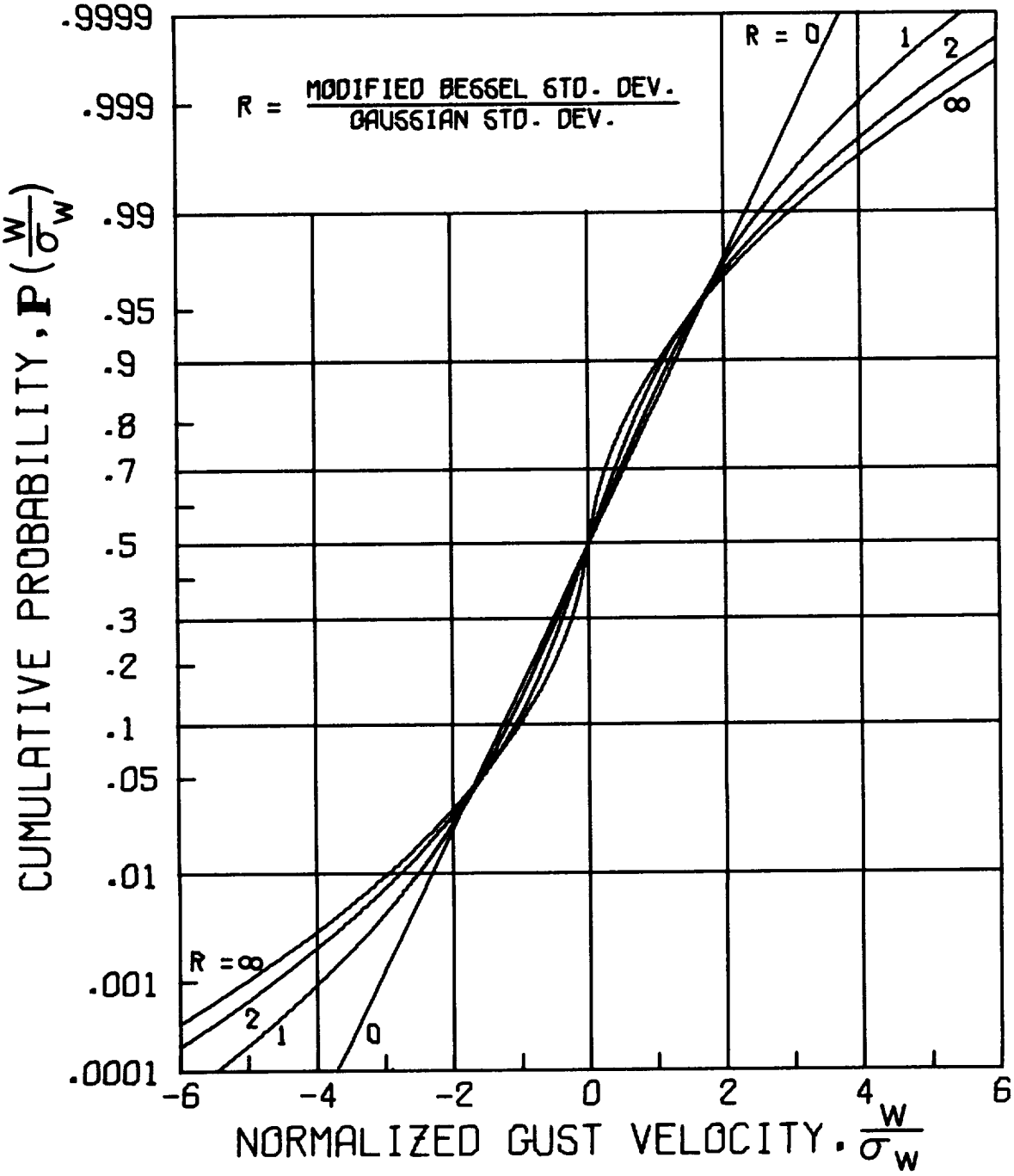


FIGURE A-10. COMPARISON OF CUMULATIVE PROBABILITY DISTRIBUTIONS FOR VARIOUS STANDARD DEVIATION RATIOS

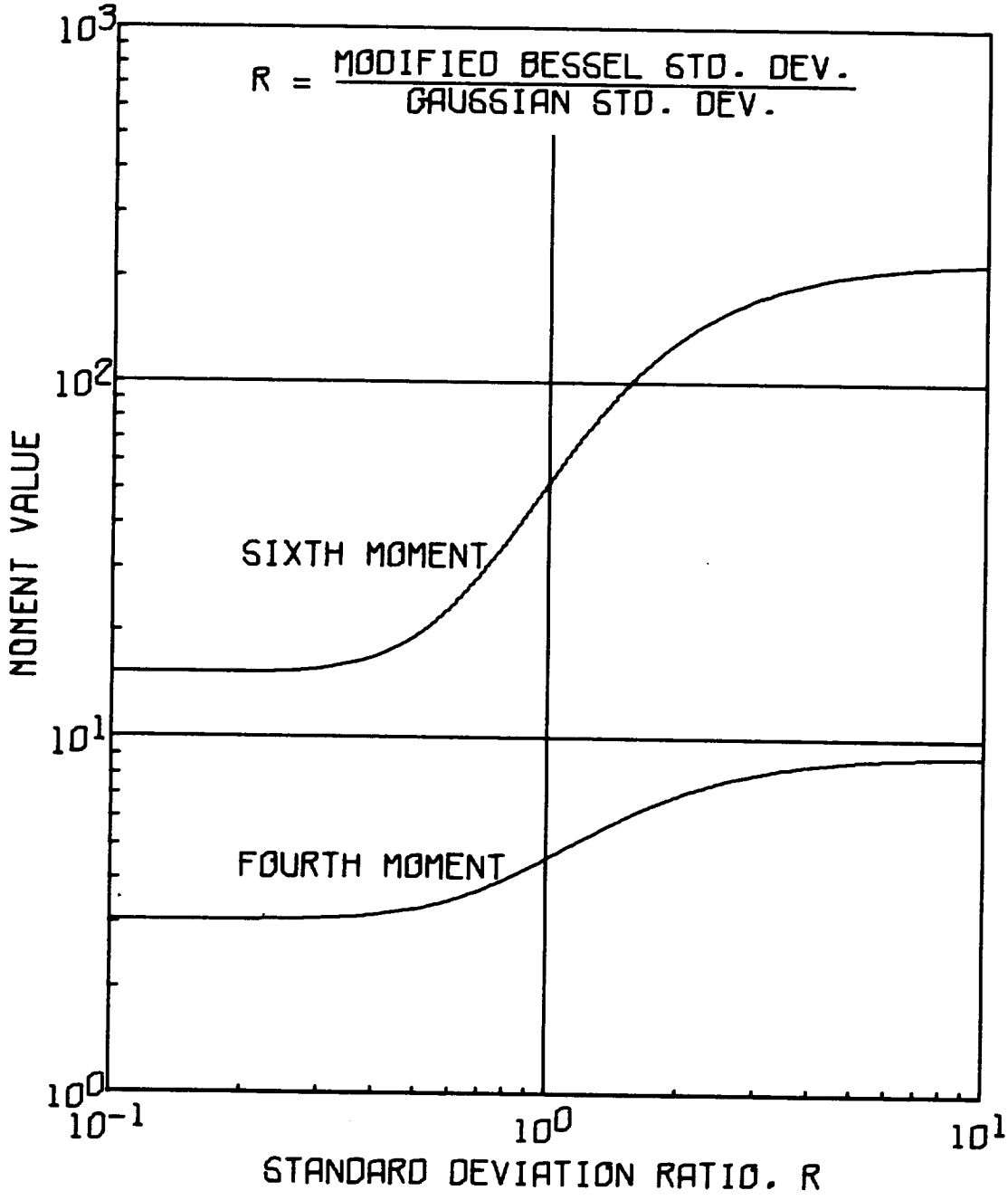


FIGURE A-11. DEPENDENCE OF THE FOURTH AND SIXTH NORMALIZED CENTRAL MOMENTS UPON THE STANDARD DEVIATION RATIO

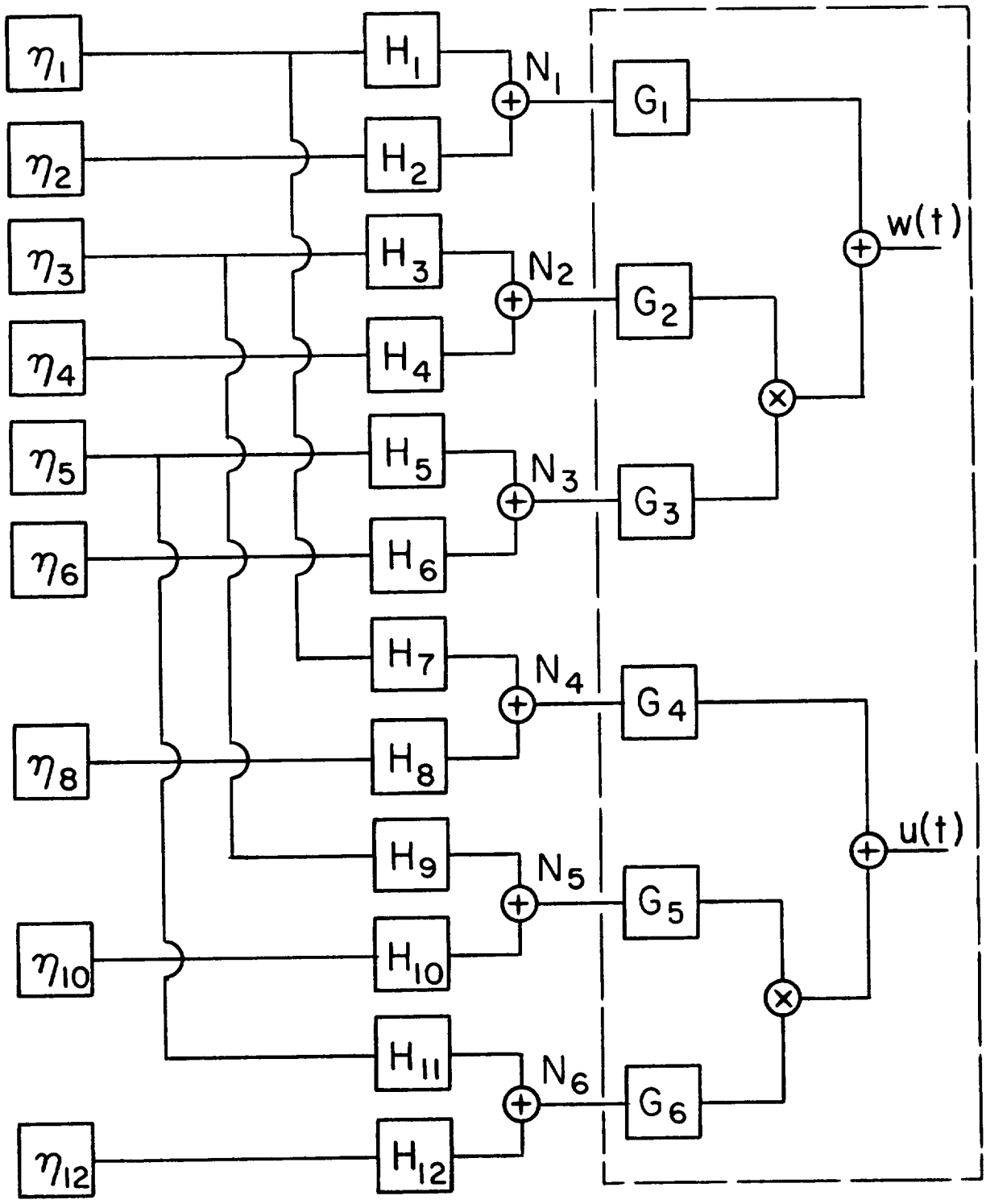


FIGURE A-12. SYSTEM FOR PRODUCING CROSS CORRELATED LONGITUDINAL AND VERTICAL GUST COMPONENTS

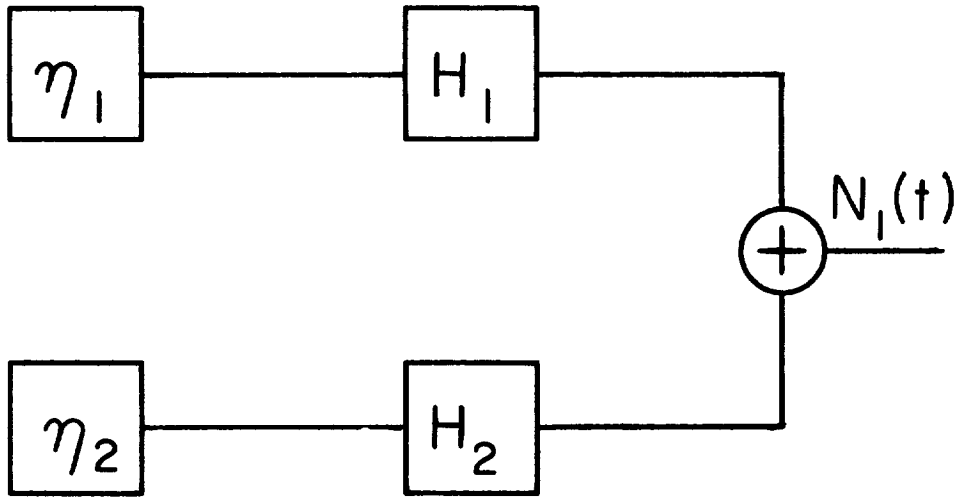


FIGURE A-13. SYSTEM FOR THE GENERATION OF GAUSSIAN WHITE NOISE

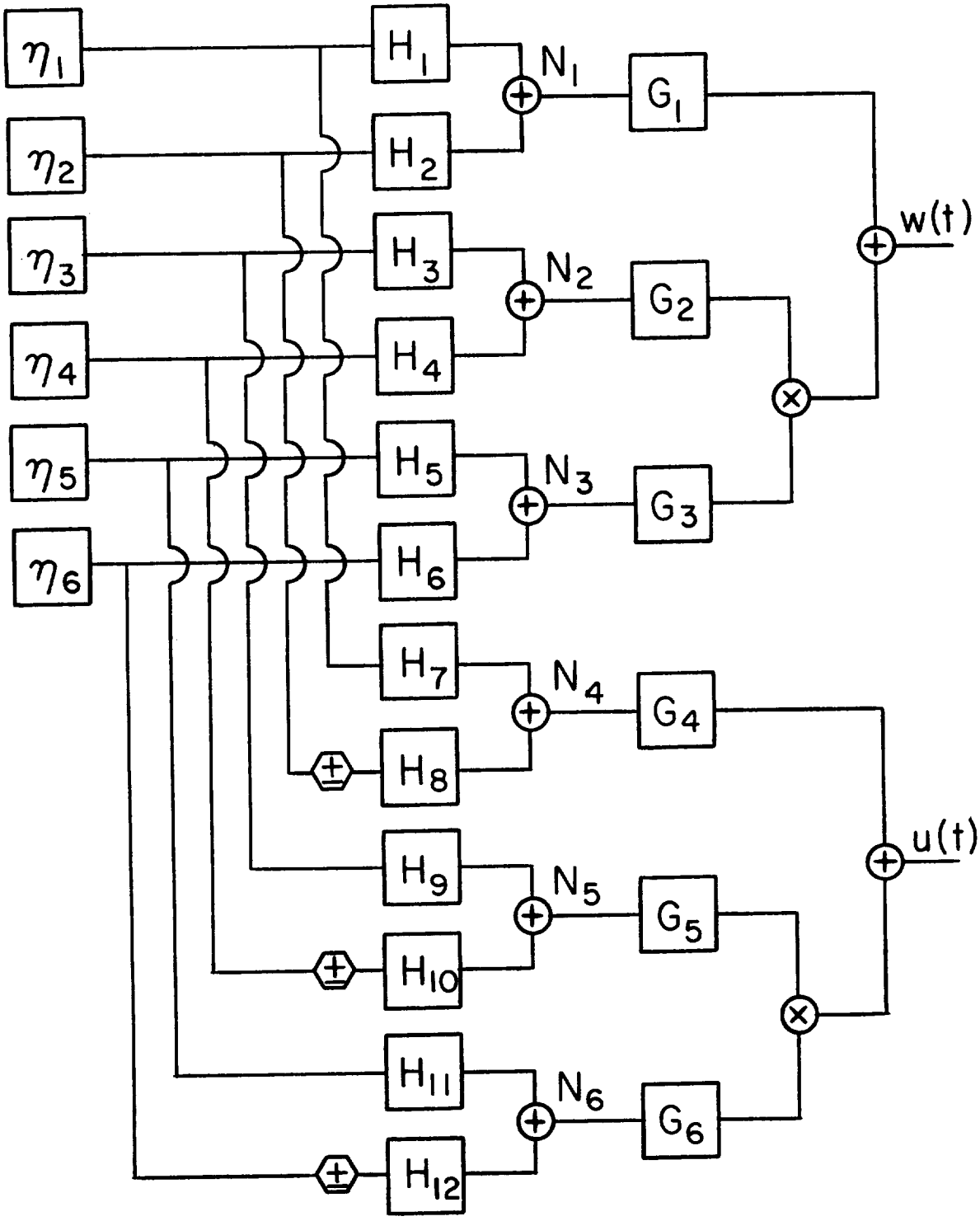


FIGURE A-14. SYSTEM FOR THE GENERATION OF CORRELATED PATCHES

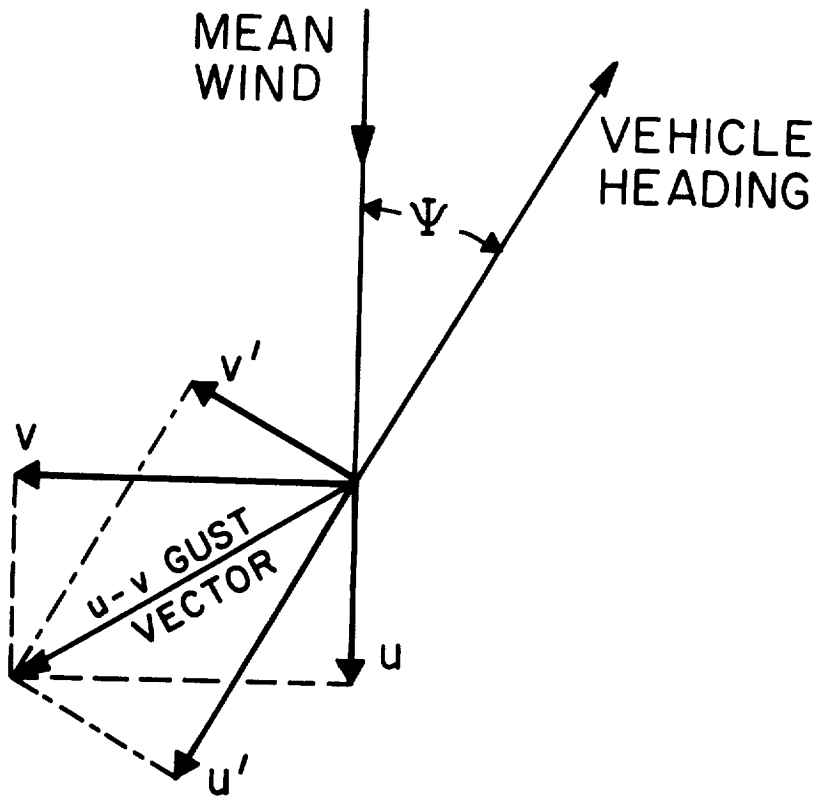


FIGURE A-15. COORDINATE ROTATION GEOMETRY

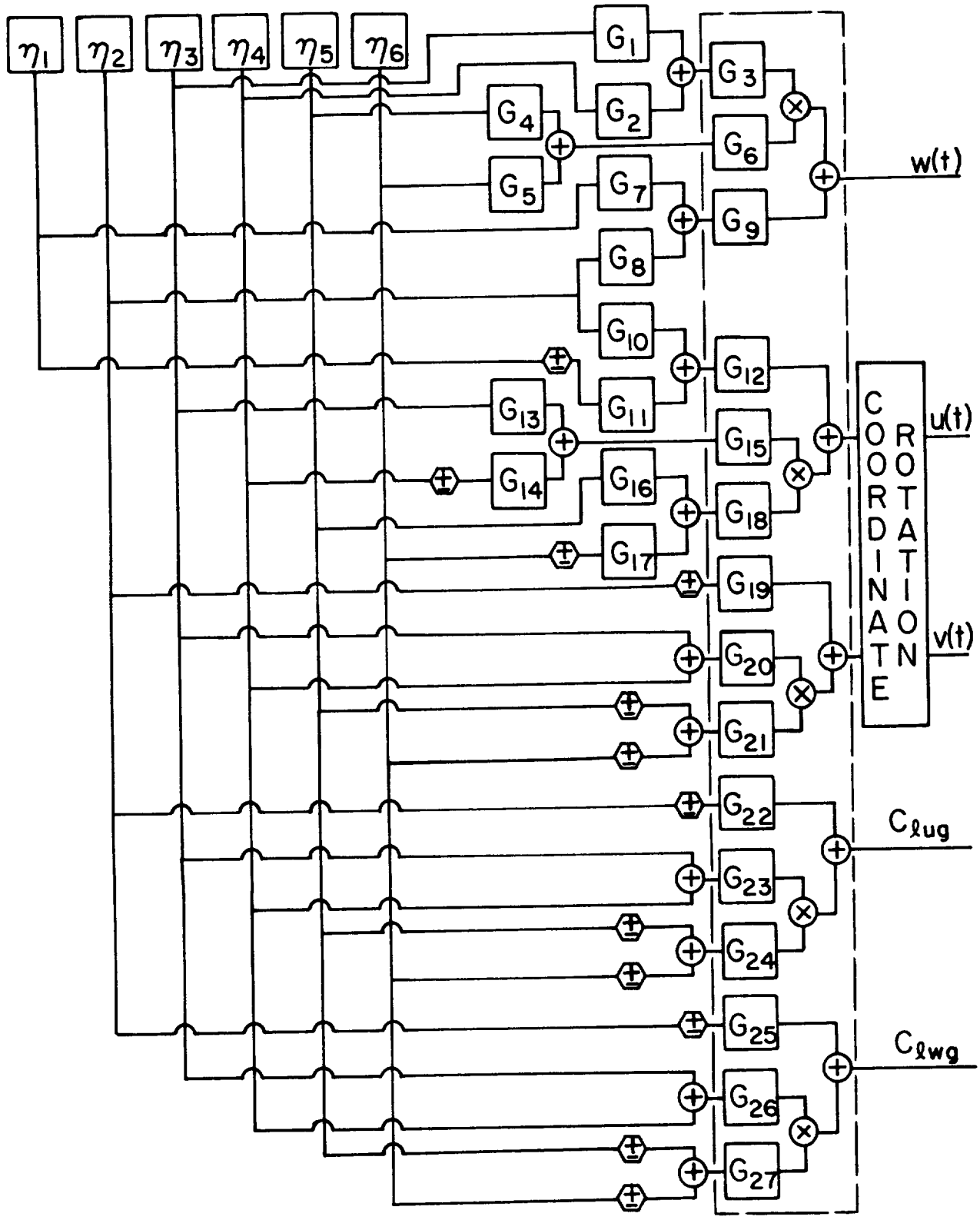


FIGURE A-16 BLOCK DIAGRAM OF COMPLETE SIMULATION

## APPENDIX B

## EQUATIONS OF MOTION

The following equations of motion are essentially those provided by NASA Ames for representing the Twin Otter for use on their simulators. They have been modified slightly to include the turbulence inputs.

The total (non-perturbation) forces and moments on the aircraft due to aerodynamic and engine forces are:

$$F_{Tx} = \bar{q}SC_x + F_{E_x} \tag{B-1}$$

$$F_{Ty} = \bar{q}SC_y + F_{Ey} \tag{B-2}$$

$$F_{Tz} = \bar{q}SC_z + F_{Ez} \tag{B-3}$$

$$M_{Tx} = \bar{q}SbC_\ell + M_{E_x} \tag{B-4}$$

$$M_{Ty} = \bar{q}ScC_m + M_{Ey} \tag{B-5}$$

$$M_{Tz} = \bar{q}SbC_n + M_{Ez} \tag{B-6}$$

The axes system (x,y,z) is a stability-axes system with the usual convention for signs. The dynamic pressure is computed using

$$\bar{q} = \frac{1}{2}\rho(u_B^2 + v_B^2 + w_B^2) \ ,$$

where $(u_B , v_B , w_B)$ are the body-axes vehicle velocities with respect to the gust air. Thus $\bar{q}$ contains the effects of gusts as well as changes in airspeed.

The engine forces and moments are

$$F_{Ex} = \bar{q}_o SC_{To} \frac{u_o}{u_B} - \bar{q}SC_{D_{CT}} C_{T_{\delta T}}(\delta T - \delta T_o) \tag{B-7}$$

$$F_{Ez} = -\bar{q}SC_{L_{CT}} C_{T_{\delta T}} (\delta T - \delta T_o) \tag{B-8}$$

$$M_{Ey} = \bar{q}SC_{m_{CT}} C_{T_{\delta T}} (\delta T - \delta T_o) \tag{B-9}$$

$$F_{Ey} = M_{Ex} = M_{Ez} = 0 \tag{B-10}$$

The thrust sensitivity is

$$C_{T_{\delta T}} = 6.5617 \frac{P_{max}}{\bar{q}s} \left(\frac{0.1311}{V_{RW}} + 0.0021\right) \tag{B-11}$$

and

$$V_{RW} = \sqrt{u_B^2 + v_B^2 + w_B^2} \tag{B-12}$$

The aerodynamic force and moment coefficients are given by

$$C_X = -C_{D_o} + C_{x_\alpha}\alpha \tag{B-13}$$

$$C_y = C_{y_\beta}\beta + \frac{b}{2V_{RW}} (C_{y_r} r + C_{y_p} p) + C_{y_{\delta a}} \delta a$$

$$+ C_{y_{\delta r}} \delta r + \frac{1}{V_{RW}} C_{y_{t\beta}} (v_{g_t} - v_{g_c}) \tag{B-14}$$

$$C_z = -C_{L_o} + C_{z_\alpha}\alpha + \frac{c}{2V_{RW}} (C_{z_{\dot{\alpha}}}\dot{\alpha} + C_{z_q} q)$$

$$+ C_{z_{\delta e}} \delta e + \frac{1}{V_{RW}} C_{z_{t\alpha}} (w_{g_t} - w_{g_c})$$

$$+ \frac{c}{2V_{RW}^2} C_{z_{t\dot{\alpha}}} (\dot{w}_{g_t} - \dot{w}_{g_c}) \tag{B-15}$$

$$C_\ell = C_{\ell_\beta}\beta + \frac{b}{2V_{RW}}\left(C_{\ell_r} r + C_{\ell_p} p\right) + C_{\ell_{\delta a}}\delta a$$

$$+ C_{\ell_{\delta r}}\delta r + C_{\ell_{ug}}(t) + C_{\ell_{wg}}(t) \qquad \text{(B-16)}$$

$$C_m = C_{m_\alpha}\alpha + \frac{c}{2V_{RW}}\left(C_{m_{\dot\alpha}}\dot\alpha + C_{m_q} q\right) + C_{m_{\delta e}}\delta e$$

$$+ \frac{1}{V_{RW}}\left(C_{m_{tu}}\left(u_{g_t} - u_{g_c}\right) + C_{m_{t\alpha}}\left(w_{g_t} - w_{g_c}\right)\right)$$

$$+ \frac{c}{2V_{RW}^2} C_{m_{t\dot\alpha}}\left(\dot w_{g_t} - \dot w_{g_c}\right) \qquad \text{(B-17)}$$

$$C_n = C_{n_\beta}\beta + \frac{b}{2V_{RW}}\left(C_{n_r} r + C_{n_p} p\right) + C_{n_{\delta a}}\delta a$$

$$+ C_{n_{\delta r}} + \frac{1}{V_{RW}} C_{n_{t\beta}}\left(v_{g_t} - v_{g_c}\right) + C_{n_{ug}}(t)$$

$$+ C_{n_{wg}}(t) \qquad \text{(B-18)}$$

Here, $\alpha$ and $\beta$ are defined so as to include the effects of gusts:

$$\alpha = \arctan\frac{w_B}{u_B} \qquad \text{(B-19)}$$

$$\beta = \arctan\frac{v_B}{\sqrt{u_B^2 + w_B^2}} \qquad \text{(B-20)}$$

The forces and moments (B-1) to (B-6) were fed into a NASA digital program which broke up the forces into a north-east-down axes system, added in the effects of gravity and earth's rotation, and performed the necessary integrations to solve the

equations of motion. The equations used in this digital program were all exact as all nonlinearities were included. The details of these equations are relatively straightforward and will not be gone into here.

# APPENDIX C

## MOTION COMPENSATION

Three different types of motion compensation were used: acceleration limits, a "quickening" circuit to improve the high-frequency response of the simulator, and a washout circuit to filter out low-frequency motions. The arrangement of these circuits is shown in figure C-1.

The drive-system for the simulator was a position-drive, i.e., a position was commanded by the computer and the simulator drive-system tried to match the commanded position.

The inputs to the motion-compensation network were the computed Euler-angle accelerations $\ddot{\phi}$, $\ddot{\theta}$, and $\ddot{\psi}$, and the computer accelerations $\dot{V}_N$, $\dot{V}_E$, and $\dot{V}_D$ in the north-east-down axis system. The accelerations $\dot{V}_N$, $\dot{V}_E$, and $\dot{V}_D$ were computed by taking the total forces (in body-axes) on the airdraft, transforming them into forces in the north-east-down axis system by using the washed-out Euler angles of the simulator $\phi_w$, $\theta_w$, and $\psi_w$, and dividing by the airplane mass $m$.

### Acceleration Limiting

In order to prevent the drive system from shutting down because the commanded accelerations were too large, limits were placed on the acceleration signals. Because the simulator was driven by position rather than by acceleration, the limiting was done on the computed values of $\dot{V}_N$, $\dot{V}_E$, and $\dot{V}_D$ instead of on actual cab accelerations in order to reduce the complexity. Thus, because the signals are passed through a quickening circuit before reaching the simulator drive, the commanded accelerations sometimes exceeded the acceleration limits set. The limiting was done digitally (as was all the compensation), and the following values were used for limits:

$$\dot{V}_N = \pm 1.524 \text{ m/sec}^2$$

$$\dot{V}_E = \pm 1.524 \text{ m/sec}^2$$

$$\dot{V}_D = \pm 0.9144 \text{ m/sec}^2$$

## Quickening

A quickening, or lead, circuit was used on all six signals in order to improve the high-frequency response of the simulator. The accelerations were first integrated twice to give distance and angle commands. The quickening input/output relations were of the form

$$e_{out} = e_{in} + K_D \dot{e}_{in} + K_{DD} \ddot{e}_{in}$$

Taking the Laplace transform,

$$\frac{E_{out}}{E_{in}} = 1 + K_D s + K_{DD} s^2$$

Note that this gives increasingly higher gain as frequency is increased, and is partly the cause of the excessive high-frequency motion that the pilots complained about in the simulation. The following values were used for $K_D$ and $K_{DD}$ in each of the channels.

| Channel | $K_D$ | $K_{DD}$ |
|---|---|---|
| $\phi$ | 0.08 | 0. |
| $\theta$ | 0.18 | 0.012 |
| $\psi$ | 0. | 0. |
| $X_{NORTH}$ (longitudinal) | 0.16 | 0.04 |
| $X_{EAST}$ (side-motions) | 0.14 | 0.037 |
| $X_{DOWN}$ (vertical) | 0.25 | 0. |

## Washout

Washout was necessary in order to prevent a low-frequency acceleration from building up motions that would cause the simulator to hit its travel limits. The washout used had an input/output Laplace transform of the form

$$\frac{E_{out}}{E_{in}} = \frac{s^2}{s^2 + As + B}$$

This provided unity gain at the high frequencies, and a gain going to zero as frequency went to zero. The values of A and B used were as follows.

| Channel | A | B |
|---|---|---|
| $\phi$ | 1.0 | 0.5 |
| $\theta$ | 1.0 | 0.5 |
| $\psi$ | 1.0 | 0.5 |
| $X_{NORTH}$ | 1.0 | 0.5 |
| $X_{EAST}$ | 1.0 | 0.5 |
| $X_{DOWN}$ | 1.0 | 0.5 |

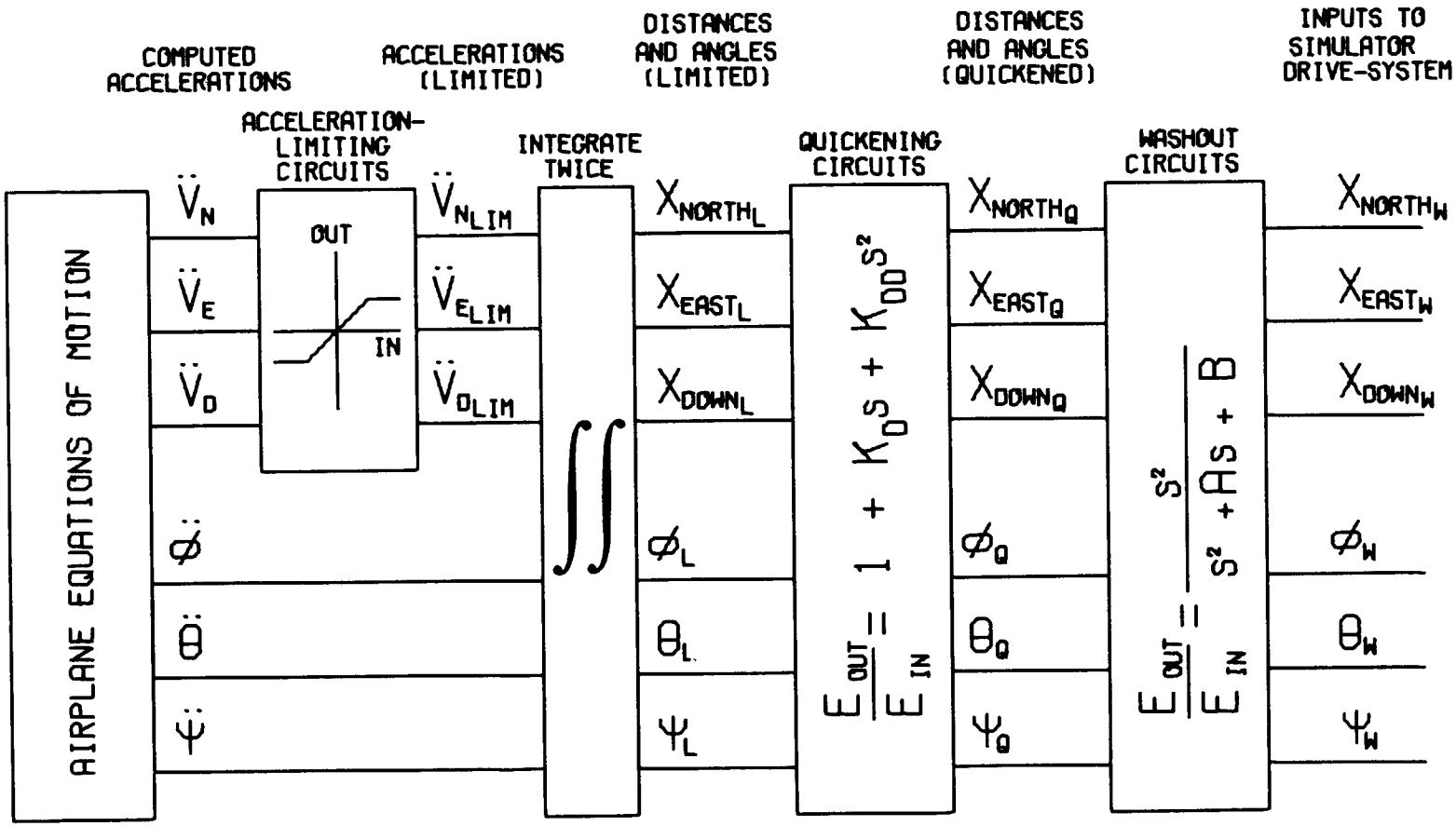


FIGURE C-1. DETAILS OF MOTION COMPENSATION USED IN SIMULATION

APPENDIX D

PILOT QUESTION SHEET

Twin Otter 6-Degree Simulation, June-July 1971

Flight Number: _____ Date: _____

Pilot: _____

1. Turbulence Intensity:

| Light | Moderate | Severe | Extreme |
|---|---|---|---|
| ( ) | ( ) | ( ) | ( ) |

2. Realism of Turbulence:

| Very Good | Good | Fair | Poor | Very Poor |
|---|---|---|---|---|
| ( ) | ( ) | ( ) | ( ) | ( ) |

3. Correctness of Relative Amplitudes of Disturbances:

| | Not Enough | About Right | Too Much | No Comment |
|---|---|---|---|---|
| Roll | ( ) | ( ) | ( ) | ( ) |
| Pitch | ( ) | ( ) | ( ) | ( ) |
| Yaw | ( ) | ( ) | ( ) | ( ) |
| Heave | ( ) | ( ) | ( ) | ( ) |
| Side-Force | ( ) | ( ) | ( ) | ( ) |

4. Patchy Characteristics (Variations of Intensity-Burst):

| Much too Continuous (monotonous) | A Little too Continuous | About Right | A Little too Patchy | No Comment |
|---|---|---|---|---|
| ( ) | ( ) | ( ) | ( ) | ( ) |

5. Frequency Content of Turbulence:

| | Not Enough | About Right | Too Much | No Comment |
|---|---|---|---|---|
| Low Frequencies | ( ) | ( ) | ( ) | ( ) |
| High Frequencies | ( ) | ( ) | ( ) | ( ) |

6. Other Comments about Realism (of turbulence or aircraft simulation):

7. Pilot Estimate of Work Load:

| Very Easy | Easy | Average | Difficult | Very Difficult |
|---|---|---|---|---|
| ( ) | ( ) | ( ) | ( ) | ( ) |

8. Pilot Estimate of Task Performance (integral-squared error for ILS tracking task):

| Very Good | Good | Average | Poor | Very Poor |
|---|---|---|---|---|
| ( ) | ( ) | ( ) | ( ) | ( ) |

9. Cooper Rating (rate aircraft as flown under these conditions of turbulence):

# APPENDIX E

## OTHER RESULTS OF PILOT QUESTIONNAIRE

The following plots show the pilot answers to the question sheet which were not discussed in the main text. They do not show any consistent differences between the various turbulence models and are shown here only for completeness. Also shown are plots of the rms values of the angles $\phi$, $\theta$, and $\psi$ . Again, there are no consistent differences between the rms values from one model to the next.

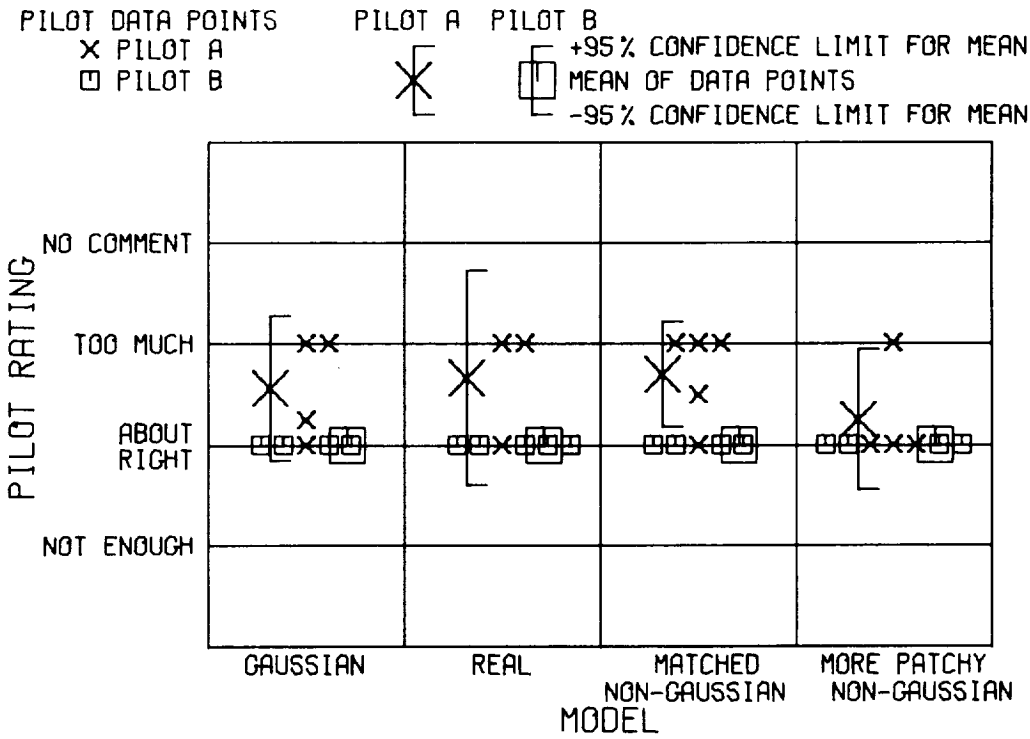


FIGURE E-1. CORRECTNESS OF PITCH

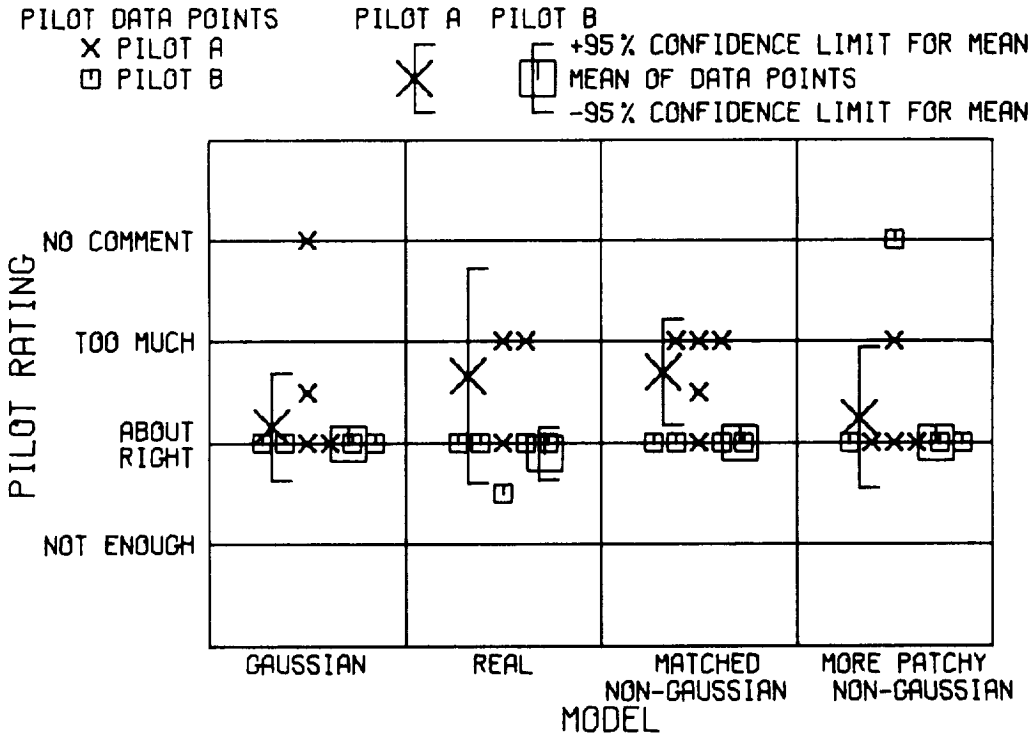


FIGURE E-2. CORRECTNESS OF HEAVE

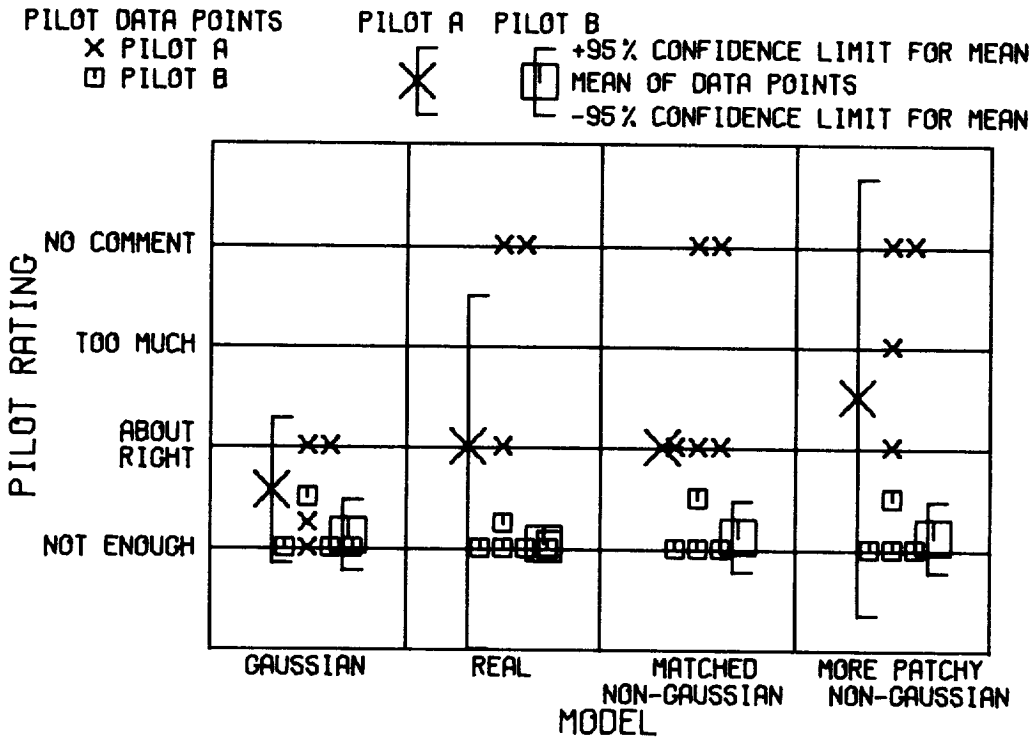


FIGURE E-3. CORRECTNESS OF SIDE-FORCE

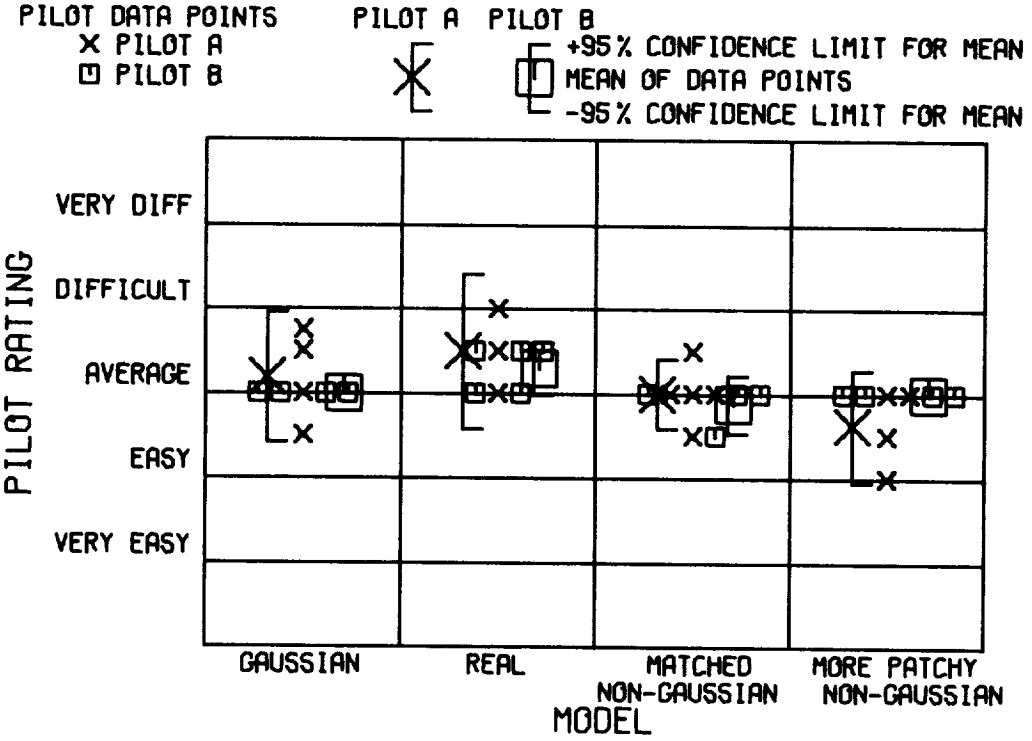


FIGURE E-4. ESTIMATE OF WORKLOAD

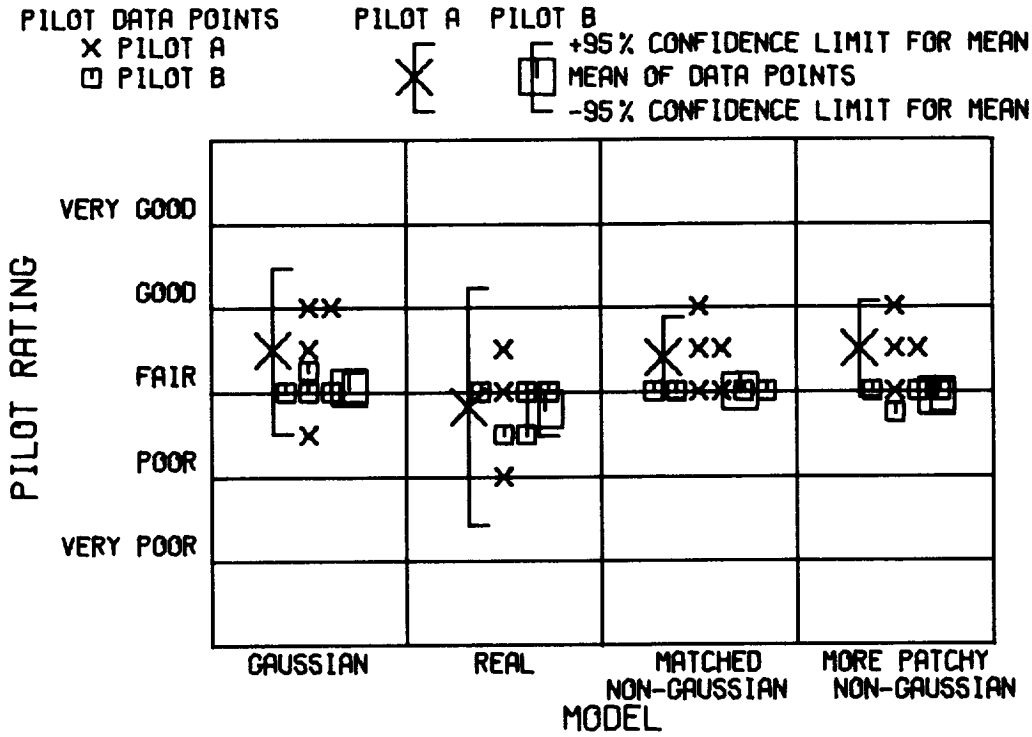


FIGURE E-5. ESTIMATE OF TASK PERFORMANCE

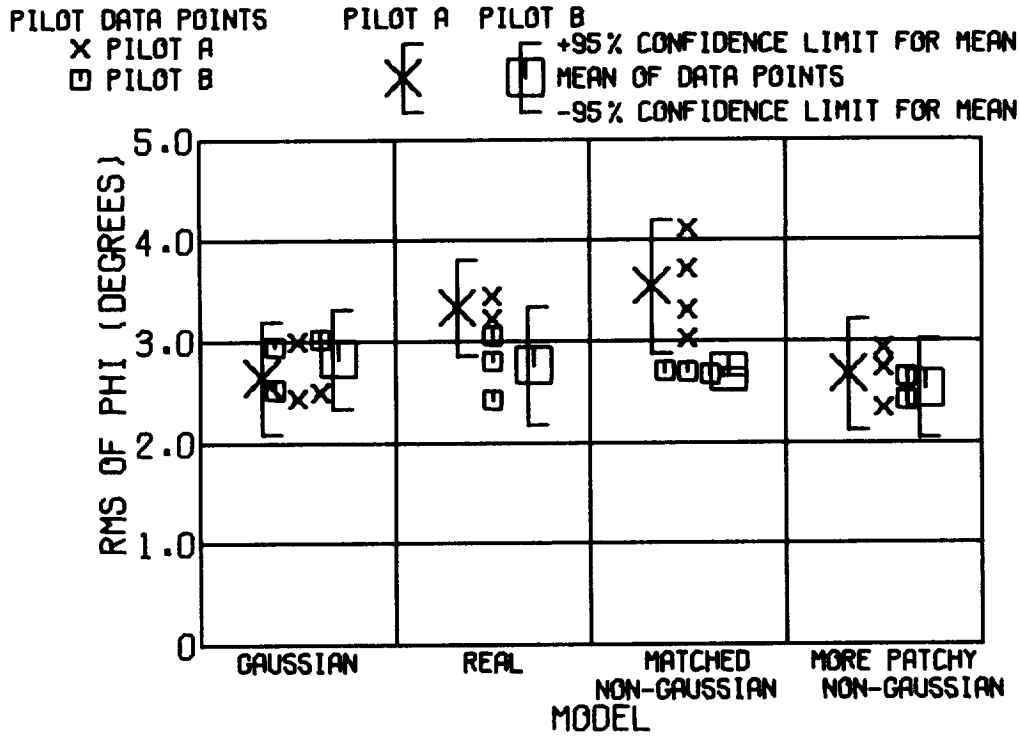


FIGURE E-6. RMS OF PHI (BANK ANGLE)

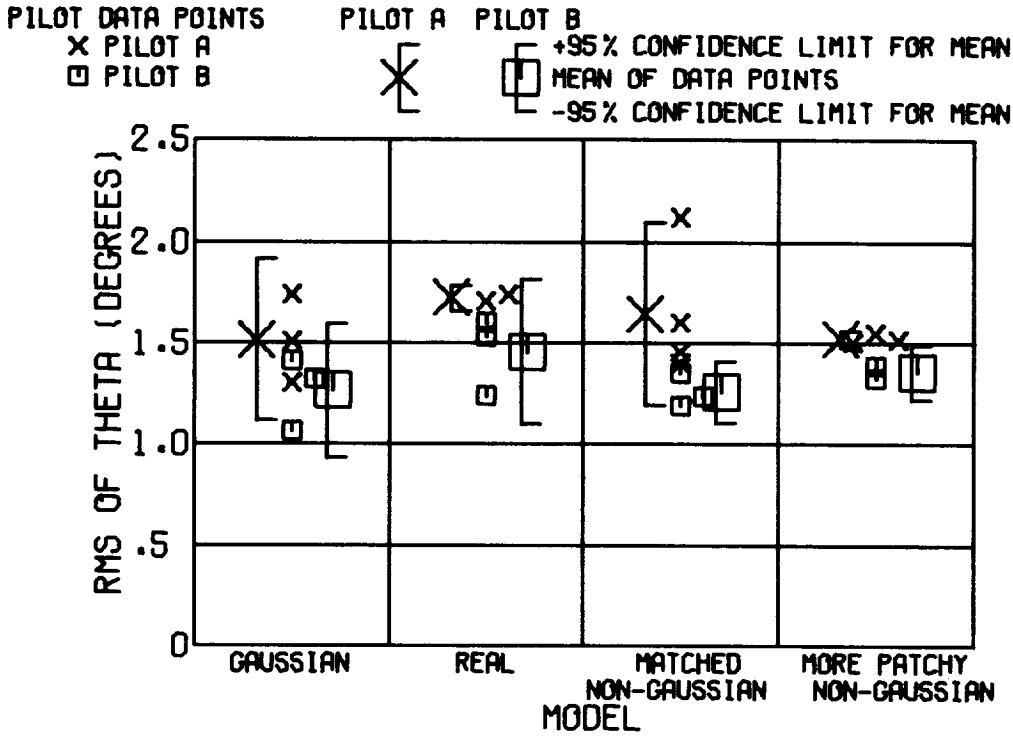


FIGURE E-7. RMS OF THETA (PITCH ANGLE)

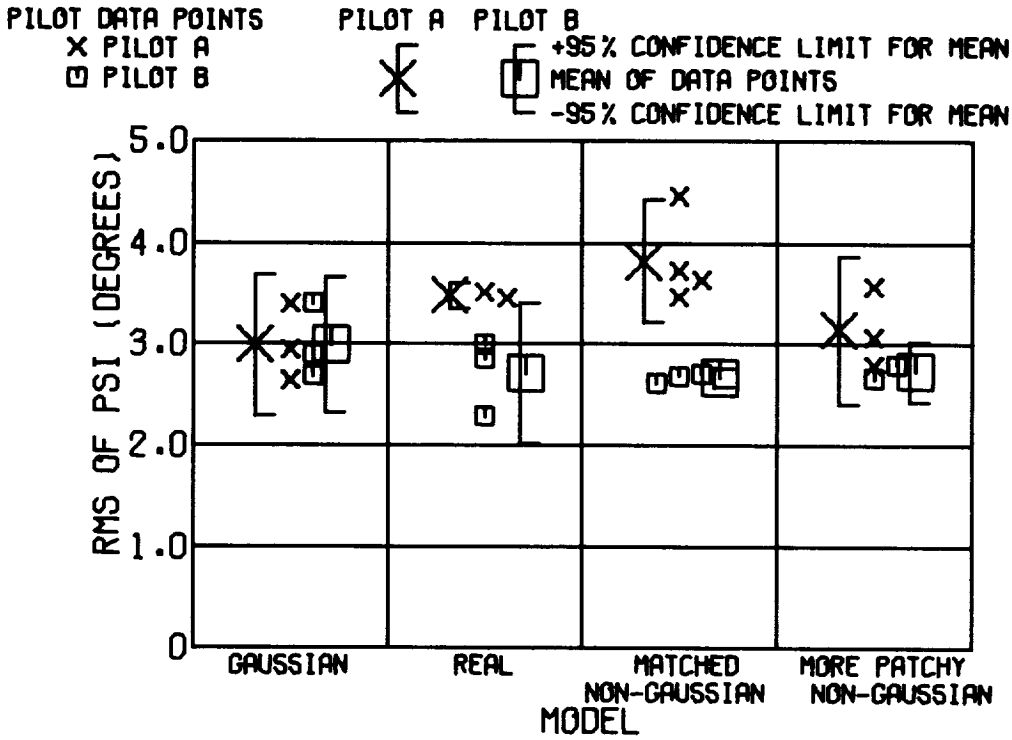


FIGURE E-8. RMS OF PSI (YAW ANGLE)



U.S. GOVERNMENT PRINTING OFFICE: 1974—635-043/19

NATIONAL AERONAUTICS AND SPACE ADMINISTRATION
WASHINGTON, D.C. 20546

OFFICIAL BUSINESS
PENALTY FOR PRIVATE USE $300

SPECIAL FOURTH-CLASS RATE BOOK

POSTAGE AND FEES PAID
NATIONAL AERONAUTICS AND SPACE ADMINISTRATION
451

U.S.MAIL

POSTMASTER: If Undeliverable (Section 158 Postal Manual) Do Not Return

*"The aeronautical and space activities of the United States shall be conducted so as to contribute . . . to the expansion of human knowledge of phenomena in the atmosphere and space. The Administration shall provide for the widest practicable and appropriate dissemination of information concerning its activities and the results thereof."*

—NATIONAL AERONAUTICS AND SPACE ACT OF 1958

# NASA SCIENTIFIC AND TECHNICAL PUBLICATIONS

TECHNICAL REPORTS: Scientific and technical information considered important, complete, and a lasting contribution to existing knowledge.

TECHNICAL NOTES: Information less broad in scope but nevertheless of importance as a contribution to existing knowledge.

TECHNICAL MEMORANDUMS: Information receiving limited distribution because of preliminary data, security classification, or other reasons. Also includes conference proceedings with either limited or unlimited distribution.

CONTRACTOR REPORTS: Scientific and technical information generated under a NASA contract or grant and considered an important contribution to existing knowledge.

TECHNICAL TRANSLATIONS: Information published in a foreign language considered to merit NASA distribution in English.

SPECIAL PUBLICATIONS: Information derived from or of value to NASA activities. Publications include final reports of major projects, monographs, data compilations, handbooks, sourcebooks, and special bibliographies.

TECHNOLOGY UTILIZATION PUBLICATIONS: Information on technology used by NASA that may be of particular interest in commercial and other non-aerospace applications. Publications include Tech Briefs, Technology Utilization Reports and Technology Surveys.

***Details on the availability of these publications may be obtained from:***

**SCIENTIFIC AND TECHNICAL INFORMATION OFFICE**

**NATIONAL AERONAUTICS AND SPACE ADMINISTRATION**

**Washington, D.C. 20546**